DOI:10.14753/SE.2021.2546

Functional cooperativity of fine-scale input patterns in the dendrites of hippocampal CA1 pyramidal cells

PhD thesis

Ádám Magó

János Szentágothai Doctoral School of Neuroscience

Semmelweis University

Supervisor: Judit K. Makara MD, Ph.D.

Official reviewers: Péter Enyedi MD, DSc

Viktor Szegedi Ph.D.

Head of the Final Examination Committee: Anita Kamondi MD, DSc

Members of the Final Examination Committee: Lucia Wittner Ph.D.

Márk Kozsurek MD, Ph.D.

Budapest

2021

DOI:10.14753/SE.2021.2546

TABLE OF CONTENTS

DOI:10.14753/SE.2021.2546

DOI:10.14753/SE.2021.2546

1. LIST OF ABBREVIATIONS

2P – 2-photon

2PGU – 2-Photon Glutamate Uncaging

ACSF – Artificial Cerebrospinal Fluid

ADP – afterdepolarization

AMPA - α-amino-3-hydroxy-5-methyl-4-isoxazolepropionic acid

AMPAR – AMPA receptor

ANOVA – Analysis of Variance

AP – action potential

AP5 – 2-amino-5-phosphonopentanoic acid

bAP – backpropagating action potential

BDNF – brain-derived neurotrophic factor

CA1, 2, 3 – cornu ammonis region 1, 2, 3

CA1PC – cornu ammonis region 1 pyramidal cell

CaMKII - Ca^{2+}/calmodulin-dependent protein kinase II

cAMP – cyclic adenosine monophosphate

Cdc42 – cell division control protein 42 homolog

clust – clustered

C_m – specific membrane capacitance

CRE – cAMP responsive element

CREB – cAMP response element binding protein

DG – Dentate Gyrus

distr – distributed

d-spike – dendritic spike

EC – Entorhinal cortex

E-LTP – early phase long term potentiation

EPSP – excitatory postsynaptic potential

ERK – extracellular signal-regulated kinases

GluA1 – glutamate ionotropic receptor AMPA type subunit 1

GTP – guanosine triphosphate

HCN - Hyperpolarization-activated cyclic nucleotide–gated channel

I_A – A-type potassium current

IEG – immediately early gene

ISD – Interspine distance

ISI – Interspine stimulus interval

L-LTP – late phase long term potentiation

LTD – long term depression

LTP – long term potentiation

MAPK – Mitogen-activated protein kinase

MEK – Mitogen-activated protein kinase kinase

MNI-glutamate – 4-methoxy-7-nitroindolinyl-glutamate

mRNA – messenger ribonucleid acid

Ni^{2+} - Nickel (II) ion

nimo – nimodipine

NMDAR – N-methyl-D-aspartate receptor

OGB-1 – Oregon Green 488 BAPTA 1

PKA – protein kinase A

PSD – postsynaptic density

Rac1 – Ras-related C3 botulinum toxin substrate

Ref – reference

DOI:10.14753/SE.2021.2546

RhoA – Ras homolog family member A

R_i – intracellular resistivity

RL – relative location

R_m – specific membrane resistivity

SD – standard deviation

SEM – standard error of mean

STDP – Spike timing dependent plasticity

Sub – Subiculum

TTX – tetrodotoxin

VGCC – Voltage gated Ca^{2+} channel

VGNC – Voltage gated Na^{+} channel

DOI:10.14753/SE.2021.2546

2. INTRODUCTION

2.1 The hippocampal structure and function

The hippocampus is part of the hippocampal formation, located in the temporal lobe. This region is one of the most extensively studied parts of the brain, particularly due to its well-established central roles in learning, memory, social behaviour and spatial navigation (Brandon et al., 2011; Hitti and Siegelbaum 2014; Kogan et al., 2000; O'keefe and Conway 1978; O'keefe and Dostrovsky 1971; Oliva et al., 2016; Sliwa et al., 2016; Wood et al., 2000). However, the functions above are more complex; although O'Keefe and Dostrovsky described place cells that code a specific certain place in the environment with a higher firing rate (O'keefe and Dostrovsky 1971), now it is clear that information in the hippocampus is not only represented by place cells, as different cells within the hippocampal formation are encoding different aspects of the space, time and environment, forming a cognitive map of the surrounding space. During navigation, the hippocampus is necessary for cue driven reward finding (Packard and Mcgaugh 1996), where recalling of learned relevance of cues for reward location is required (Ainge et al., 2007). This finding reinforces the fact that the cognitive map is supported by hippocampus (Eichenbaum 2017). Aside from spatial memory, it has been shown that the hippocampus also plays a role in memory formation and consolidation as after removing the medial temporal lobe bilaterally from the famous epileptic patient Henry Molaison, he suffered from severe anterograde amnesia (Corkin 1984). Nevertheless, the hippocampus only temporally stores new memories and supports the permanent storage of memories, which takes place in the neocortex (Eichenbaum 2013).

These functions are produced by a network of principal cells and interneurons, which are located in well-defined subregions within the hippocampus: the dentate gyrus (main principal neurons: granule cells) and the CA1, CA2 and CA3 subregions of the Cornu Ammonis region (main principal neurons: pyramidal cells)(Amaral and Witter 1989; Lorente De Nó 1934) (**Fig.1 A)**. These cells are connected via an excitatory trisynaptic loop (Andersen et al., 1971): layer 3 and layer 2 of the entorhinal cortex (EC) form synapses via the perforant path onto granule cells (**Fig.1 Bi**) and also send axons to CA1 and CA3 pyramidal cells, respectively (**Fig.1 Biii, Bvii**). Granule cells connect via

DOI:10.14753/SE.2021.2546

their axons, the mossy fibers, to the proximal (mostly apical) dendrites of CA3 pyramidal cells (**Fig.1 Bii**). CA3 pyramidal cells give recurrent collaterals to other CA3 pyramidal cells (**Fig.1 Biv**) and innervate the apical oblique and basal dendrites of CA1 pyramidal cells via the Schaffer collaterals in the stratum radiatum and stratum oriens, respectively (**Fig.1 Bv**). Finally, CA1 pyramidal cells, the main output of the hippocampus, send axons back to the EC deep layers (**Fig.1 Bvi**) (Andersen 2007; Cenquizca and Swanson 2007). Since these connections allow transmission and storage of crucial information about the environment, it is important to understand how principal cells integrate their different input patterns with various spatiotemporal profiles and how this integration shapes the output of the neurons. Although there are also numerous types of interneurons located in the hippocampus (Freund and Buzsaki 1996; Klausberger 2009; Pelkey et al., 2017) which are also reciprocally interconnected, and modulate the activity of principal cells, I will not discuss them in details, because they were not the focus of my research providing the topic of this thesis.

DOI:10.14753/SE.2021.2546

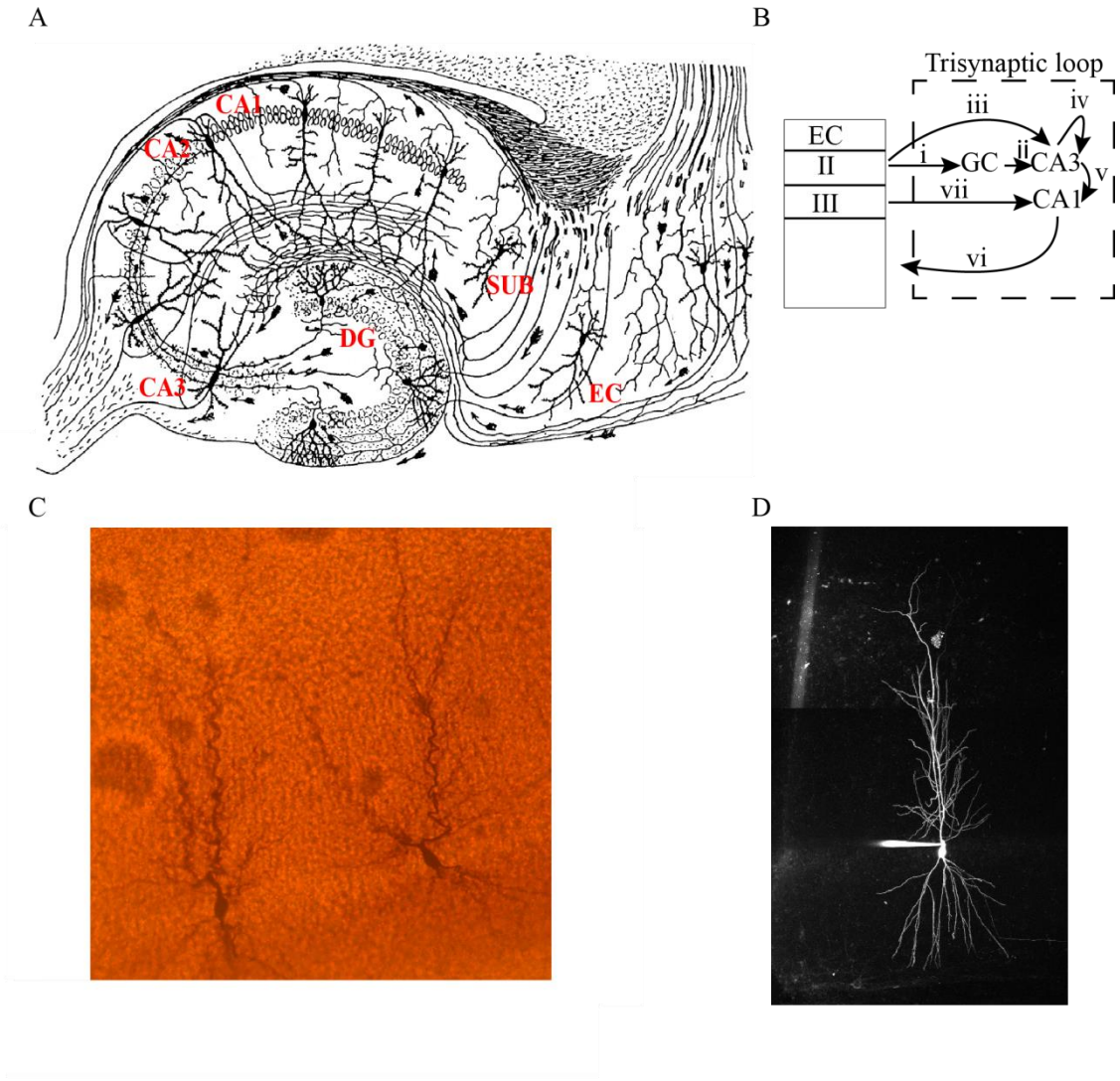

Figure 1 Anatomy of the hippocampus. ***(A)*** *Classical illustration of hippocampus by Ramon y Cajal.* ***(B)*** *The trisynaptic loop and the entorhinal cortical inputs. (i-vii) indicating the specific inputs, arrows showing their direction.* ***(C)*** *Two biocytin loaded CA1 pyramidal neurons in acute hippocampal slice using DAB reaction.* ***(D)*** *2-photon z-stack image of a CA1 pyramidal neuron, loaded with fluorescent dye Alexa fluorophore 488. CA: Cornu Ammonis; DG: dentate gyrus; SUB: Subiculum; EC Entorhinal cortex.*

DOI:10.14753/SE.2021.2546

2.2 Dendritic and synaptic organization of CA1 pyramidal cells

The CA1 region is located between the CA2 and subiculum regions. The laminar organisation consists of multiple layers, which is typical across the whole cornu ammonis region of hippocampus: stratum oriens (SO), stratum pyramidale (SP), stratum radiatum (SR) and stratum lacunosum-moleculare (SLM) (Amaral and Witter 1989; Andersen 2007). The layers above are separated based on the location of the cell bodies and dendrites, which have a characteristic anatomical arrangement (Andersen 2007). CA1 pyramidal cells have a basal and apical dendritic tree; the apical has typically one trunk and multiple bifurcating oblique dendrites, while the basal dendritic tree consists of multiple thin, bifurcating branches originating from the soma (Bannister and Larkman 1995; Dougherty et al., 2012; Malik et al., 2016). On a large scale, it has been for long established that different types of synaptic information arrive to different regions of the dendritic tree. Excitatory inputs from CA3 pyramidal cells are predominantly terminate on single or bifurcating families of basal and relatively proximal apical oblique dendrites, which have long (>40 μm), thin (diameter ~0.3-0.7 μm) and tapering terminal branches (Bienkowski et al., 2018). These inputs are the Schaffer collaterals, which are highly plastic (Jones and Mchugh 2011), and the most prominent intrahippocampal excitatory inputs of CA1 principal cells; typically ~300 000 CA3 pyramidal cells innervate ~400 000 CA1 pyramidal neurons in rodents (Amaral et al., 1990). Numerically smaller entorhinal cortical excitatory inputs from L3 neurons are located on the most distal apical dendrites in the SLM (Masurkar et al., 2017).

Altogether, the dendritic tree of a typical CA1 pyramidal cell receives synaptic information from ~20.000 presynaptic cells, and constantly integrates the activity of these inputs to determine the neuronal output (Andersen 2007), which depends on the spatiotemporal pattern of the actual activated inputs. While we have reasonable understanding of behaviourally relevant input activity on large scale (i.e. EC and Schaffer collateral inputs), little is known about the fine, micron scale spatiotemporal organization of physiologically relevant input patterns. In recent years more and more studies suggested the existence and importance of fine scale input activity; recent data suggest that in CA1 pyramidal cells developmentally related inputs arriving

from CA3 pyramidal neurons can form small clusters on short segments of individual basal or oblique dendrites (Druckmann et al., 2014) suggesting functional organization (Deguchi et al., 2011). Moreover, Ca^{2+} hotspots consistent with coactivation of multiple synapses can be observed in dendrites of hippocampal pyramidal cells *in vitro* (Takahashi et al., 2012), where Ca^{2+} signals were observed locally in dendritic spines within small dendritic segments, and during virtual spatial navigation *in vivo* (Sheffield and Dombeck 2015; Sheffield et al., 2017), where local dendritic spikes (d-spikes) often preceded place field formation. However, the impact of such finely clustered synaptic arrangement on the interaction, cooperation or plasticity is not well elucidated.

2.3 Function of CA1 pyramidal cells

CA1 pyramidal cells receive inputs from different areas, carrying spatial as well as nonspatial information (Deshmukh and Knierim 2013; Knierim et al., 2014), which lead to large functional heterogeneity during different behaviours. CA1 pyramidal cells show place field activity and they are neural substrates of a cognitive map (O'keefe and Nadel 1978). Recent data showed that activation of specific place cell populations in CA1 can bias the animal's behaviour during spatial navigation and supports spatial memory (Robinson et al., 2020). This is consistent with the idea, that on a population level, place cells also represent memory traces (Poucet et al., 2000). Aside from space coding, there is stable population activity during goal-oriented learning tasks (Danielson et al., 2016), and they also have a role in social memory (Okuyama et al., 2016), anxiety related and contextual fear behaviour as well as memory retrieval (Xu et al., 2016).

In addition, CA1 pyramidal cells also play a role in contextual representation and recall via the autoassociative CA3 system (processed through pattern separation and pattern completion mechanisms), where CA3PCs activate CA1 cell ensembles (Jones and Mchugh 2011). This processed information is recoded and conveyed by CA1 pyramidal cells back to neocortical areas (Rolls 2018). On a network level, aside from entorhinal cortex, Schaffer inputs can also provide intrahippocampal theta oscillation to the CA1 area (Buzsaki 2002; Colgin 2013). In addition, synchronous population burst of CA3

pyramidal cells can cause fast network oscillations called ripples (140-200 Hz) in CA1 region via Schaffer collaterals by activating the local pyramidal cells and inhibitory neurons. These oscillations are embedded in a large, irregularly occurring activity caused by the recurrent system of CA3, resulting the complex sharp wave ripple oscillation, which is observed during immobility, memory consolidation and affect decision-making (Buzsaki 2015).

Another indicator of the importance of CA1 region is its involvement in various neurodegenerative diseases, such as Alzheimer's disease (Giannakopoulos et al., 1997), epilepsy (Dam 1980) or ischemic episodes (Victor and Agamanolis 1990).

2.4 Dendritic properties of pyramidal cells

It has long been appreciated that dendrites profoundly influence processing of excitatory inputs due to their electrical properties that determined by several factors. In addition, in principal neurons most excitatory synapses are formed on dendritic spines. These small protrusions are connected to the dendrite via the thin spine neck, compartmentalize not only synaptically evoked Ca^{2+} transients but also voltage signals, due to the high neck resistance (~ 500 MΩ) (Harnett et al., 2012).

The dendritic integration mode of active inputs and the propagation of voltage signals are determined by the active and passive properties of dendrites. Understanding the passive properties of the dendrites is based on the application of cable theory by Wilfrid Rall in the 1960's. The passive properties are largely determined by a) the three main parameters of passive dendritic properties are the specific membrane resistivity (R_m), intracellular resistivity (R_i) and specific membrane capacitance (C_m) for a unit membrane area; and b) the morphology of the dendrites, such as branch diameter and length, as well as the presence of branch points, i.e. the complexity of the dendritic tree

While C_m is considered to be uniform across different neurons (~1 μF/cm^2) (Gentet et al., 2000; Larkum et al., 2009), R_m and R_i are more heterogeneous in different cells (Norenberg et al., 2010; Rall 1960; Roth and Hausser 2001; Szoboszlay et al., 2016).

DOI:10.14753/SE.2021.2546

It is important to mention that (in accordance with Ohm's law) larger resistance (or impedance in case of dynamic signals) causes larger voltage change by the same amount of current. Since dendritic branches get thinner with distance from soma, distal dendrites typically have larger impedance (Harnett et al., 2012). This, together with the boundary condition at sealed ends, result in much larger (and faster) local dendritic depolarization by the same synaptic input in distal thin terminal dendrites than in thicker proximal dendrites. On the other hand, voltage signals become attenuated and filtered as they travel along dendrites, due to the cable property of dendrites (Spruston et al., 1994). As a result of the above mentioned dendritic impedance gradient, the efficiency of propagation is asymmetric: propagation of EPSPs is more effective towards the tip of the dendrite (where the impedance is higher) compared to propagation towards the soma (where impedance is lower) (Branco et al., 2010; Branco and Hausser 2011). In addition, the passive membrane properties filter fast EPSPs stronger than slower voltage signals (Johnston and Brown 1983; Nevian et al., 2007; Spruston et al., 1994; Spruston et al., 1993; Williams and Stuart 2002).

Even though the larger local depolarization can partly compensate the attenuation of inputs arriving to distal branches, if dendrites of pyramidal cells had only passive properties, EPSPs from most distal apical dendrites would attenuate so strongly that they would fail to shape the neuron's output (Spruston et al., 1994; Tran-Van-Minh et al., 2015). However, dendrites also have active properties provided by various voltage-dependent mechanisms in the membrane, such as voltage gated ion channels (e.g. Na^+, Ca^{2+}, K^+ channels) and NMDA receptors (Bloodgood and Sabatini 2007a; Bloodgood and Sabatini 2007b; Johnston et al., 1999; Losonczy and Magee 2006; Makara and Magee 2013). While many channel types are known to be expressed in dendrites, their density, subunit composition and regulation is not well established (Benarroch 2013; Matsuzaki et al., 2001; Shah et al., 2010; Simms and Zamponi 2014). This is partly due to the fact that the expression pattern of active conductances along the dendrites may be variable not just across different cells or cell types, but also within a single cell, showing a gradient. For example, A-type K^+ current and the hyperpolarization activated cation current I_h increase along the apical dendritic axis, which affects the attenuation of active voltage

signals (Desjardins et al., 2003; Hoffman et al., 1997), and compensate the location dependence of temporal summation (Day et al., 2005; Johnston et al., 1999; Magee 1999), respectively. Although channel expression profiles are not known within single dendritic branches, potential heterogeneous channel expression patterns could lead to different integration properties even in different branches of the dendritic tree, e.g. the propagation strength of dendritic spikes (see below) (Losonczy et al., 2008). It is worth to mention that expression of neurotransmitter receptor channels may also be non-uniform in CA1 pyramidal cells, both along the apical trunk (Bittner et al., 2012; Magee and Cook 2000), as well as within individual branches of basal dendritic tree and apical oblique branches (Menon et al., 2013). These ion channel expression profiles can allow the neuron to keep the somatic EPSP amplitude of Schaffer collateral synapses independent of dendritic location.

2.4.1 Individual dendrites as distinct integration compartments

The highly branching structure of the dendritic tree raised the idea that dendritic branches may serve as individual integration compartments. For example, branchpoints limit the propagation of regenerative voltage signals, such as Na^+ spikes, into other branches (Larkum et al., 2009; Losonczy and Magee 2006; Losonczy et al., 2008; Polsky et al., 2004). In addition, even shorter dendritic segments, with a group of coactive synapses may also represent integration compartments by producing local spikes mediated by NMDARs (Polsky et al., 2004), which are key modulators of synaptic plasticity (Bliss and Collingridge 1993). This compartmentalization is supported by multiple in vivo studies using Ca^{2+} imaging techniques, which suggest correlated, spatially clustered synaptic activity on relatively short dendritic segments both in developing and adult hippocampus as well as other brain regions, as indicated by Ca^{2+} signals spatially restricted along the dendrites of principal neurons independently of somatic activity (Iacaruso et al., 2017; Kerlin et al., 2019; Sheffield et al., 2017). Some studies also suggest that neighbouring synapses, with less than 16 micrometres interspine distance are more likely to be coactive than random (Kleindienst et al., 2011; Takahashi

et al., 2012). Thus, it is highly important to explore the wide range of local interactions of inputs both within small dendritic compartments as well as on the branch level to understand their relevance and potential roles in the neuron's function.

2.4.2 Integration modes of dendrites

The integration of synaptic inputs in general can be either sublinear, linear or supralinear (Tran-Van-Minh et al., 2015) (**Fig. 2**), depending on the relationship of the actual compound voltage response and the arithmetic sum of the individual responses.

Sublinear integration (i.e. the measured depolarization is smaller than the arithmetic sum of individual EPSPs) can occur either passively, when synapses at close proximity are activated synchronously and the driving force is reduced resulting in smaller current flow **(Abrahamsson et al., 2012; Cash and Yuste 1999; Norenberg et al., 2010; Tran-Van-Minh et al., 2015; Vervaeke et al., 2012)**, or actively, when strong outward currents are activated reducing depolarization. In CA1PCs, passive sublinear summation is often compensated by voltage-dependent ion channels and NMDARs (Cash and Yuste 1999)

During linear integration (**Fig. 2A, B**), the amplitudes of summed EPSPs are roughly equal to their arithmetic sum. This may be a result of two complementary mechanisms; a passive one, where the coactive inputs are spatially distributed and therefore the local depolarization of the coactive inputs cannot affect each other's driving force significantly. Thus, the linear summation of EPSPs is caused by simple addition (Cash and Yuste 1998) and cannot be disrupted by blocking Na_V channels or NMDA receptors. However, in pyramidal neurons, linear integration also can be an active mechanism, where a limited numbers of spatially clustered inputs are summated linearly due to the contribution of active channels that can counterbalance passive sublinearity (Cash and Yuste 1998; Cash and Yuste 1999). In addition, on a larger scale, EPSPs from different branches located at basal or proximal apical dendrites are also integrated linearly (Cash and Yuste 1999) with the support of NMDA, Na^+ and Ca^{2+} channels

DOI:10.14753/SE.2021.2546

When a large number of inputs is co-activated that reach the threshold of the generation of regenerative dendritic spikes, dendritic integration can become strongly supralinear (**Fig. 2A, B**). Three basic types of dendritic spikes have been described so far depending on the channels that are responsible for their generation: Na^+ (**Fig 2C**), Ca^{2+} (not shown), and NMDA (**Fig. 2C**) spikes, generated by voltage-gated Na^+ channels (VGNCs), voltage-gated Ca^{2+} channels (VGCCs), and NMDARs, respectively. In cortical pyramidal neurons, Ca^{2+} spikes are global events, which are thought to be generated in apical trunk dendrites (Larkum and Zhu 2002) by robust conjunctive input to a large dendritic area, including tuft and perisomatic activity. In contrast, local inputs in individual dendrites typically generate Na^+ and NMDA spikes but not Ca^{2+} spikes; below I will discuss these two types of regenerative dendritic voltage events in details.

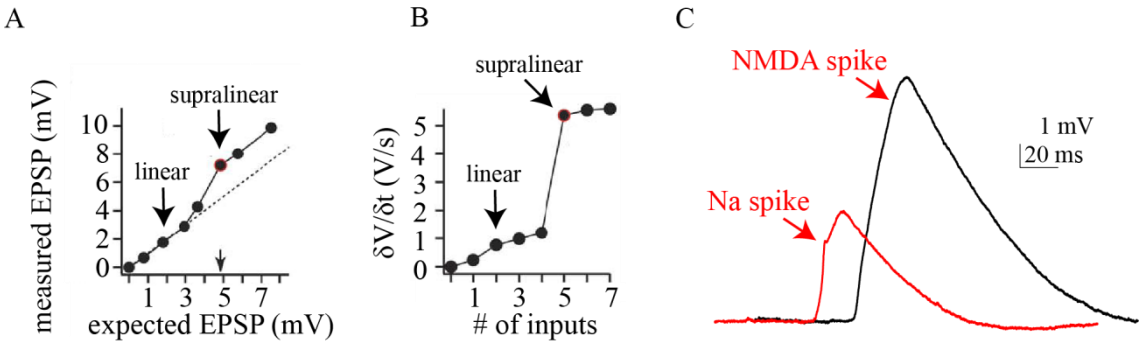

Figure 2 Examples for linear and supralinear dendritic integrations ***(A)*** *Input-output graph showing the expected vs measured EPSPs in a rat CA1 PC dendrite. Arrows indicate the linear (measured EPSP is equal to expected EPSP) and supralinear (measured EPSP is larger than expected) part produced by dendritic Na^+ spike.* ***(B)*** *Speed of voltage increase due to the costimulation of 1-7 inputs. Note the sudden increase in the speed when the integration is supralinear due to the coactivation of the required number of inputs (threshold indicated by red dot).* ***(C)*** *Representative NMDA and Na^+ spikes. NMDA mediated spike amplitude is larger, and more prolonged in time than Na^+ spikes, while Na^+ spikes are faster and the voltage step is steeper. Panels* ***(A)*** *and* ***(B)*** *are adopted and modified from Losonczy and Magee 2006.*

2.4.3 Dendritic Na^+ spikes

When sufficiently large amount of inputs are active highly synchronously (within a few ms time window), the magnitude of postsynaptic depolarization reaches a voltage threshold where VGNCs are activated, generating an additional depolarization leading to a local action potential-like steeply regenerative voltage event, called dendritic Na^+ spike (Golding and Spruston 1998; Losonczy and Magee 2006) (**Fig 2C**). The main characteristic parameter of a Na^+ spike as determined at the soma is its "strength", which can be measured as the magnitude of the spikes-associated component on the first temporal derivative of the voltage response (dV/dt, given in V/s) (**Fig 2B**). The somatic strength of the Na^+ spike depends primarily on its propagation from the site of initiation (Losonczy et al., 2008). Although it propagates more effectively towards the soma compared to subthreshold EPSPs, the Na^+ spike also attenuates strongly, a feature that depends on the activity of A-type K^+ channels (mediated mainly by $K_v4.2$ channels) in the dendritic branch (Losonczy et al., 2008). These channels are activated by local depolarization and limit the propagation of both dendritic spikes and back-propagating action potentials (Hoffman et al., 1997; Losonczy et al., 2008) (Johnston et al., 2000). In addition to the voltage amplification, the large local depolarization can contribute to the generation of NMDA spikes (Kim et al., 2015).

2.4.4 Dendritic NMDA-spikes

Another important dendritic spike type is the NMDA spike, which is mediated by postsynaptic NMDA receptors (**Fig. 2C**). In the hippocampus, pyramidal cells can elicit such spikes (Losonczy and Magee 2006; Makara and Magee 2013). Since the ionotropic NMDAR activation requires the release of voltage dependent Mg^{2+} block **(Crunelli and Mayer 1984; Mayer et al., 1984; Nowak et al., 1984)** as well as the binding of the neurotransmitter glutamate, the receptor acts as a coincidence detector of glutamate release and postsynaptic depolarization (Major et al., 2008; Rhodes 2006; Schiller et al., 2000). As a consequence of this two-component activation, NMDA spikes do not propagate actively from the input site, since they require glutamate binding (Stuart and

Spruston 2015). The characteristics of NMDA spikes as measured at the soma are different from those of Na^+ spikes: they are usually larger in amplitude, and have much slower kinetics, lasting for tens to hundreds of milliseconds **(Major et al., 2008; Polsky et al., 2004; Rhodes 2006; Schiller et al., 2000)**. Although they can effectively drive the neuron to produce somatic action potentials (APs), the local roles of NMDARs are also highly important (Milojkovic et al., 2007). Since the NMDAR is permeable to Ca^{2+}, its activation causes not only Na^+ influx, but provides substantial Ca^{2+} influx too (Major et al., 2008; Milojkovic et al., 2007; Takahashi and Magee 2009). As a second messenger, changes in the intracellular Ca^{2+} concentration can lead to the activation of different signaling pathways, which in turn can induce various effects (e.g. new protein synthesis) on the cellular level. Thus, the NMDAR has been for long considered to be a major mediator of memory formation on the synaptic level, in particular by inducing long-term potentiation (LTP) (Gordon et al., 2006; Holthoff et al., 2006; Nimchinsky et al., 2002).

2.4.5 Backpropagating action potentials

Somatic APs propagate not only forward along the axon, but also backward to the dendritic tree of pyramidal neurons, typically with intermediate attenuation (decrease to ~50% at 200 µm). The spread of backpropagating action potentials (bAPs) is mostly modulated by dendritic Na_v channels, A-type K^+ channels (Frick et al., 2003; Hoffman et al., 1997; Johnston et al., 2003; Magee et al., 1998), activity of synaptic inputs (Williams and Stuart 2003) and the morphological properties of the dendritic tree such as the length of apical trunk (Galloni et al., 2020), diameter of the dendrites (Goldstein and Rall 1974; Vetter et al., 2001) and branching. Although bAPs usually cannot propagate to the very distal dendrites, at more proximal dendrites they can modify the impact of local synaptic transmission either on short or long timescales. For example, it can increase local dendritic Ca^{2+} levels (via activation of voltage gated Ca^{2+} channels), or the local depolarization of the membrane caused by bAPs leads to the release of Mg^{2+} block of NMDA receptors (Kampa et al., 2004; Larkum et al., 1999a; Larkum et al., 1999b). In a widely accepted model of Hebbian synaptic plasticity, postsynaptic bAPs are considered

DOI:10.14753/SE.2021.2546

to be crucial for both synaptic strengthening and weakening depending on their timing relative to the presynaptic activity (Celikel et al., 2004; Magee and Johnston 1997; Markram et al., 1997). This type of plasticity, i.e. spike timing dependent plasticity (STDP) (Song et al., 2000) will be discussed in details in section 2.5.1.

2.5 Postsynaptic long-term plasticity

The contribution of a synapse to the output of a neuron depends on its strength (the amplitude of the EPSP at the soma), which is mostly determined by the number and conductance of postsynaptic AMPARs (Matsuzaki et al., 2001) and its location in the dendritic tree. The strength of an input is not constant, but depends on its activity history (Lee et al., 2000). During long-term potentiation, synaptic strength increases either by the increased number of AMPARs in the postsynaptic density, and/or the increase of the conductance of the pre-existing AMPARs (Kerchner and Nicoll 2008; Kessels and Malinow 2009; Makino and Malinow 2009; Nicoll 1988). It is a generally accepted view, that synaptic plasticity is a major mechanism in learning and memory (Dudai and Morris 2013; Holtmaat and Caroni 2016; Kandel et al., 2014). Although in the thesis I will only focus on the 'classical' long-term potentiation mechanism characteristic at Schaffer collateral synapses, it is important to mention that both synaptic depression and potentiation can be long- (hours, days) or short-lasting (few seconds) and can be mediated by several other mechanisms apart from NMDA receptors (e.g. metabotropic glutamate receptors or the endocannabinoid system, see review by Sjöström et al., 2008).

2.5.1 The activity-dependent requirements of long-term plasticity

The classical view of potentiation of synapses was coming from Hebb's postulate (Hebb 1949); when cell A repeatedly or persistently takes part in firing of cell B, their synaptic connection will be strengthened. The first experimental demonstration of long term potentiation was performed by Bliss and Lomo in the hippocampus of an anesthetized rabbit, published in 1973 (Bliss and Lomo 1973). Decades later, a refined

idea was developed that potentiation of an input requires the co-occurrence of presynaptic activity and subsequent backpropagating action potential within a short (few tens of milliseconds) time window (Abbott and Nelson 2000; Magee and Johnston 1997; Markram et al., 1997). As the precise timing of pre- and postsynaptic activity is a crucial determinant of the generation of LTP, this type of plasticity was termed as "spike timing dependent plasticity" (STDP).

However, the requirement of bAPs does not allow plasticity in synapses located at distal dendritic branches, since they cannot propagate effectively to those locations. So, the question arises: can other mechanisms replace the role of bAPs? One possibility is the role of local regenerative dendritic voltage events that can spread effectively even to distal dendritic locations. It turned out that this hypothesis is correct, as it has been shown both *in vitro* (Golding et al., 2002) and *in vivo* **(Gambino et al., 2014)** that dendritic spikes are able to generate potentiation even at distally located synapses. Golding and colleagues were able to induce plasticity by strong synaptic activation without bAPs in CA1 pyramidal cells, while the Holtmaat group using whole cell recordings in somatosensory cortex, observed LTP during whisker stimulation without APs but in the presence of NMDA receptor dependent plateau potentials. While this finding proved that local dendritic activity is *sufficient* to induce synaptic plasticity, it still remained unknown whether regenerative dendritic voltage events are also *necessary* for synaptic potentiation.

Another important aspect of LTP generation is the location within the dendritic tree; in L5 pyramidal neurons, STDP for example shows the typical time window requirements at inputs located at proximal dendritic locations (Froemke et al., 2010). On the other hand, at more distal locations the requirements were different as pre-before-post pairing during STDP induction led to LTD instead of LTP (Letzkus et al., 2006; Sjostrom and Hausser 2006). This finding highlights the important thought that generally accepted concepts may not true globally along the whole dendritic tree.

Aside from functional synaptic clusters, recent studies suggest the existence of plasticity clusters of synapses as well. A very elegant study from Makino and Malinow showed evidence of LTP of spatially clustered inputs by tagging GluR1 subunits of

AMPARs in the layer 2/3 pyramidal cells of mouse barrel cortex. When they stimulated the whisker of the mice, they observed an accumulation of tagged GluR1 subunits in spatially clustered dendritic spines (Makino and Malinow 2011). Similar results were published by Zhang and colleagues (Zhang et al., 2015). The connection between clustered spine turnover and learning and memory was also shown in other brain regions, such as in the retrosplenial cortex (Frank et al., 2018). Thus, these findings suggest that even the plasticity "compartment" can be substantially smaller than a dendritic branch.

2.5.2 Homo- and heterosynaptic plasticity

Synaptic plasticity can be categorized as homosynaptic or heterosynaptic plasticity, based on what synapses are potentiated or depressed due to a synaptic activity pattern (Bliss and Collingridge 1993; Citri and Malenka 2008). Both operate on the same timescale but may have different computational roles and consequences in learning systems (Chistiakova et al., 2014). During homosynaptic plasticity, active synapses can undergo LTP or LTD and the inactive synapses are not affected. It can theoretically be input specific and therefore fit well in Hebb's classic postulate (Nicoll et al., 1988).

During heterosynaptic plasticity the strength of non- or asynchronously active synapses also change. In contrast to homosynaptic plasticity, heterosynaptic plasticity is a non-Hebbian form of plasticity. It has been first described in the hippocampus in a study, where LTP was induced on a subset of synapses, while they also observed a permanent depression in another subset of inactive synapses on the same pyramidal cell (Lynch et al., 1977) suggesting that homosynaptic LTP is accompanied by heterosynaptic LTD. These findings point out that heterosynaptic plasticity can be a practical mechanism to counterbalance the effect of homosynaptic plasticity, keeping net synaptic weight on a set level (Muller et al., 1995). Later on, more forms of heterosynaptic plasticity have been described; another manifestation of heterosynaptic interactions is metaplasticity, where the plasticity rules of a synapse are modified by the activity of other synapses (Sjostrom et al., 2008), in other words "plasticity of synaptic plasticity" (Abraham and Bear 1996). A prominent form of metaplasticity is synaptic "tagging" described by Richard Morris

and colleagues (Frey and Morris 1997). During synaptic tagging, there is an interaction between a strongly activated potentiated synapse with an adjacent weakly activated one; the weakly activated synapse can receive newly synthesized, plasticity-related proteins from the strongly activated potentiated synapse via diffusion, which can facilitate the generation of LTP even by weak stimulation that would otherwise be ineffective to induce potentiation (Frey and Morris 1997; Rogerson et al., 2014). Another interesting form of heterosynaptic plasticity was demonstrated in a very nice study, where strong stimulation of a single spine potentiated the activated synapse, but simultaneously decreased the threshold for potentiation of an adjacent spine (Harvey and Svoboda 2007). Although this mechanism seems similar to synaptic tagging, there are several differences between the two phenomena; in contrast to synaptic tagging, this mechanism is only available on a second-minute time scale and it does not depend on protein synthesis. The findings above suggest that heterosynaptic plasticity can be more than just a compensatory mechanism, and input specificity is not always fulfilled within shorter dendritic segments.

2.5.3 The molecular mechanism of long-term potentiation in principal cells

The process of long-term potentiation consists of two phases: an early and a late phase. The most important difference between them is that while the early phase does not require protein synthesis, the late phase of LTP does, and it also lasts longer (up to few hours and at least 24 hours, respectively) (Kandel 2001).

In CA1 pyramidal cells, the generation of LTP is typically NMDAR dependent (Collingridge 1992; Volianskis et al., 2015), and takes place postsynaptically. A crucial determinant of the process is the strong rise of local intracellular Ca^{2+} concentration (Lee et al., 2012) The role of NMDARs in hippocampal plasticity was suggested also *in vivo*, as the knock-out of the NMDAR subunit NR1 led to learning deficits in rodents (Rondi-Reig et al., 2006). As a next step in the process of plasticity, local elevated Ca^{2+} level initiates second-messenger systems involved in the molecular effects leading to the long-lasting change in synaptic strength. Various kinases have been shown to be crucial (Soderling and Derkach 2000); an essential kinase during both early

and late phase of LTP (E- and L-LTP, respectively) is CaMKII (Lee et al., 2009; Mower et al., 2011; Shen and Meyer 1999; Takao et al., 2005). At E-LTP, CaMKII phosphorylates the GluA1 subunit of AMPARs, which results in an increase in the receptor conductance (Derkach et al., 1999). In addition, via the Ras/ERK pathway CaMKII also regulates the lateral diffusion of AMPARs (termed as AMPAR trafficking) from outside of the synapse into the postsynaptic density (Hayashi et al., 2000; Zhu et al., 2002), leading to increased synaptic strength (Makino and Malinow 2009). The process is often accompanied by the enlargement of the spine head volume, a typical sign of structural plasticity via the activation of small GTPase proteins (Bosch et al., 2014; Penzes et al., 2008).

The late-phase LTP (L-LTP) is dependent on de novo protein and mRNA synthesis, modulated by various proteins, enzymes, seconder messengers and transcription factors. In the hippocampus, the first step of L-LTP is the activation of PKA by the seconder messenger cAMP, which can act via two pathways. PKA can phosphorylate CREB at the nucleus, which initiates gene transcription (Laviv et al., 2020; Nguyen and Woo 2003). The other pathway, PKA induces the phosphorylation of MEK (Pittenger and Kandel 2003; Vossler et al., 1997), which activates MAPK (English and Sweatt 1997). The activation of MAPK also leads to plasticity related immediate early gene (IEG) transcription by activating CREB and Elk-1 (Bozon et al., 2003; Laviv et al., 2020).

During L-LTP another important regulator of plasticity and the related protein synthesis is BDNF (brain-derived neurotrophic factor) by regulating protein translation (Lu et al., 2014). For example, it causes enhanced local protein synthesis by indirectly activating the ERK pathway (Baudry et al., 2015; Briz et al., 2013) which will be important in our study.

Surprisingly, some of these proteins such as small GTPases are able to diffuse to adjacent weakly or asynchronously active synapses, promoting potentiation in these spines. A classic study about the subject (mentioned above in Section 2.5.2.) was performed by Harvey and Svoboda in 2007, where they were able to reduce the threshold

DOI:10.14753/SE.2021.2546

for potentiation of a synapse, after they induced LTP in an adjacent spine within 10 μm (Harvey and Svoboda 2007). Later, other studies showed diffusion of LTP-related small proteins such as RhoA, Ras, Rac1 from potentiated active spines to adjacent inactive spines within similar distance (Harvey et al., 2008; Hedrick et al., 2016).

2.6 Unexplored aspects of integration and plasticity of synaptic input patterns

Although, as I have shown in the introduction so far, there is a large literature of dendritic integration and plasticity, there are several aspects that are not clear yet. Among the three dendritic integration modes, the role of suprathreshold integration in synaptic plasticity is extensively studied; however, very little is known about the roles of small input patterns -which are integrated in the linear integration regime- in synaptic plasticity and their possible local interactions. One reason that may explain why subthreshold activity patterns are out of focus of research, is that most of the electrophysiological studies use whole cell current clamp recordings, and the measured linearly summated EPSPs of a few co-active inputs are strongly attenuated recorded from the soma and seemingly do not affect the output of the cell. Thus, it is an important, and yet unanswered question, whether linear summation of various spatiotemporal input patterns can also have any local impacts, which may be relevant for the neuron's activity but their presence is masked by global activities.

In order to investigate the interactions and plasticity rules of small numbers of coactive inputs, a proper technique is required, which is able to precisely control the spatiotemporal activation of the given inputs. So far, most LTP studies used bulk electrical stimulation of axons in order to evoke synaptic activity and induce plasticity, which does not allow precise spatiotemporal control of the activated input patterns or specific pharmacological manipulation of postsynaptic (but not presynaptic) mechanisms. More specifically, the drawback of electrical stimulation of the presynaptic axons is that we do not know how many inputs and in what distribution are stimulated. However, with a specific technical approach, it is possible to circumvent these constrains; using 2P

DOI:10.14753/SE.2021.2546

glutamate uncaging combined with whole cell current clamp recordings, it is possible to control precisely the spatiotemporal profile of stimulation of multiple synapses.

DOI:10.14753/SE.2021.2546

3. OBJECTIVES

Within a broader investigation of the subthreshold interactions of spatially colocalized Schaffer collateral synapses in dendrites of CA1 pyramidal neurons, the main aim of my PhD work was to elucidate what are the local synaptic plasticity rules at different dendritic locations, and how these rules are affected by different input patterns.

I aimed to address the following specific questions using in vitro 2P imaging, 2P glutamate uncaging and Ca^{2+} imaging combined with whole cell current clamp recordings from adult male Wistar rats:

1. How sensitive is the function of a synapse to the coactivation of other closely located synapses? How does this property depend on the position of the synapse in the dendritic tree?

2. Do local interactions between spatially clustered coactive synapses lead to synaptic plasticity? How does this phenomenon depend on the number and spatial pattern of the inputs?

3. How are local synaptic plasticity rules affected by the dendritic integration mode of input patterns, in particular by the generation of dendritic spikes?

CONTRIBUTIONS

The majority of the LTP experiments presented in the thesis were performed and analyzed by myself; my postdoctoral colleague Jens Weber has performed the initial series of LTP experiments describing subthreshold LTP by 4 inputs (Figures 10-1). Ca^{2+} imaging experiments were performed by Judit Makara. Computational simulations were performed by Balázs Ujfalussy.

.

DOI:10.14753/SE.2021.2546

4. MATERIALS AND METHODS

4.1 Hippocampal slice preparation and patch-clamp recordings

Adult male Wistar rats (7-11 week old) were used to prepare 400 μm thick transverse slices from the hippocampus. The slice preparation was performed according to methods approved by the Animal Care and Use Committee of the Institute of Experimental Medicine, and in accordance with the Institutional Ethical Codex, Hungarian Act of Animal Care and Experimentation (1998, XXVIII, section 243/1998), and European Union guidelines (86/609/EEC/2 and 2010/63/EU Directives).

Animals were deeply anaesthetized with 5% isoflurane (~5 minutes) and quickly perfused through the heart with ice-cold cutting solution containing (in mM): sucrose 220, $NaHCO_3$ 28, KCl 2.5, NaH_2PO_4 1.25, $CaCl_2$ 0.5, $MgCl_2$ 7, glucose 7, Na-pyruvate 3, and ascorbic acid 1, saturated with 95 % O_2 and 5 % CO_2. After the perfusion, the brain was quickly removed, and "magic cut" (Bischofberger et al., 2006) was applied for both hemispheres in order to best preserve the dendritic arbour of dorsal CA1 pyramidal cells. 400 μm thick slices were prepared in cutting solution using a vibratome (Vibratome, St. Louis, MO, or Leica VT1000A, Leica Biosystems GmbH, Nussloch, Germany). Slices were incubated in a submerged storing chamber containing ACSF at 35 °C for 30 min, and then stored in the same chamber at room temperature. For recordings, slices were transferred to a custom-made submerged recording chamber under the microscope where experiments were performed at 32–35 °C in ACSF containing (in mM): NaCl 125, KCl 3, $NaHCO_3$ 25, NaH_2PO_4 1.25, $CaCl_2$ 1.3, $MgCl_2$ 1, glucose 25, Na-pyruvate 3, and ascorbic acid 1, saturated with 95 % O_2 and 5 % CO_2.

Cells were visualized using an Olympus BX-61 or a Zeiss Axio Examiner epifluorescent microscope equipped with differential interference contrast optics under infrared illumination and a water immersion lens (60X, Olympus or 63X, Zeiss). Current-clamp whole-cell recordings from the somata of hippocampal CA1PCs were performed using a BVC-700 (Dagan, Minneapolis, MN, USA) or an EPC800 (HEKA) amplifier in the active „bridge" mode, filtered at 3–5 kHz and digitized at 50 kHz. Patch pipettes (2–6 MΩ) and puffer pipettes were pulled with a P-97 Flaming/Brown Micropipette Puller

(Sutter Instruments, Ignacio, CA, USA). Patch pipettes were filled with a solution containing (in mM): K-gluconate 134, KCl 6, HEPES 10, NaCl 4, Mg_2ATP 4, $Tris_2GTP$ 0.3, phosphocreatine 14 (pH=7.25) complemented with Alexa Fluor 488 (100 μM) in order to visualize neurons. In some experiments where Ca^{2+} imaging was performed, intracellular solution contained the Ca^{2+} dye Oregon Green BAPTA 1 (OGB-1, 100 μM) and Alexa Fluor 594 (50 μM). In these experiments different Alexa dye was used because OGB-1 and Alexa Fluor 488 have similar two-photon excitation wavelength (imaged at 920 nm). Only those experiments were used for data analysis where series resistance was <30MΩ. Voltages were not corrected for liquid junction potential. Only CA1PCs with a resting membrane potential (V_{rest}) more negative than -55 mV were used. Cells were kept at -63– -65 mV.

4.2 Two-photon imaging and uncaging

A dual-galvanometer-based two-photon scanning system (Prairie Technologies, Middleton, WI, USA) was used to image the neurons and to uncage glutamate at individual dendritic spines. Two ultrafast pulsed laser beams (Chameleon Ultra II; Coherent, Auburn, CA, USA) were used, one for imaging of fluorophores at 920 or 860 nm wavelengths. The other laser was used at 720 nm to photolyse MNI-caged L-glutamate (Tocris; 10 mM, applied through a puffer pipette with an approximately 20-30 μm diameter, downward-tilted aperture above the slice, using a pneumatic ejection system (PDES-02TX (NPI, Tamm, Germany). MNI-caged glutamate uncaging is a suitable technique for stimulating individual synapses with high temporal and spatial resolution, allowing mimicking desired input patterns. Briefly, the caged glutamate becomes active only when the laser photolyses (on a microsecond timescale) the covalent bond between MNI and glutamate, so that glutamate can act locally substituting the neurotransmitter. Laser beam intensity was independently controlled with electro-optical modulators (Model 350-80, Conoptics, Danbury, CT, USA). Emitted light was collected by multi-alkali or GaAsP photomultipliers (Hamamatsu Photonics K.K, Iwata City, Japan).

All neurons included in the study had mostly complete apical and basal dendritic arbours, with no major dendrites cut. The selected basal (stratum oriens; 65% of all experiments) and apical oblique (proximal stratum radiatum; 35% of all experiments) dendrites were carefully examined and only intact branches with >70 μm length were used. We adjusted the laser power during glutamate uncaging to evoke physiological-like excitatory postsynaptic potentials (EPSPs) (~ 0.2-0.8 mV) similar to the somatically measured mEPSPs (see also Fig. 5), based on local puffing of high osmolarity artificial cerebrospinal fluid (containing 300 mM sucrose, 0.5 μM TTX and 10 μM gabazine; (Magee and Cook 2000) to induce presynaptic vesicle release locally, (**Figure 3A-C**; data by Bertalan Andrásfalvy). During the course of the project, we did not detect significant differences between results obtained in basal and apical oblique dendrites, thus the experiments from apical and basal branches were pooled. Individual spines with an average phenotype and separated from their neighbours were selected for stimulation. Stimulation was performed by uncaging glutamate ≤0.5 μm lateral to the head of visually identified spines, using 0.5 or 0.2 ms uncaging duration. The uncaging points were placed more than ~1.1 μm apart to allow individual stimulation of selected spines on the same side of the dendrite. I note that spines at the same dendritic location but on opposing sides of the dendrite could be stimulated separately. Time interval between the stimulated spines (termed interspine stimulus interval, ISI) within a recorded trace was 200 ms for recording individual voltage responses of spines, or 0.1 ms for their quasi-synchronous activation during the LTP protocol. Unitary EPSPs and Ca^{2+} signals were measured repeatedly (usually 6-12 times, repeated every 5 minutes for EPSPs, and 2-5 times for Ca^{2+} signals).

DOI:10.14753/SE.2021.2546

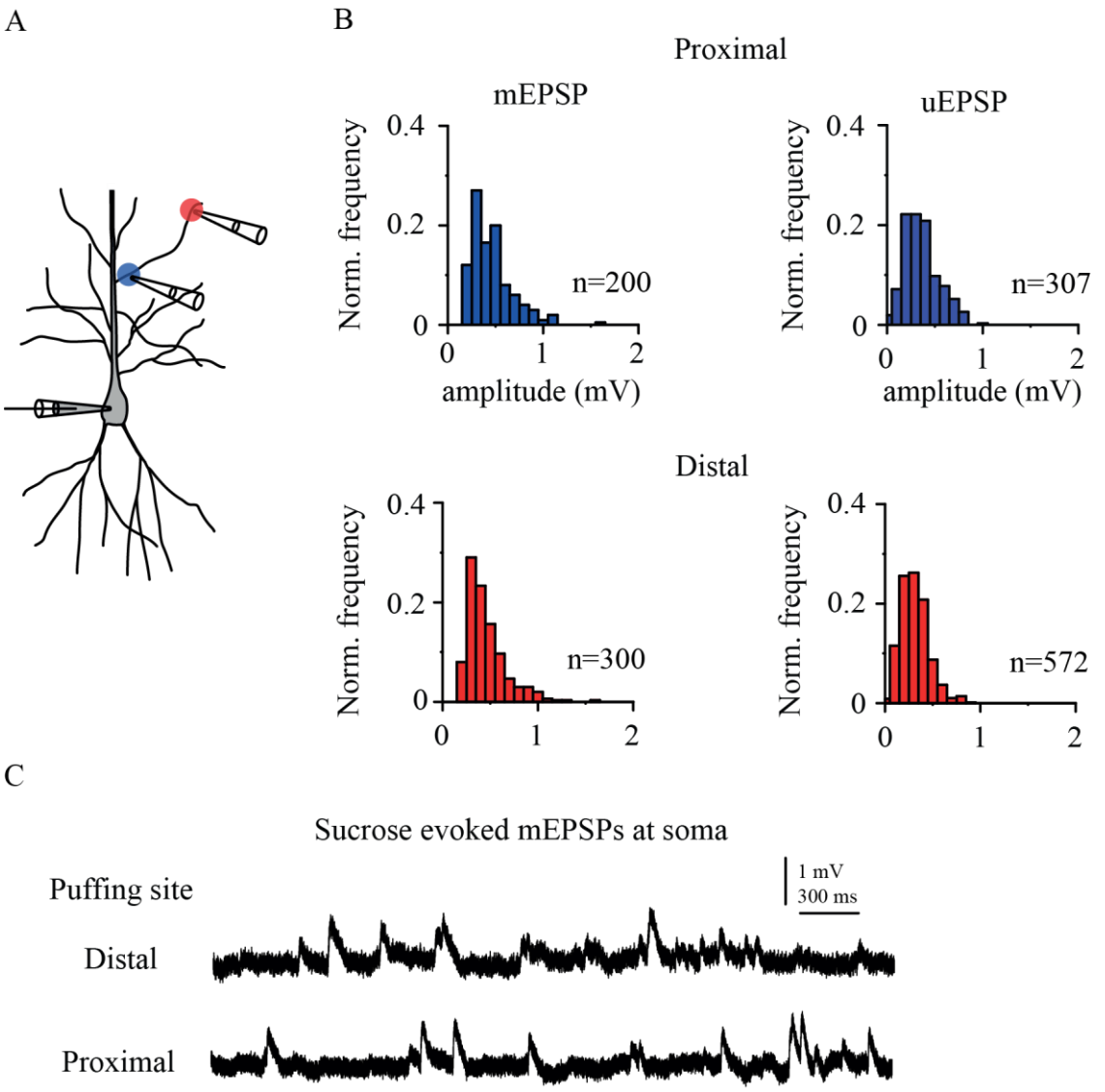

Figure 3 Properties of somatic miniature EPSPs at different dendritic locations. *(**A**) Illustration of different puffing locations with the high osmolarity ACSF. (**B**) Left: Distribution of miniature EPSPs (mEPSP) at different proximal and distal dendritic locations, indicated by blue and red, respectively. Right: normalized distribution of uncaging evoked EPSPs (uEPSP) stimulated at proximal and distal locations, indicated by blue and red, respectively. (**C**) Representative traces of mEPSPs at different puffing locations, measured at the soma.*

4.3 Ca^{2+} measurements

In experiments measuring spine Ca^{2+} signal nonlinearity, the bath solution contained 0.5-1 μM TTX to eliminate nonlinearities arising from dendritic Na^{+} spike generation, except where indicated. Freehand linescan imaging through spines was performed at 200-500 Hz with 8-12 μs dwell time. At the beginning of the experiment, the set of two to four spines were first stimulated individually (200-305-ms intervals) and the laser power was adjusted to yield physiological unitary EPSPs and reliable associated spine Ca^{2+} signals. Next, stimulation of various numbers of the selected spines was performed with the same laser power synchronously (0.1ms ISI for galvo movement, plus 0.2 ms uncaging duration per spines). In some experiments, longer ISIs (5-10 ms) or uncaging duration (0.5 ms, with 0.1 ms ISI) were used. In experiments examining the effect of larger proximal input clusters (up to 12 spines), Ca^{2+} signals were measured only in the first four spines. Following synchronous stimulation, spines were stimulated individually again to confirm the stability of single spine responses. Recordings were repeated three to five times for each condition. Ca^{2+} signals were expressed as $\Delta F/F=(F-F_{rest})/F_{rest}$ x 100. During pharmacological experiments, drugs were applied in the bath for > 10 min. When testing the effects of AP5, Ca^{2+} channel blockers on spine Ca^{2+} signaling, the drugs were included in the puffed MNI glutamate solution as well to ensure maximal efficiency, and separate cells were measured under control conditions (no drug in puffer pipette) and in the presence of the drugs (with drug-containing puffer pipette) from different slices of the same animals. Ca^{2+} signals and nonlinearity in control experiments with or without including 0.01% dimethylsulphoxide (DMSO; solvent of nimodipine) did not differ; therefore data of these two control groups were pooled. To ensure comparable stimulation conditions, only experiments with 1-2.1 mV expected EPSP were included in the analysis of these experiments.

4.4 LTP experiments

To measure changes in synaptic function induced by LTP protocols (**Fig. 4**), we recorded EPSPs evoked by 2PGU in whole-cell current-clamp mode. This allowed us to ensure that the applied uncaging stimuli produced EPSPs are in the physiological amplitude range regardless of the depth of the spines, requiring fine adjustments in uncaging laser power in each experiment. Furthermore, in our experience, electrophysiological recordings provide the best way to detect even subtle signs of photodamage to confidently distinguish plasticity related effects from phototoxicity. Accordingly, experiments showing electrophysiological signs of photodamage (sudden large irregular depolarization with uneven and slow repolarization during LTP protocol with consecutive loss of reliable single spine responses, often accompanied by morphological changes including spine swelling and contour changes or dendritic swelling) were terminated and excluded from the analysis. We chose not to measure fluorescence based spine volume for monitoring structural LTP (Matsuzaki et al., 2004) because Alexa Fluor 488 fluorescence continuously increased in the repatched cells due to dialysis from the patch pipette.

To prevent washout of intracellular components by whole-cell dialysis (Matsuzaki et al., 2004), we developed a method where LTP protocol could be started within <10 minutes after establishing the whole-cell configuration. Neurons (usually three to four per slice) were first patched with a pipette solution containing Alexa Fluor 488 (100 μM), the cell was dialysed for 30–60 s (usually facilitated by gently blowing into the pipette), and then the pipette was carefully withdrawn. After 30–100 min, the dye diffused sufficiently to visualize most of the dendritic arborisation. A proximal (relative distance along branch: <0.4; total distance from soma: 82 ± 9 μm, n=20) or distal (relative location along branch: >0.6; total distance from soma: 181 ± 4 μm, n=160) fluorescent dendritic segment with well visible individual spines was selected and a z-stack was obtained (0.5 μm z-steps). Then, the soma of the same cell was patched again, guided by fluorescent identification using either 2PI or a camera (Andor Zyla 4.2). Success rate for repatching exceeded 90%, and repatched neurons had normal V_{rest} (more negative than -55 mV). After establishing whole-cell configuration again and measurement of V_{rest}, uncaging started immediately.

DOI:10.14753/SE.2021.2546

A set of four individual spines were first stimulated separately (200 ms between spines; trials repeated typically with 0.02-0.5 Hz) and the uncaging laser power was adjusted to yield physiological-sized EPSPs at each stimulated spine (**Fig. 3B, C** and **Fig. 5A**). Spines that did not respond reliably to uncaging were replaced by new ones until four test spines with relatively uniform EPSP amplitudes were found (note that as a result of this selection procedure, the final four spines may have received variable numbers of pre-LTP test stimuli). After the test recording, an LTP induction protocol (50 stimulations at 3 Hz at a group of spines, unless otherwise indicated) (**Fig. 4**) was applied as soon as possible (within 2 minutes from the last test stimulus and within 10 minutes after break-in), in various configurations (as indicated in the text and figures).

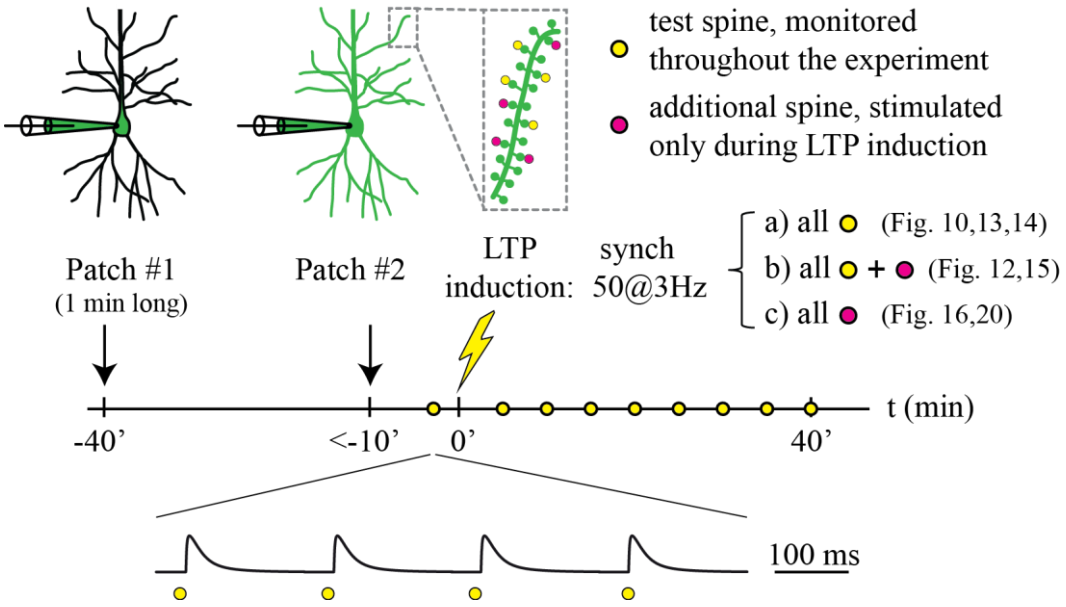

Figure 4 LTP induction protocol. *Experimental procedure of LTP induction. Different subset of dendritic spines stimulated on the pre-loaded CA1 pyramidal cells (yellow and magenta dots). After LTP induction, the yellow test spines were stimulated individually every five minutes (bottom, timeline). Note that corresponding figures of the different LTP inducing arrangements (which subsets of spines were stimulated) are indicated.*

In all homosynaptic LTP experiments the same laser power was used for the LTP induction protocol as that for monitoring the test spines throughout the experiment. In

some of the heterosynaptic LTP experiments the laser power was increased by ~15% during the LTP induction protocol, in order to increase the likelihood to evoke d-spikes by the LTP induction spines, then we commenced monitoring the test spines with the original test laser power. The uncaging locations were manually readjusted if necessary between test pulses (every 5 min) due to occasional changes in shape, position or loading-related fluorescence of the stimulated spines. Care was taken not to move the uncaging location closer to the spine head during the experiment, to avoid the possibility of artificial increases in EPSP amplitudes. In experiments where d-spikes were evoked during LTP protocol, we accepted experiments if we could either detect a clear transient rise in the dV/dt (related to dendritic Na^+ spikes; (Losonczy and Magee 2006; Losonczy et al., 2008; Makara et al., 2009) or measured at least 2 mV peak nonlinearity comparing the measured compound EPSP to the arithmetic sum of the individual EPSPs (Losonczy and Magee 2006; Losonczy et al., 2008; Makara et al., 2009) (**Fig. 5B**). The presence of d-spike(s) by at least one stimulus was always confirmed by visual inspection of the LTP trace by at least two investigators, and in most cases was also evaluated using a semiautomated spike detection algorithm. D-spikes were usually most clearly detected at the first stimulus of the LTP induction protocol. Because in some cases the presence of a fast d-spike was ambiguous at later stimuli (most likely due to partial inactivation of voltage-gated Na^+ channels (VGNCs; (Remy et al., 2010)), we did not attempt to systematically calculate the proportion of stimuli with and without d-spikes in the full dataset.

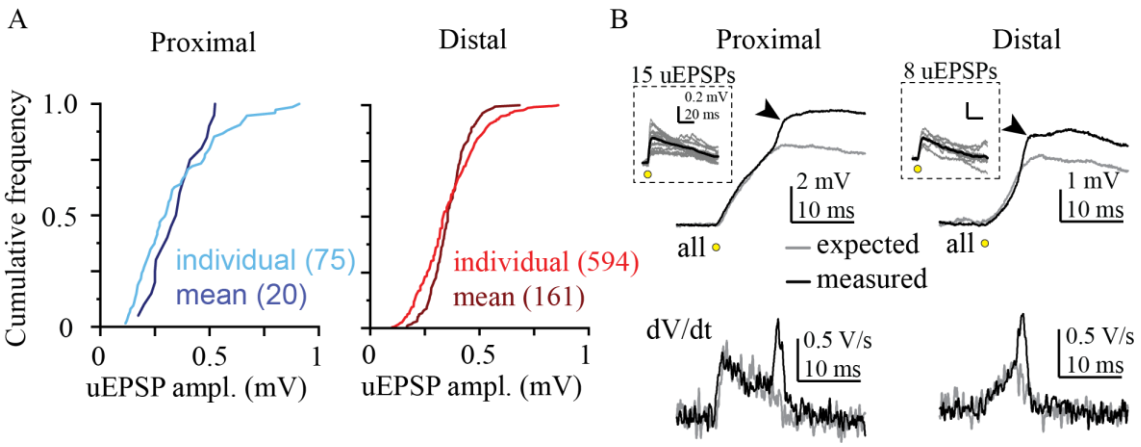

Figure 5 Parameters of LTP experiments. *(**A**) Cumulative frequency of all individual test spine EPSP amplitudes and the mean EPSP amplitudes of the test spines in individual experiments at proximal (left, blue) and distal (right, red) dendritic locations. (**B**) Representative somatic recordings of d-spikes evoked by quasi-synchronous multisynaptic glutamate uncaging at proximal (left) and distal (right) segments (in two different cells). Top, recorded response to the first stimulus during the LTP protocol (black), and the arithmetic sum (gray) of the individual EPSPs (inset). Arrows indicate the fast somatic spikelet mediated by dendritic Na^+ spikes. Bottom, dV/dt of the voltage traces. dV/dt component associated with the fast Na^+ spikelet.*

In low-Mg^{2+} experiments, wash-in of ACSF with reduced Mg^{2+} concentration (0.1 mM) was started immediately before seal rupture to establish the whole-cell configuration (~5-7 min before delivering the LTP induction protocol; control test pulse was measured during this wash-in period), and washout was started immediately after completing the LTP induction protocol.

4.5 Chemicals

D-AP5, TTX (all from Tocris), Ba^{2+} and NiCl2 (Sigma) were dissolved in distilled water; nimodipine (Tocris) and U0126 (Sigma) were dissolved in DMSO. Aliquots of the stock solutions were stored at -20°C and dissolved into ACSF on the day of experiment. Inhibitors were applied by perfusing the slice with ACSF containing the blocker(s) for 10-15 minutes before repatching the cells. Solution containing nimodipine and Ni^{2+} was protected from light.

4.6 Data analysis

Analysis was performed using custom-written macros in IgorPro (WaveMetrics, Lake Oswego, OR, USA). Voltage signals were analysed offline using averaged traces of typically 3-12 trials with no smoothing. Individual traces where the rising phase or the peak of an uncaging-evoked EPSP was contaminated by spontaneous EPSPs were not

included in the average. Calculated EPSP amplitudes were measured offline as the peak of the arithmetic sum of the individual responses (shifted and added, mimicking the same input timing as used experimentally). Test spines were typically monitored in every 5 minutes. For assessing temporal changes, data were pooled between 5-10 minutes, 15-25 minutes and 30-40 minutes.

The magnitude of plasticity was quantified as the mean normalized change in EPSP amplitude of all test spines, averaged between 30 and 40 min after the LTP protocol. An individual spine was considered to be potentiated with normalized EPSP >1.3 after LTP (Matsuzaki et al., 2004), which corresponded to a cut-off at 95% of the spines measured in control experiments with no LTP protocol. We did not analyse spines with <0.1 mV initial EPSP amplitude to avoid overestimation of LTP due to division by small numbers. Occasionally (<5%), we observed a retraction or disappearance of the stimulated spine, usually accompanied by a strong reduction (<40% of the control value) or unreliability of response amplitudes. This seemed to occur independently of the location of the spines or the experimental protocol; therefore, we omitted such spines from the analysis. Spines were excluded also if their head moved close to other neighbouring spines due to the shape or size changes throughout the course of the experiment. Spines were included in the analysis only if: (1) initial EPSP amplitude was between 0.1-1 mV, (2) either all three normalized EPSP amplitudes (at 30, 35 and 40 min) after LTP induction were >1.8 or <0.6, or the s.d. was <0.35 in case of average change >1 or s.d. was <0.6 in case of average change ≤1. Experiments with 4 test spines where more than one spine failed to fulfil these criteria were discarded; in experiments using 2 or 3 test spines, all spines fulfilled the criteria.

Morphological and distance measurements were performed on dye-loaded neurons using ImageJ (NIH, Bethesda, MD, USA). Distance of input site from the soma or trunk was measured from the approximate midpoint of the input site on stacked images. Interspine distances were measured between spine insertion points to the shaft (either visible or the perpendicular projection of the spine head centre to the shaft) on stacks or single-focal images. Relative distances along branch were measured as the distance of the input site centre divided by the total branch length, measured from the soma (basal

dendrites) or the originating branch point from the trunk (apical oblique dendrites). In cases when the dendrite bifurcated distal to the input site (e.g. proximal stimulation sites), the longer daughter was measured for total branch length.

4.7 Statistical analysis

Statistical analysis was performed using Wilcoxon matched pairs test (two paired groups), one-sample Wilcoxon test (some analysis of LTP experiments, comparison to median=1), Mann–Whitney U test (two unpaired groups), Kruskal–Wallis test and post hoc multiple comparisons with Holm-Bonferroni adjustment (multiple unpaired groups), or χ^2 test (comparing proportions) using Statistica (Statsoft, Tulsa, OK, USA) software. All statistical tests were two tailed. Differences were considered significant when $p<0.05$.

4.8 Computational modeling

We used a detailed biophysical CA1 pyramidal cell model (Ujfalussy and Makara 2020) based on (Jarsky et al., 2005), optimized for reproducing the dendritic processing of synaptic inputs in CA1 pyramidal neurons (Losonczy and Magee 2006).

The default passive parameters of the model were: C_m=1 µF/cm^2, R_a = 100 Ωcm and R_m=20 kΩcm^2 in the dendrites, R_m= 40 kΩcm^2 in the soma and in the axon and R_m= 50 kΩcm^2 in the axonal nodes. Activated synapses were placed on high-impedance dendritic spines consisting of a spine neck (length: 1.58 µm, diameter: 0.077 µm) and spine head (length: 0.5 µm, diameter: 0.5 µm) with total neck resistance ~500 MΩ (Harnett et al., 2012). To correct for the presence of spines, C_m was increased and R_m was decreased by a factor of 2 in dendritic compartments beyond 100 µm from the soma. In the simulations shown in Fig 17F we increased R_a to 200 Ωcm (high R_a) and changed R_m to 10 (low R_m), 20 (medium R_m) or 40 (high R_m) kΩcm^2 in compartments beyond 100 µm from the soma. These manipulations altered Na^+ spike dV/dt amplitude in a range of

75-120%, and EPSP amplitude in a range of 87-116% (both parameters still remaining in the physiological range).

Ion channel parameters were adjusted to replicate the most important features of dendritic integration of excitatory synaptic inputs. The model contained voltage gated Na^+, KDR and KA channels with the following densities (all in S/cm^2): Na^+: axon initial segment: 15; soma: 0.2; dendrites: 0.03 and increasing from 0.04 S/cm^2 to 0.06 S/cm^2 along the apical trunk between 100 and 500 µm. KDR: axon, soma, and apical trunk: 0.04; all other dendritic branches: 0.02. KA: axon: 0.004; soma and dendritic branches: 0.02; and increasing from 0.048 to 0.29 along the apical trunk between 100 and 500 µm.

The model included AMPA and NMDA excitation with synaptic conductances modeled as double-exponential functions with the following parameters: AMPA: τ_1=0.1 ms, τ_2=1 ms, g_{max}=0.6 nS and E_{rev}=0 mV; NMDA: τ_1=2 ms, τ_2=50 ms, g_{max}=0.8 nS and E_{rev}=0 mV. The voltage dependence of the NMDA conductance was captured by a sigmoidal activation curve: $g_{NMDA} = g_0 (1 + C_{Mg} / 4.3 \exp^{(-0.071V)})^{-1}$ where V is the local dendritic membrane potential, C_{Mg} = 1 mM is the Mg^{2+} concentration.

The model captures several somatic and dendritic properties of these cells measured under in vitro conditions, including the generation and propagation of Na^+ action potentials at the soma and along the apical dendritic trunk; the generation of local Na^+ spikes in thin dendritic branches; amplitude distribution of synaptic responses; nonlinear integration of inputs via NMDA receptors; the similar voltage threshold for Na^+ and NMDA nonlinearities and the major role of A-type K^+ channels in limiting dendritic excitability. When stimulated with in vivo-like synaptic inputs distributed throughout the entire dendritic tree, the same biophysical model shows place-selective activity, with several features of the somatic membrane potential activity falling in the physiological range (Ujfalussy and Makara 2020). The simulations were performed with the NEURON simulation environment (version 7.4) embedded in Python 2.7.

DOI:10.14753/SE.2021.2546

5. RESULTS

5.1 Spatial gradient of cooperative spine Ca^{2+} signaling.

In order to quantitatively investigate potential cooperative nonlinearities of interactions between nearby synaptic inputs, we first determined how voltage intagration and spine Ca^{2+} signals were affected by coactivation of small clusters of synapses. These experiments (performed by Judit Makara) provided the theoretical basis of the plasticity experiments described in my thesis; therefore I will briefly discuss the results (see Weber et al., 2016).

We measured the somatic voltage and spine Ca^{2+} responses to increasing number (up to four on an approximately 3-6 μm dendritic segment) of individually or synchronously stimulated nearby synapses, and compared the measured signals with that expected from independent (arithmetically summated) synapses. Initial experiments were performed at the two extremes of the branch impedance gradient, that is, at proximal (relative distance: 21±3% of branch length, n=7) and distal (relative distance: 93±1%, n=10) dendritic locations along thin apical oblique and basal dendrites (**Fig. 6A, D**). The laser power was always adjusted to yield uncaging-evoked EPSPs at each spine with somatic amplitudes similar to that of miniature EPSP (see Materials and Methods). To minimize the contamination of spontaneous synaptic activities, and to better assess the impact of passive dendritic properties, in these set of experiments, 0.5-1 μM tetrodotoxin (TTX) was included in the bath solution.

Uncaging-evoked EPSPs were typically accompanied by NMDAR-mediated Ca^{2+} signals (see also Fig. 8), which were largely restricted to the stimulated spine head, and had similar amplitudes at proximal and distal dendritic locations (**Fig. 6B, E**). When stimulating the four synapses (4S condition) quasi-synchronously, at distal dendritic locations we observed a pronounced amplification of peak spine Ca^{2+} signals, with a gradual nonlinear increase by activation of each additional nearby spine (**Fig. 6C, G**), accompanied by elevated dendritic Ca^{2+} levels near the input site. Surprisingly, the large Ca^{2+} signal amplification was not associated with suprathreshold voltage integration of EPSPs: summation remained linear (**Fig. 6F, H**).

DOI:10.14753/SE.2021.2546

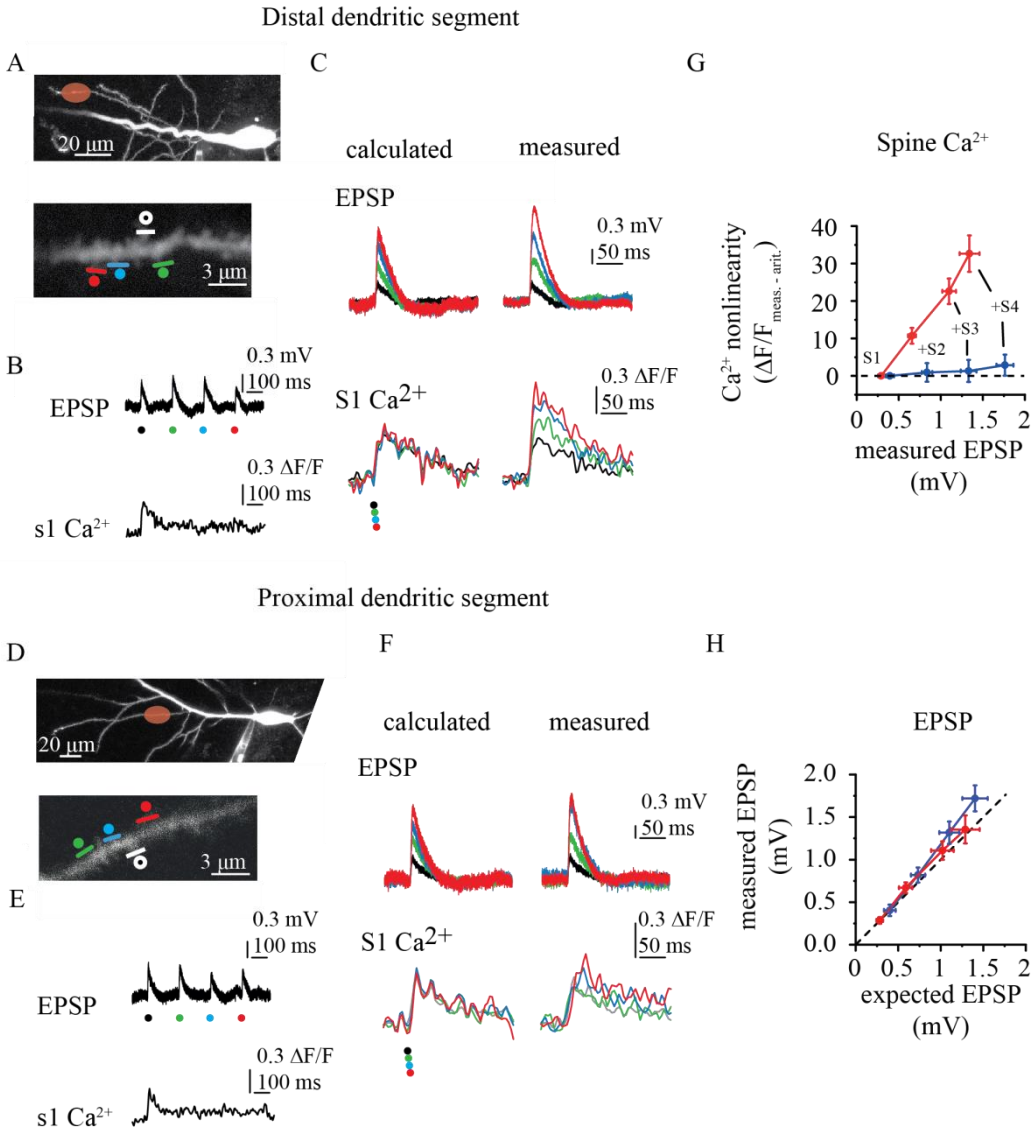

Figure 6 Cooperative spine head Ca^{2+} signaling in distal but not proximal dendritic segments. ***(A)*** *Left: 2P z-projection of a CA1PC, with the uncaging location indicated in red at a distal site on an oblique dendrite. Right: magnified image of the stimulated segment. The four stimulated spines are indicated.* ***(B)*** *Representative recording of uncaging-evoked somatic EPSPs (upper trace) and Ca^{2+} signal in the first spines (lower trace) by individual stimulation of the four spines shown in* ***A****.* ***(C)*** *Calculated (left) and measured (right) somatic voltage traces (upper) and spine Ca^{2+} signals in s1 (lower) achieved by synchronous stimulation of the spines in increasing numbers (black: s1 alone; green: s1+s2; blue: s1+s2+s3; red: s1+s2+s3+s4). Note that, in the absence of*

interspine interactions, spine Ca^{2+} signals are expected to remain unaffected by stimulation of other inputs. ***D-F*** *same as* ***A-C****, for spines stimulated at a proximal site on an oblique dendrite. (****G****) Quantification of cooperativity of synaptic Ca^{2+} signaling by calculating the nonlinear component of spine Ca^{2+} signals (measured minus calculated) at distal (red, n=18 spines, 6 cells, s1 and s2 data pooled) and proximal (blue, n=13 spines, 5 cells, s1 and s2 data pooled) dendritic segments, as a function of the somatically measured EPSP with increasing number of stimulated spines. (****H****) Measured versus calculated peak somatic EPSPs evoked at distal (red, n=10 experiments) and proximal (blue, n=8 experiments) dendritic segments with increasing number of stimulated spines. Group data are presented as mean± SEM cal, calculated; meas., measured).*

On the other hand, coactivation of similar synapse clusters at proximal dendritic locations led to little if any nonlinearity of spine Ca^{2+} signals (**Fig. 6D,G**; two-way repeated measures analysis of variance (ANOVA): interaction between spine N and location: $P<0.01$, effect of location: $P<0.001$, effect of spine N: $P<0.001$) along with linear voltage summation.

Testing clusters of four synapses at various relative distances along basal and apical oblique thin dendrites revealed a clear proximodistal increasing gradient of cooperative amplification of spine Ca^{2+} signals (**Fig 7A**), whereas the position of the branch in strata radiatum and oriens did not matter (**Fig. 7C**). In contrast to Ca^{2+} cooperativity, the small EPSP nonlinearity slightly decreased with distance along dendrites towards the tip (**Fig. 7B**). At proximal segments, only synapse clusters of at least ~12 inputs (12S condition) were sufficient to produce similar Ca^{2+} nonlinearity as that measured with four inputs at distal sites (**Fig. 7E**). In summary, the threshold sensitivity of synaptic Ca^{2+} cooperativity increases gradually along thin dendrites from their base to their tip systematically in the dendritic target area of Schaffer collaterals (**Fig. 7F**), a pattern well matching the passive impedance profile of the dendritic arbour (Harnett et al., 2012). In contrast, the corresponding EPSPs sum at the soma largely linearly with little location dependence (**Fig. 7B, D**).

DOI:10.14753/SE.2021.2546

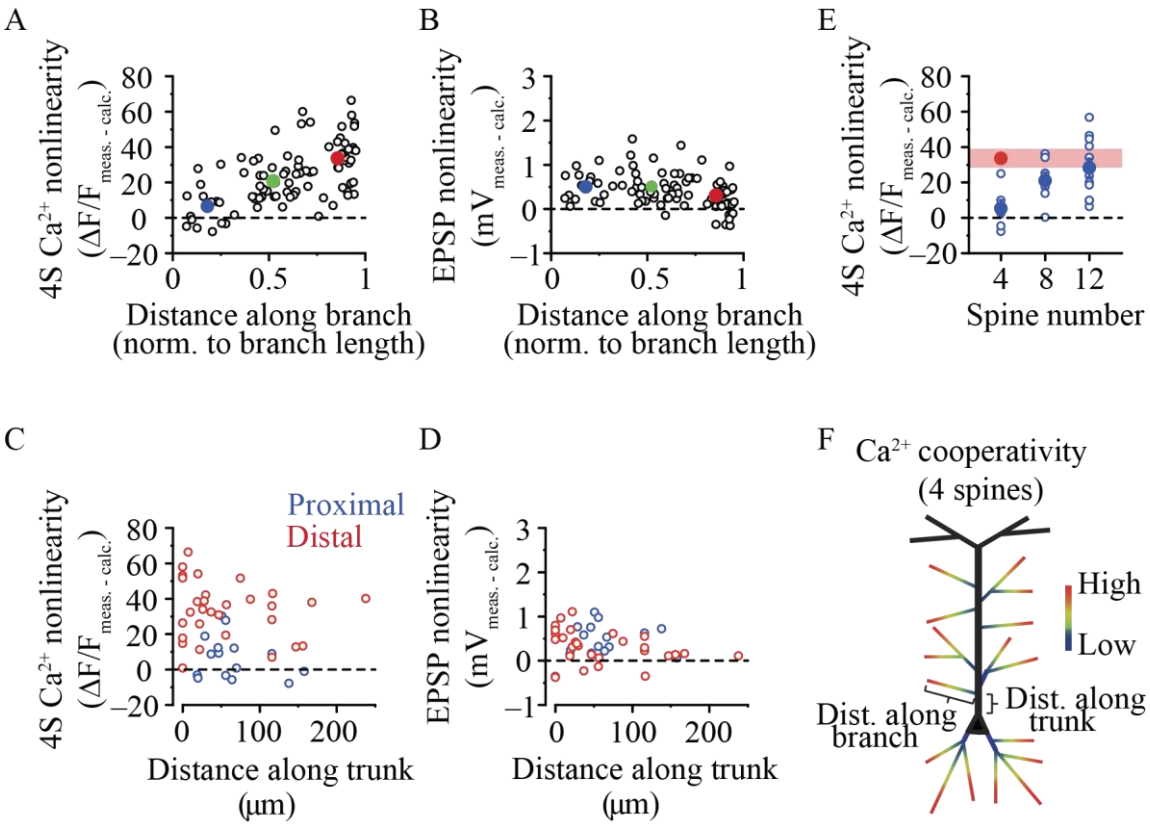

Figure 7 Dendritic map of synaptic cooperativity. *(**A**, **B**) Cooperative spine Ca^{2+} nonlinearity (**A**, as described in Fig. 6G) and somatic EPSP nonlinearity (**B**, difference between measured and calculated peak amplitudes) evoked by four coactivated spines at different relative locations along individual branches. Open circles represent individual spines sets (results of all four spines averaged, 1 set/branch). Filled symbols represent mean for proximal (relative location (RL)<0.33, blues, n=16 experiments in 11 cells), middle (RL=0.33-0.67, green, n=33 experiments in 20 cells) and distal (RL>0.67, red, n=37 experiments in 25 cells) locations. Correlations: spine Ca^{2+} nonlinearity (**A**): Spearman R=0.606, P<0.001; somatic EPSP nonlinearity (**B**): Spearman R=-0.379, P<0.001. (**C**, **D**) Cooperative spine Ca^{2+} nonlinearity (**C**) and somatic EPSP nonlinearity (**D**), evoked by four coactivated spines located proximally (blue) or distally (red) within apical oblique dendrites, as a function of the distance of the originating branch point from the soma. Spearman rank correlations; (**C**) proximal: R= -0.193, P= 0.490, n=15; distal: R= -0.097, P= 0.608, n= 30; (**D**) proximal: R= 0.044, P= 0.874; distal: R= -0.370, P= 0.044. (**E**) Spine Ca^{2+} nonlinearity using increasing number of inputs in*

*proximal dendritic segments (blue, n=6/7/11 for clusters of 4, 8 and 12 spines, respectively). Red symbol and band represent mean and 95% confidence interval, respectively, of the data obtained in distal segments with four spines. Comparison of 12S proximal and 4S distal data: Mann-Whitney test, P= 0.404. (**F**) Schematics of the dendritic cooperativity map and distance measurements. dist, distance; calc, calculated; meas., measured; norm., normalized.*

Pharmacological experiments using blockers of various possible sources of spine Ca^{2+} signals revealed (only AP5 experiments are shown here, for the effects of other Ca^{2+} source blockers, see Weber et al., 2016) that the Ca^{2+} nonlinearity evoked in spines and the dendrite at distal locations was mediated by NMDARs (**Fig. 8A, B**). In addition, similar cooperative spine Ca^{2+} nonlinearity was measured at distal dendritic locations without TTX as well (data not shown, see Weber et al 2016), indicating that four coactive synapses were subthreshold to dendritic Na^{+} spike generation, as expected (Losonczy and Magee 2006). Furthermore, we found no signs of NMDA spike generation by four distal synapses (neither larger peak EPSP nonlinearity (**Fig. 6C, F, H, Fig. 7B**) nor substantial prolongation of EPSPs compared to proximal clusters (half $width_{measured}$/half $width_{calculated}$, proximal: 1.08±0.03, n=16; distal: 1.17±0.03, n=34, P=0.082, Mann-Whitney test).

In summary, the results showed that NMDAR-mediated spine Ca^{2+} signals are highly sensitive to coincident activation of even low number of spatially close synapses in distal dendritic compartments. This local cooperative function takes place in the linear electrical integration regime, where voltage recordings at the soma remain uninformative about the spatial distribution or cooperation of the synapses involved.

DOI:10.14753/SE.2021.2546

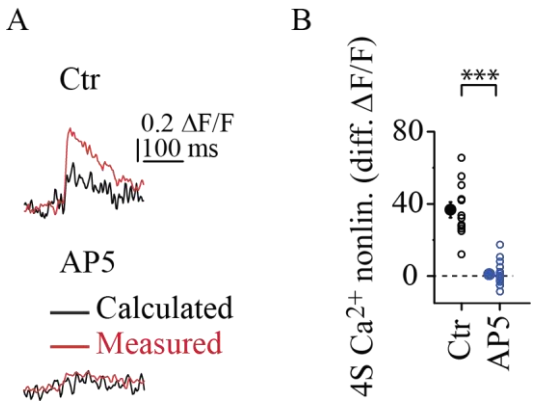

Figure 8 Cooperative spine Ca^{2+} signaling at distal dendritic locations is mediated by NMDARs. ***(A)*** *Calculated and measured spine Ca^{2+} signals from representative experiments using the 4S protocol (averaged data from all four spines) at distal segments of oblique and basal dendrites under control conditions (top) and in the presence of AP5 (100 μM, bottom).* ***(B)*** *Summary of cooperative spine Ca^{2+} nonlinearity (multiple comparisons after Kruskal-Wallis test with P<0.001) measured with the 4S protocol under control conditions (black, n=12 in 12 dendrites, five cells) and in the presence of AP5 (blue, n=16 in 10 dendrites, four cells). For the effect of other Ca^{2+} source blockers see Weber et al., 2016.*

5.2 Spatial requirements for cooperativity

We next explored the spatial requirements for cooperative interaction of NMDAR-mediated spine Ca^{2+} signals in distal dendritic compartments. When four synchronously activated inputs were evenly spread on an approximately 15-20 μm long dendritic segment close to the tip, average spine Ca^{2+} cooperativity decreased but still remained substantial (**Fig. 9A, C-E, H**), with decreasing distal-to-proximal nonlinearity profile in individual spines (**Fig. 9E**). EPSP summation by four inputs showed similar albeit weaker dependence on spatially distributed input arrangement (**Fig. 9G**). Finally, stimulating only two synapses we found small but detectable Ca^{2+} cooperativity between synchronously activated spines located within ~5-10 μm (**Fig. 9F**). These experiments highlight the importance of tight spatial requirement for effective cooperativity of

DOI:10.14753/SE.2021.2546

coactive synapses. Although I do not present the temporal requirements for cooperativity, we found that sub millisecond stimulus synchrony leads to the largest Ca^{2+} cooperativity (Weber et al., 2016).

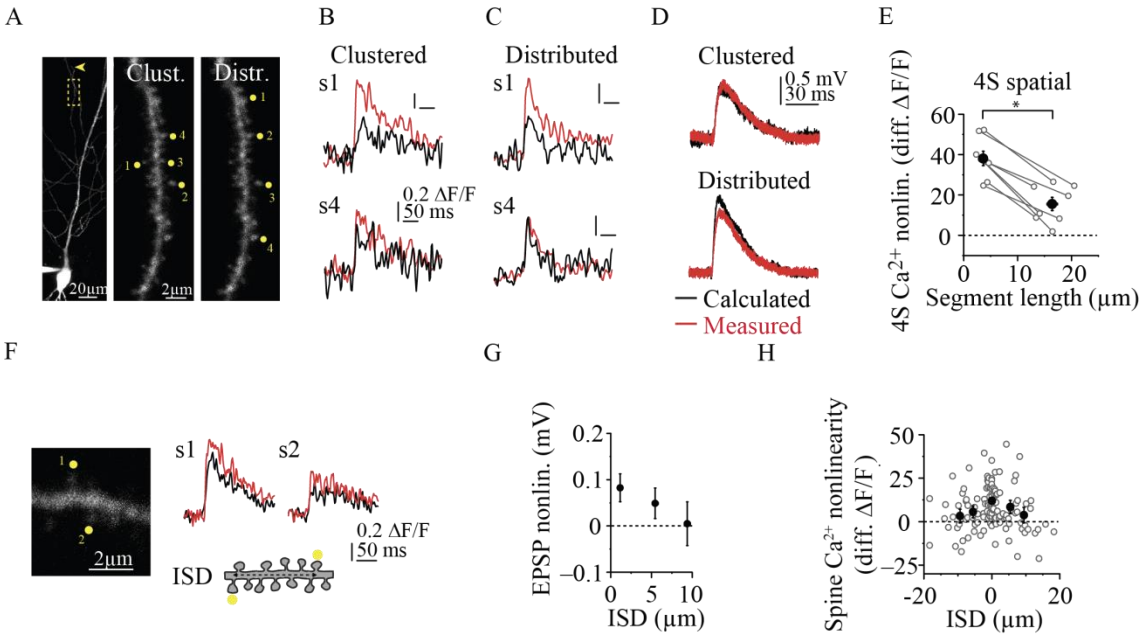

Figure 9 Spatiotemporal properties of cooperative spine Ca^{2+} signaling in distal compartments. *(**A**) Left: low-magnification z-stack of a CA1PC, stimulation site on oblique dendrite indicated by yellow box. Arrowhead points to dendrite tip. Middle and right: high-magnification z-stack of the stimulated segment, with clustered (middle) and distributed (right) arrangement of inputs. Distributed inputs were always activated distal to proximal. (**B, C**) Representative Ca^{2+} signals from spine #1 (upper) and spine #4 (lower) in clustered (**B**) and distributed (**C**) arrangement using the 4S protocol (ISI= 0.1 ms). (**D**) Integrated somatic EPSPs corresponding to (**B, C**). In **B-D**, black traces represent calculated responses and red traces represent measured responses. (**E**) Spine Ca^{2+} nonlinearity (average of all four spines) in clustered versus distributed arrangement ($P<0.05$, Wilcoxon test). Grey lines represent experiments in individual dendrites. (**F**) Left: single 2P image of a distal segment with two stimulated spines indicated. Right: Ca^{2+} signals in the two spines during synchronous stimulation. Cartoon depicts measurement of interspine distance (ISD). (**G**) EPSP nonlinearity as a function of ISD*

*(grouped by absolute ISD values binned as in (**H**). Filled symbols and error bars represent mean±SEM (**H**) Ca^{2+} cooperativity among spine pairs as a function of ISD (n=122 spines. Positive or negative ISD value represents spine sequence towards tip or soma, respectively. Symbols represent mean±SEM for data binned in 0±2.5, 2.5-7.5 and 7.5-12.5 μm. Kruskal-Wallis test for 0±2.5 (n=62), 2.5-7.5 (n=27) and 7.5-12.5 μm (n=23) bins, P= 0.003.*

5.3 Location-dependent cooperative synaptic LTP

Spine Ca^{2+} signaling is considered to be fundamental in determining the sign and strength of long-term synaptic plasticity. We hypothesized that cooperative enhancement of spine Ca^{2+} signals in coactive synapses even in the linear voltage integration regime, as shown above, may promote clustered forms of synaptic plasticity, with lowest input threshold in distal high-impedance dendritic compartments. To examine this hypothesis, we measured peak amplitude changes of EPSPs (initial amplitude; proximal: 0.42±0.03 mV, n=61 spines) in response to a cooperative 2PGU LTP induction protocol that involved synchronous stimulation of various number of spatially clustered spines (0.1 ms ISI, 0.5 ms uncaging duration per spine) depending on the experiments, repeated 50x at 3 Hz in normal ACSF near the resting membrane potential (~ -64mV) (see Materials and Methods). In most experiments, EPSPs were also measured at an additional nearby (<15 μm) reference spine that was not stimulated during the cooperative LTP protocol. Cells were first loaded with Alexa Fluor 488, via brief (30-60 s) whole-cell recordings, and patched again after allowing 30-100-min recovery period when spines could be clearly visualized throughout the dendritic arbour. This allowed us to induce LTP at identified spines within 5-10 min after membrane rupture, avoiding disruption of the intracellular milieu critical for LTP.

The costimulation of 4 spines during the LTP protocol led to an increase of somatic EPSP amplitude to 139±10% of control values at the four LTP-induced spines (s1-s4) at distal dendritic locations (**Fig. 10A, B, E, F**, P<0.01, one-sample Wilcoxon test, n=17 experiments; data from s1 to s4 averaged). The effect was heterogeneous among

spines even within spine sets (**Fig. 10B**), but followed a normal distribution (**Fig. 10G**). The heterogeneity in LTP depended neither on spine order in the activation sequence, nor on initial EPSP amplitude. Importantly, EPSP amplitude did not increase (in fact, slightly decreased) in the reference spine that was not stimulated during the LTP protocol, indicating input specificity of potentiation (**Fig. 10A, B, F**; 83±5% of control, n=16, $P<0.01$, one-sample Wilcoxon test; comparison with LTP spines: $P<0.001$, Wilcoxon test). While these experiments were performed mostly on apical oblique dendrites, in an extended dataset we found similar cooperative LTP in basal distal segments (apical: 131±10%, n=18; basal: 152±14%, n=6, $P=0.193$, Mann-Whitney test). Control experiments confirmed that LTP appeared only when both caged glutamate and uncaging laser pulses were presented during the induction protocol.

DOI:10.14753/SE.2021.2546

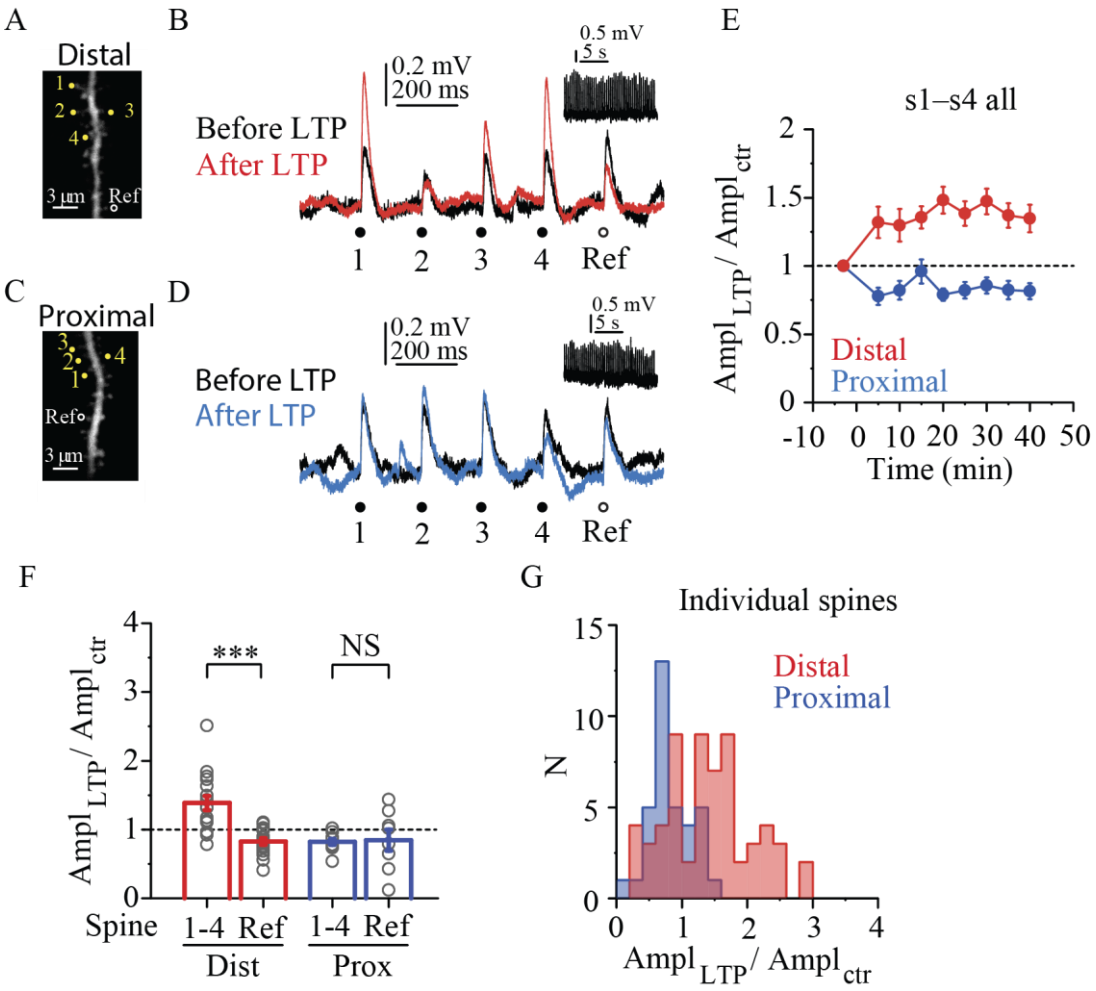

Figure 10 Spatial gradient of cooperative LTP along dendrites. *(**A**) 2P image of a distal segment in an oblique branch. Spines s1-s4 were included in the LTP protocol; the reference spine did not receive LTP induction stimulus. (**B**) Somatic EPSPs by the five spines (s1-s4 (yellow dots) and reference spine (black circle) in **A**), before (black) and >30 min after (red) delivering the LTP induction protocol to test spines. (inset shows LTP induction voltage trace). (**C**, **D**) Similar experiment as in A and B on a proximal segment in an oblique branch. (**E**) Time course of the effect of cooperative LTP protocol on somatic EPSP amplitude at the yellow test spines in distal and proximal dendritic segments. (**F**) Summarized effect of the cooperative LTP protocol on peak somatic EPSP amplitude evoked in distal versus proximal segments in s1-s4 (distal (red), n=17 cells; proximal (blue), n=10 cells, grey circles represent averaged data from s1-s4 in individual experiments) and in reference spines (distal (red), n=16; proximal (blue), n=8, grey*

*circles represent individual spines). (**G**) Histogram of EPSP amplitude change in distal (red) and proximal (blues) s1-s4 spines. Note the normal distribution of the LTP effect in distal spines (Shapiro-Wilks test, P=0.120). Group data are presented as mean±SEM.*

In contrast to distal locations, no cooperative LTP could be induced at proximal dendritic locations using the same protocol; instead, a long-lasting slight decrease of EPSP amplitude was observed (**Fig. 10C-G**; 82±4% of control, n=10, P<0.01, one-sample Wilcoxon test) that did not differ from the amplitude change at reference spines (85±16% of control, n=8, P=0.888, Wilcoxon test).

Cooperative LTP in distal dendritic segments was eliminated by the NMDAR inhibitor D-AP5 (50 μM), but was not significantly affected by the VGNC inhibitor TTX (1 μM), demonstrating that NMDARs but not VGNCs are required for LTP (**Fig. 11A, B**).

To examine whether the difference in LTP between proximal and distal locations is due to the difference in voltage-dependent alleviation of Mg^{2+} block of NMDARs, we stimulated single spines alone with an LTP induction protocol with the same activity pattern (50x at 3 Hz) at distal and proximal locations in low Mg^{2+} (0.1 mM) containing ACSF, where the voltage-dependent block of NMDARs by Mg^{2+} is strongly reduced. Consistent with previous studies (Matsuzaki et al., 2004; Tonnesen et al., 2014), this single-spine protocol induced LTP in most spines at both distal and proximal locations (**Fig. 11C, D**). In contrast, using the same induction protocol in normal ACSF (containing 1 mM Mg^{2+}), spines stimulated alone failed to undergo LTP at both locations (**Fig. 11C, D**; two-way ANOVA: no interaction between location and Mg^{2+} treatment, P=0.735, P=0.681 for location, P<0.05 for Mg^{2+} treatment). These results together indicate that LTP induction and expression are functional in both proximal and distal spines, and suggest that the larger dendritic depolarization generated by coactive inputs in distal, high-impedance dendritic compartments was sufficient to unblock NMDARs and produce cooperative LTP even with low number of clustered inputs.

DOI:10.14753/SE.2021.2546

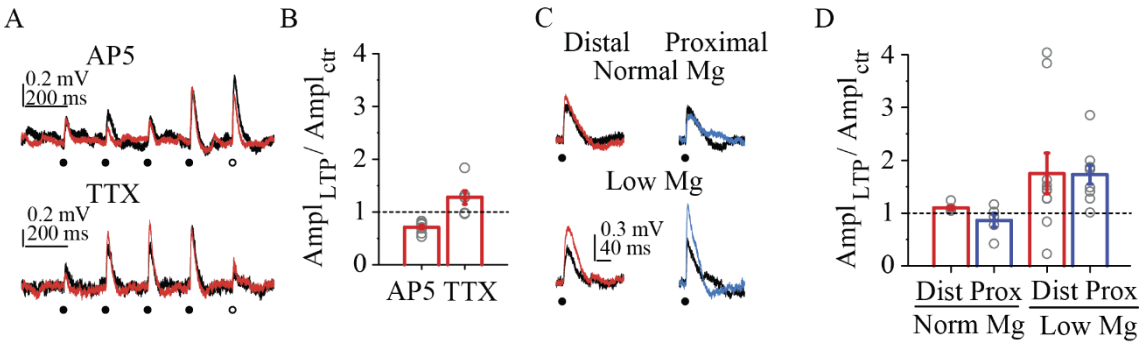

Figure 11 LTP is mediated by voltage-dependent NMDARs but not Na^+ channels. *(**A**) Representative cooperative LTP experiment at a distal oblique segment in the presence of 50 µM AP5 (upper) or in the presence of 1 µM TTX (lower). (**B**) Summary of the effect of AP5 (n= 8 cells, P<0.001 for comparison with control, multiple comparisons after Kruskal-Wallis test with P<0.001) and TTX (n=6 cells, P=0.649 for comparison with control) on cooperative LTP at distal locations. Grey circles: averaged data from s1-s5 in individual experiments. (**C**) Representative EPSPs before (black) and >30 min after a single spine LTP protocol at distally (red) and proximally (blue) located spine in normal ACSF (upper traces) and in ACSF containing 0.1 mM Mg^{2+} (lower traces). (**D**) Summary of single spine LTP experiments in normal ACSF (distal, n=5 spines; proximal, n=5 spines) and in 0.1 mM Mg^{2+} ACSF (distal, n=10 spines; proximal, n=9 spines). Grey circles: individual spines. Group data are presented as mean±SEM Two-way ANOVA: no interaction between location and Mg^{2+} treatment, P=0.735, P=0.681 for location, P<.05 for Mg^{2+} treatment.*

5.4 Regenerative d-spikes are required for efficient cooperative LTP at proximal dendritic locations

Since we did not observe LTP by subthreshold coactivity of small input clusters (4 spines) at the proximal sites of perisomatic dendrites, we asked whether larger clusters of proximal inputs were able to evoke subthreshold LTP. During the following experiments, the mode of voltage integration during the LTP induction protocol, specifically the presence of d-spikes, was carefully evaluated by comparing the amplitude and kinetics of the expected and measured compound EPSPs (**Fig. 5B**).

DOI:10.14753/SE.2021.2546

We increased the size of the synapse cluster costimulated during the LTP protocol to 12-16 inputs, by uncaging at additional neighbour spines together with the test spines, covering a ~10-15 μm long dendritic segment (**Fig. 12Aii**). Synchronous activation of such a sizable synapse cluster evoked substantial somatic EPSPs (first EPSP during LTP protocol: 3.9±0.5 mV, n=5 experiments; **Fig. 12Aiii**) with small peak EPSP nonlinearity (0.7±0.5 mV, measured in n=4 experiments), but regenerative d-spikes were not triggered (**Fig. 12Aiii**), likely due to the low impedance of proximal dendritic segments. Surprisingly, even with this high local input density, with the subthreshold pattern no LTP was observed at the test synapses; indeed, the mean EPSP amplitude of test spines tended to rather decrease (**Fig. 12Ai, D**; EPSP amplitude relative to baseline at 30-40 min: 0.82±0.09, mean±SEM of n = 5 experiments, p=0.079, one-sample Wilcoxon test).

DOI:10.14753/SE.2021.2546

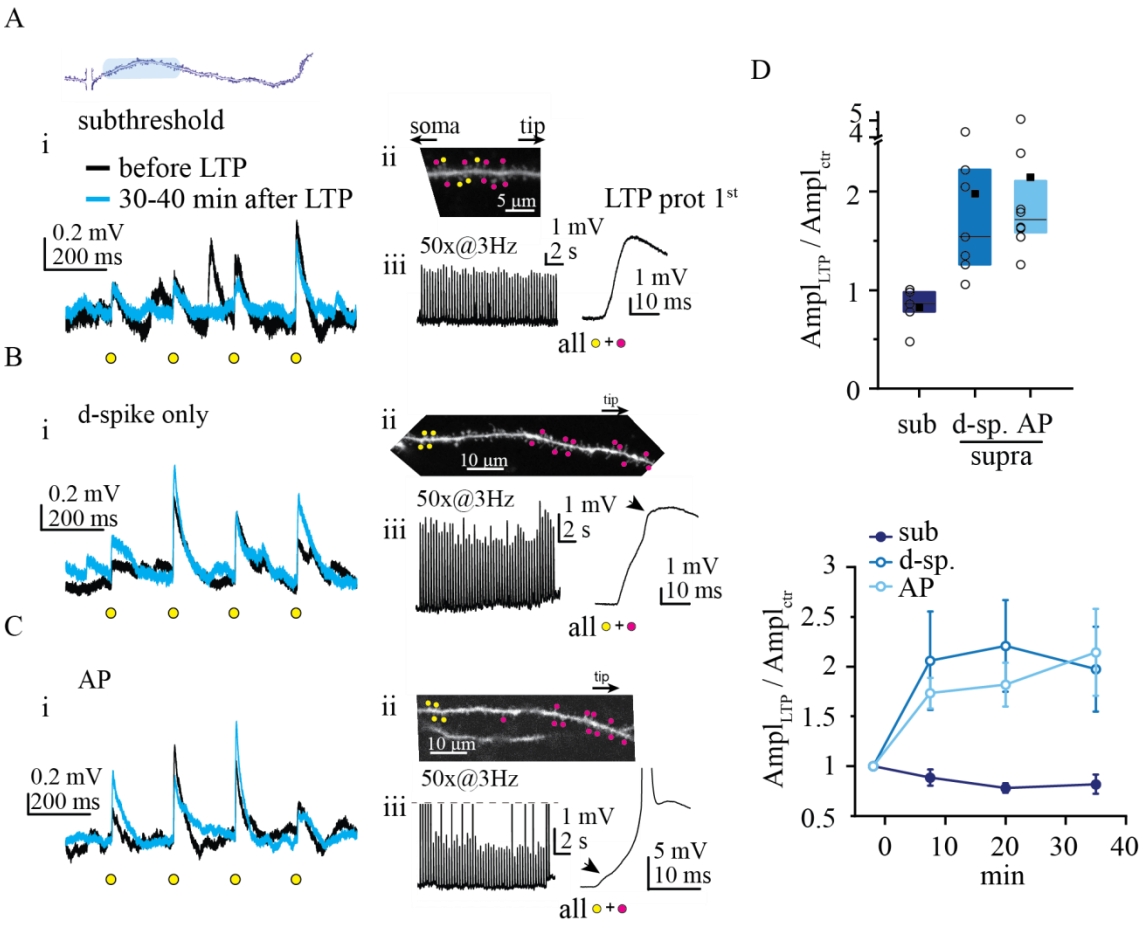

Figure 12 D-spikes are required for cooperative LTP at proximal dendritic locations. *(**A**) Top, Schematic of an individual dendrite. Blue represents proximal area. (**A-C**) Representative recordings using clustered subthreshold (**A**), dendritically suprathreshold (**B**), and somatically suprathreshold (**C**) input patterns. (**Ai**, **Bi**, **Ci**) Representative recordings (average traces) of individual EPSPs evoked by 2PGU (yellow circles) at the four test spines before (black) and >30 min after (blue) the LTP protocol. (**Aii**,**Bii**,**Cii**) 2P images (z stack or single plane) of the stimulated segments. Yellow dots indicate test spines 2PGU sites. Magenta dots indicate additional spines costimulated with test spines during the LTP protocol. (**Aiii**, **Biii**, **Ciii**) LTP induction protocol trace (left) and the first stimulus enlarged (right). Arrows point to dendritic Na^+ spikes as detected at the soma. APs are truncated in **Ciii**. (**D**) Summary of LTP experiments at proximal dendritic segments. Top, Mean (square), median (line), and interquartile ranges*

(box) of EPSP amplitude changes at 30-40 min relative to baseline. Circles represent data (mean of the four test spines in individual experiments. Bottom, Time course of EPSP amplitude changes (mean±SEM of experiments).

We next asked whether proximal synapses can undergo LTP if they contribute to input patterns triggering d-spikes. As explained in the Introduction, d-spikes in thin perisomatic dendrites comprise of fast Na^+ spikes and/or slow NMDA spikes. To facilitate d-spike initiation, we costimulated the four proximal test spines during the LTP protocol with a group of 11 additional spines located more distally on the same dendrite (~25 μm distance between group centers; **Fig. 12B**). This input pattern evoked d-spikes more efficiently, likely due to extending to higher impedance dendritic segments. Generation of d-spikes was indicated by either a transient increase in the rate of rise (dV/dt) of the compound EPSPs, a sign of dendritic Na^+ spikes (**Figs. 5B, 12Biii**), and/or a peak somatic nonlinearity ≥2 mV, indicating NMDA spikes. We prevented somatic APs by slight hyperpolarization during the LTP protocol. Triggering d-spikes induce robust long-lasting increase in the mean EPSP amplitude of the four proximal test spines (1.98±0.43, n=7 experiments; **Fig. 12B, D**; different from subthreshold with p=0.024, multiple comparisons after Kruskal-Wallis test with p=0.004), and potentiated synapses were found in every experiment. Similar LTP was measured when APs were also evoked by at least 1 of the 50 LTP stimulus pulses: EPSP amplitude increased to 2.15±0.44 (**Fig. 12C, D**; n=8 experiments, different from subthreshold with p=0.004, not different from d-spike only, p=1, multiple comparisons after Kruskal-Wallis test with p=0.004), and potentiated synapses were found in all experiments. These data suggest that large depolarization, involving regenerative dendritic spikes (local or backpropagating AP), is needed for cooperative LTP induction of synapses located in proximal segments of perisomatic dendrites.

DOI:10.14753/SE.2021.2546

5.5 Subthreshold LTP at distal dendritic locations depends on fine-scale input configuration

Next, we explored the rules of cooperative LTP at distal segments of perisomatic dendrites. To have a reliable control group, we repeated the experiments using coactivation of four clustered distal test spines (dendritic stretch: 4.59±0.25 μm), and we have found similar results to the previous dataset, as test spines increased their net EPSP amplitude to 1.32±0.11 (n=14 experiments; **Fig. 13A, E**), and potentiation occurred in at least one spine in most (11 of 14) experiments (**Fig. 13A**). D-spikes were not detected during the LTP protocol based on our detection criteria (**Fig. 13A**), and the LTP was input specific, as the reference spine showed, on average, no change in EPSP amplitude (1.03±0.12 in n=12 experiments; comparison with test spines: p=0.012, Wilcoxon test; **Fig. 13E**). In experiments where EPSPs of four test spines were monitored without coactivation (no LTP protocol), EPSPs did not increase, indeed slightly decreased (**Fig. 13B, E**; EPSP amplitude: 0.86±0.05, n=11, p=0.029, one-sample Wilcoxon test; comparison of experiments with and without LTP protocol: p=0.001, Mann-Whitney test), similarly to what we have observed in reference spines.

To determine the minimum cluster size required for subthreshold cooperative LTP, we reduced the number of test synapses coactivated during LTP induction. With three synapses, we still observed input-specific increase in EPSP amplitude (1.35±0.13, n=8; **Fig. 13C, E**), similar to that measured with four inputs. In contrast, LTP protocol with only two synapses did not induce their potentiation (0.81±0.11, n=8; **Fig. 13D, E**); their EPSP amplitude changes were similar to those of reference spines (0.84±0.09, n=8, p=0.89, Wilcoxon; **Fig. 13E**). Statistical analysis showed similar LTP with coactivation of 3 or 4 spines (p=1), which was larger than that with 2 spines (p=0.025 and p=0.018, respectively, multiple comparison test after Kruskal-Wallis ANOVA with p=0.010).

DOI:10.14753/SE.2021.2546

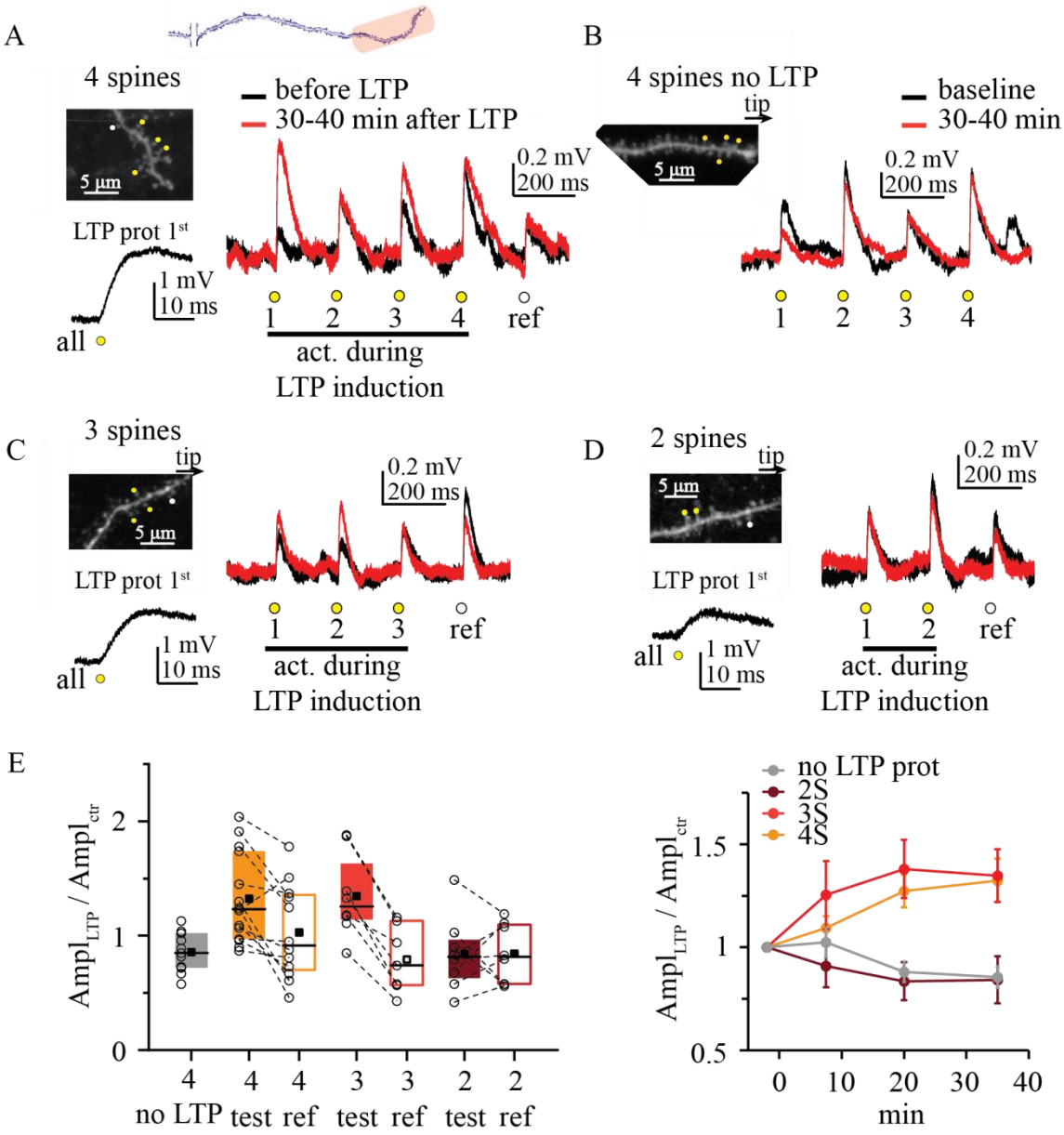

Figure 13 Cluster size requirements for subthreshold cooperative LTP at distal dendritic locations. *(**A**) Top, Schematic of an individual dendrite, with stimulated distal area indicated in red. (**A-D**) Representative experiments. (**A**) Left, Top, 2P image of the distal segment of a perisomatic dendrite. Test spines marked by yellow dots were costimulated in the LTP protocol; the reference spine (white dot) was not. Left, Bottom, First stimulus of the LTP protocol. Right, Somatic EPSPs by the five spines (s1-4, yellow circles; and reference spine, white circle), before (black) and >30 min after (red) the LTP protocol. (**B**) Experiment where four test spines (yellow dots in 2P image) were monitored*

*but no LTP protocol was applied. (**C**, **D**) Similar experiment as in **A**, but with only 3 (**C**) or 2 (**D**) test spines stimulated during the LTP protocol. (**E**) Summary of experiments with clustered distal spines. Circles represent mean data of the test spines or data from individual reference spines in each experiment. Test and reference spine data from the same experiment are connected. Note that data from individual (reference) spines have inherently higher variance that that of mean data of multiple (test) spines. Right, Time course of EPSP amplitude changes in test spines (mean±SEM).*

Next, we examined the spatial pattern requirements for subthreshold LTP. LTP protocol with four coactivated test spines that were distributed evenly on longer dendritic stretches (17.4±0.5 μm, ISD: 5.8±0.2 μm; **Fig. 14A,C**) did not produce subthreshold LTP effectively (EPSP amplitude: 0.91±0.05, n=21, $p<0.001$ for comparison with tightly clustered arrangement with 3 or 4 spines, Mann-Whitney test; **Fig. 14A-C**; 13% of all spines potentiated, comparison with tightly clustered: $p<0.001$, χ^2 test), with strong negative correlation between ISD and EPSP change (**Fig. 14C**; $p<0.001$, Spearman R= -0.548, n=43). No significant difference was found between tip-to-soma (0.98±0.09, n=7) and soma-to-tip (0.88±0.07, n=14) sequences ($p=0.681$, Mann-Whitney test; **Fig. 14D**). Together, the above results show that tight clusters of ≥3 coactive distal inputs can be strengthened by subthreshold cooperative LTP, even without regenerative dendritic activity.

DOI:10.14753/SE.2021.2546

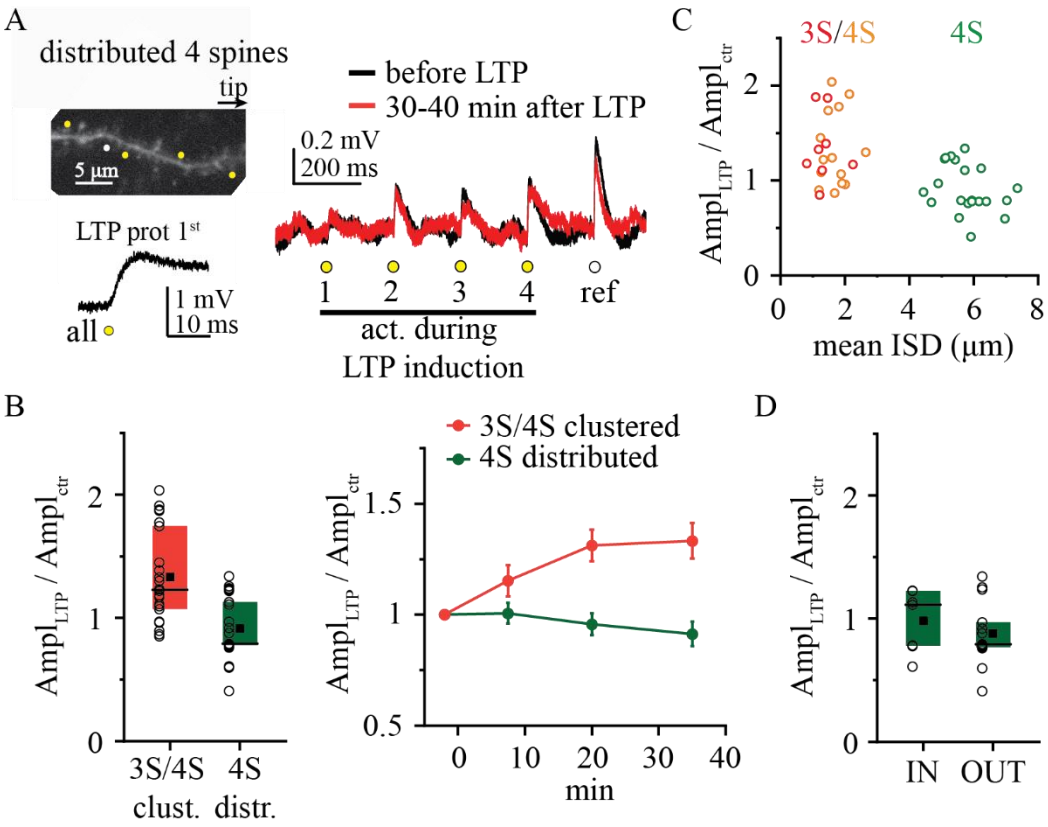

Figure 14 Spatial requirements for subthreshold cooperative LTP at distal dendritic locations. *(**A**) Representative experiments similar to Fig. 3 but using more distributed spines. (**B**) Summary of experiments with clustered (experiments with 3 and 4 spines pooled) and distributed arrangements. (**C**) Mean ISD between two neighboring test spines in clustered and distributed arrangements. (**D**) Results of experiments with distributed inputs in tip-to-soma (IN) and soma-to-tip (OUT) sequences.*

5.6 D-spikes alleviate the tight clustering requirements of LTP

Are the strength and/or the spatial rules of plasticity at distal dendritic segments different if synapses participate in a stronger input pattern that can evoke local d-spikes? To address this question, during the LTP protocol, additional neighbour spines were coactivated together with the four clustered test inputs to trigger d-spikes. (**Fig. 15A**). In most cases, eight synchronous synapses were enough to evoke at least one regenerative dendritic event during the LTP protocol without somatic APs (**Fig. 5B, 15A**; see also **Fig.**

16A). This clustered, locally suprathreshold input pattern induced LTP in at least one test spines in all experiments (9 of 9). Surprisingly, neither the magnitude of LTP (1.37±0.08, n=22 for subthreshold LTP with 3 or 4 spines, p=0.727, Mann-Whitney test) nor the ratio of potentiated synapses (47% vs 39%, p=0.456, χ^2 test) was significantly different from that measured with subthreshold LTP by 3 or 4 clustered inputs (**Fig. 15B**).

We next explored how LTP with d-spikes depends on the spatial arrangement of the inputs. We hypothesized that more extended propagation of d-spikes, especially toward the sealed tip, may allow more distributed input patterns to potentiate. To test this, we again distributed the four test spines (total stretch: 23.2±2.6 μm, average ISD=8.3±0.8 μm, n=5), but during LTP induction we coactivated them with four additional (more proximal) synapses in order to trigger d-spikes (**Fig. 15C**). In most experiments (4 of 5), we found at least one synapse to be potentiated, and an average LTP of 1.52±0.20 was induced (n=5; **Fig. 15C, D**). The effect was significantly stronger than that measured with only four distributed (subthreshold) synapses (p=0.004, Mann-Whitney test; **Fig. 15D**).

Previous reports using electrical stimulation indicated that d-spikes can trigger synaptic potentiation with fewer stimulus repetitions than other LTP-inducing activity patterns (Bittner et al., 2017; Remy and Spruston 2007). To test whether there is a difference in this regard between locally subthreshold and suprathreshold input patterns, we performed experiments with a short LTP protocol, consisting of only 5 coactivations of 4 (subthreshold) or 8 (suprathreshold for d-spikes) clustered spines. We found that suprathreshold clustered inputs did develop robust LTP (1.50±0.05, n=4), whereas only 5 synchronous activations were not sufficient to induce LTP with subthreshold clustered inputs (0.79±0.05, n=5, p=0.019 compared with d-spikes, Mann-Whitney test; **Fig. 15E, F**).

DOI:10.14753/SE.2021.2546

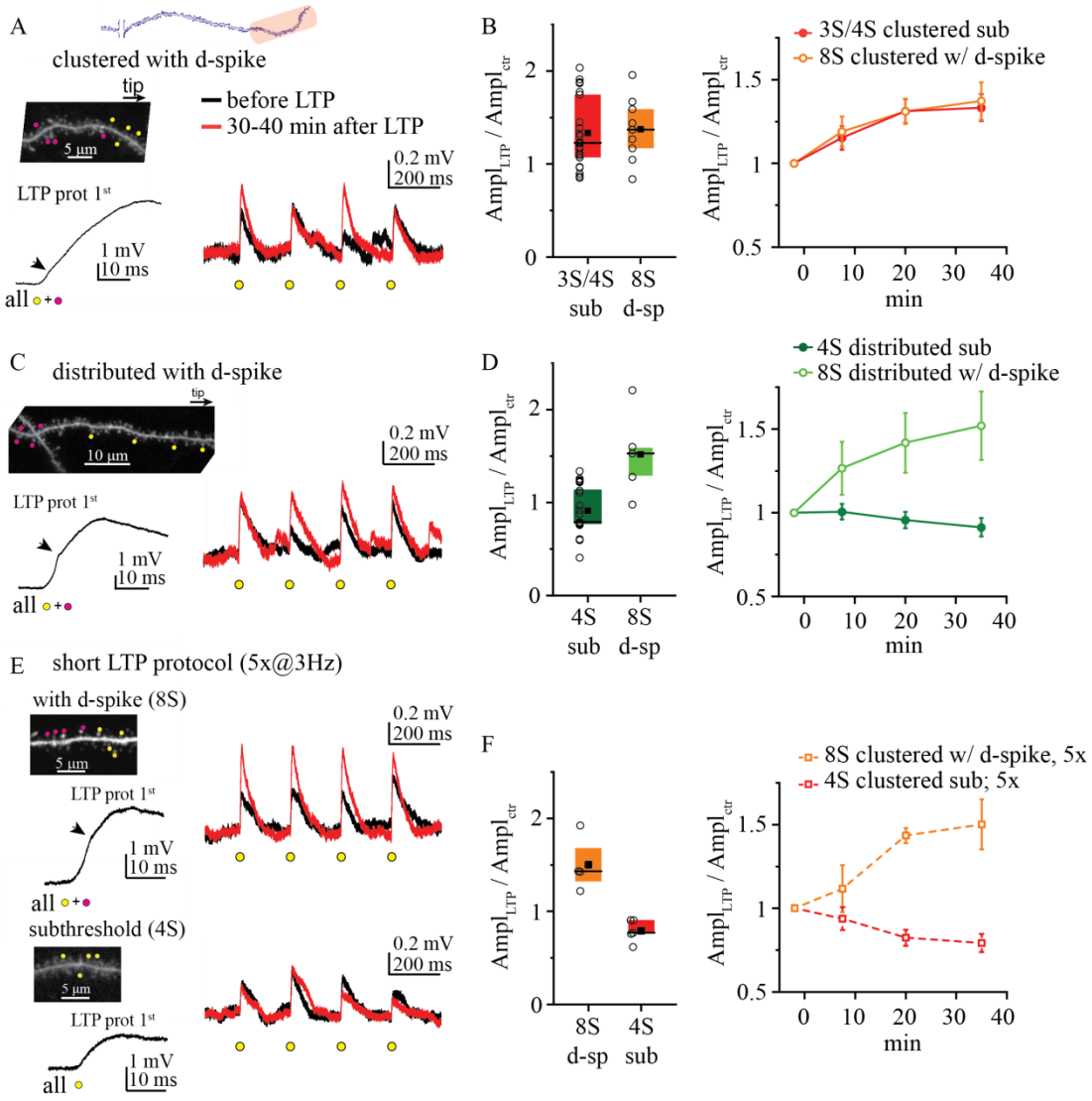

Figure 15 Role of d-spikes in cooperative LTP at distal dendritic locations. ***(A)*** *Representative experiment with clustered input pattern. Left, Top, 2P image of a distal dendritic segment. Four clustered test spines (yellow dots) were costimulated during the LTP protocol with four additional spines (magenta dots) to triggered-spikes on at least one stimulus. Left, Bottom, First stimulus of the LTP protocol. Right, Somatic EPSPs by the four test spines before (black) and >30 min after (red) the LTP protocol.* ***(B)*** *Comparison of LTP with subthreshold (red; pooled data with 3 and 4 spines from Fig. 11E) and locally suprathreshold clustered input patterns with 8 spines (orange). Left, Mean (square), median (line), and interquartile ranges (box) of relative EPSP amplitude changes. Circles represent individual experiments (mean data of the four test spines).*

*Right, Time course of EPSP amplitude changes (mean±SEM of all experiments). (**C**) Similar representative experiment as in **A**, but with distributed test spine arrangement. (**D**) Comparison of LTP with subthreshold (dark green; data from Fig. 12B) and locally suprathreshold (light green) distributed patterns. (**E**) Representative experiments with short LTP protocol (costimulation 5 times, 3 Hz). Top, Experiment with four clustered test spines and four additional spines coactivated during the short LTP protocol triggering d-spikes. Bottom, Four clustered test spines costimulated in the short LTP protocol, evoking no d-spikes. Right, Somatic EPSPs bz the four test spines before (black) and >3 min after (red) the LTP protocol. (**F**) Comparison of the effect of short LTP protocol with subthreshold (red) and locally suprathreshold input patterns (orange). Left, Mean (square), median (line), and interquartile ranges (box) of relative EPSP amplitude changes. Circles represent individual experiments (mean data of the four test spines). Right, Time course of EPSP amplitude changes (mean±SEM). (**A, C, E**) Arrows indicate dendritic Na^+ spikes.*

These results together indicate that d-spikes, although not necessarily required for LTP at distal dendritic segments, can alleviate the tight spatial clustering requirements and reduce the number of coincident activity events needed to induce cooperative LTP.

5.7 Strong input patterns allow local plasticity crosstalk

D-spikes, evoking robust voltage and Ca^{2+} signals in the branch, may activate signaling mechanisms that affect the function of not only those synapses that evoked them but other neighbour synapses as well. To examine this possibility, we coactivated a group of eight spines during LTP induction, triggering d-spikes ("LTP induction spines"), and measured the impact of this stimulus on EPSP amplitudes of a different set of nearby four test spines (up to ~20 μm distance; **Fig. 16A**). The test spines were thus only activated before (≤2 min, on average 94 s) and after (≥5 min, on average 369 s), but not during the LTP protocol. Surprisingly, we observed variable effects: although the long-term change in test spines EPSP amplitude (1.25±0.12, n=30) was smaller than that by homosynaptic

LTP with d-spikes (clustered and distributed suprathreshold data from Fig. 12A-D pooled; 1.43±0.10, n=14, p=0.03, Mann-Whitney test), in a substantial fraction of experiments, we detected signs of potentiation in the test spines (**Fig. 16A, B, E**). First, in the majority of experiments (20 of 30), EPSP increased >30% in at least one of the test spines (**Fig. 16A, B**). Second, in 12 of 30 experiments, the mean EPSP amplitude change in the test spines was larger than the mean +2 SD measured in control experiments with no LTP protocol (**Fig. 16E**; compare with **Fig. 13E**). We also examined whether the relative location of test spines to the LTP induction spines matters, but our observation showed that this heterosynaptic "crosstalk" potentiation could occur both if the test spines were proximal or distal from the LTP induction spines (**Fig. 16C**).

To better understand the nature of this effect, we tested whether crosstalk potentiation is evoked when test spines and LTP induction spine groups are located at short Eucledian distance, but on different dendrites of the cell (Eucledian distance: 7.1±1.4 μm, dendritic path: 228±19 μm; n=6; **Fig. 16D**). Under these conditions, no LTP was found in any of the test spines, and their EPSP amplitude rather decreased (0.77±0.05, n=6, p=0.013 compared with arrangement with all spines on the same dendrite, Mann-Whitney test; **Fig. 16E**), similar to the control experiments with no LTP protocol (**Fig. 16B**). This indicates that the crosstalk mechanism involves intracellular rather than extracellular signal(s), and affects only the activated dendrite segment. These results also excluded that the effect could be attributed to the diffusion of uncaged glutamate or other nonspecific effects of 2PGU.

DOI:10.14753/SE.2021.2546

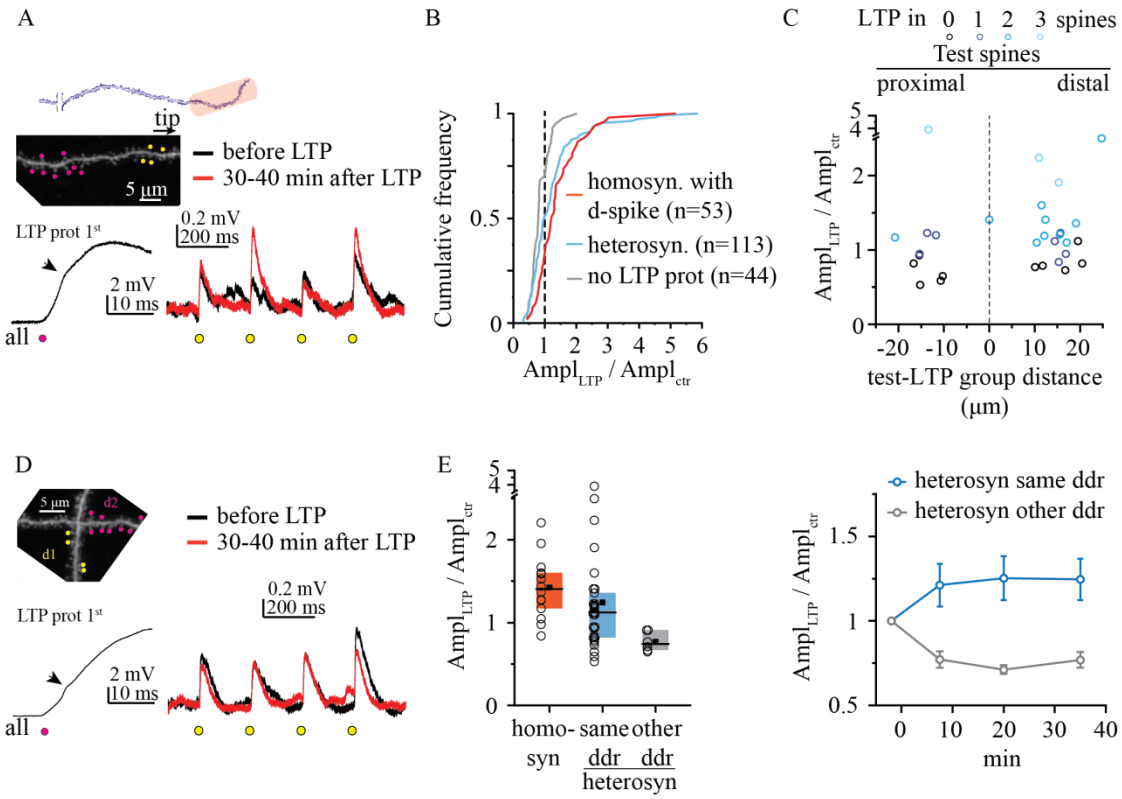

Figure 16 Heterosynaptic plasticity by suprathreshold input patterns at distal dendritic locations. *(**A**) Representative experiment. Left, Top, 2P z stack image of a distal dendritic segment. Four clustered test spines (yellow dots) were monitored but during the LTP protocol, only nearby spines (magenta dots) were stimulated to trigger d-spikes on at least one stimulus. Left, Bottom, First stimulus of the LTP protocol. Right, Average somatic EPSPs at the four test spines before (black) and >30 min after (red) the LTP protocol. (**B**) EPSP amplitude changes of individual test spines homosynaptic (orange suprathreshold experiments from Fig. 13B-D) and heterosynaptic (blue) LTP experiments. Number of spines included in the analysis is indicated in parentheses for each condition. Spines from no LTP experiments (Fig. 11B, E) are shown in gray for reference. (**C**) Impact of relative dendritic distance between the test spine and LTP induction spine groups. (**D**) Similar as in (**A**), but test spines and LTP induction spines are located on two different dendritic branches of the same cell. (**E**) Left, Comparison of homosynaptic LTP and heterosynaptic LTP, with test spines located on the same dendrite as the LTP induction spines (light blue) or on a nearby other dendrite (grey). Right, Time course of mean EPSP changes in heterosynaptic experiments.*

DOI:10.14753/SE.2021.2546

We considered the possibility that the LTP induction protocol, triggering repeated dendritic spikes, perhaps produced a general change in the electrical properties of the stimulated dendrite, leading to a virtual increase of synaptic voltage signals at the soma. However, the somatic strength of dendritic Na^+ spikes (dV/dt), a parameter expected to increase by enhanced dendritic excitability, did not systematic differ from the value measured during the first pulse of the LTP induction protocol to that evoked again at the end of the experiments (n=8, p=0.67, Wilcoxon test; **Fig. 17A**).

To further explore whether changes in the dendritic excitability can explain our data, my colleague Balázs Ujfalussy implemented a detailed biophysical model of a CA1PC and measured the somatic response amplitude to near-synchronous stimulation of 1-30 excitatory synaptic inputs (see Materials and Methods). In agreement with the experimental data, sufficiently strong stimulations elicited local dendritic Na^+ and NMDA spikes in the biophysical model, visible as small fast spikelets and slow plateaus, respectively, in the soma (**Fig. 17B**). We used this model to explore which mechanisms can increase synaptic EPSP amplitudes without changing the strength of the Na^+ spikelets as measured in the soma. Increasing the local excitability of the branch by changing passive parameters (increasing the local membrane resistivity [R_m] and decreasing axial resistivity [R_a]) within the branch increased the amplitude of individual EPSPs, but it also significantly increased dV/dt of the somatic spikelets (**Fig. 17C-E**). Changing the local excitability by locally eliminating K^+ channels also increased dV/dt of the somatic spikelets but failed to increase EPSP amplitudes (**Fig. 17 C-E**). On the other hand, increasing the AMPA conductance of the synapses by 40% (mimicking LTP) increased the amplitude of the EPSPs without changing the spikelets (**Fig. 17B-E**). These effects were robust against changing the passive parameters in the model (**Fig. 17F**). These simulations made it unlikely that changes in dendritic excitability by so far described mechanisms could alone explain the increase in somatically measured amplitude of the test spine EPSPs, and suggest that crosstalk was most likely mediated by synaptic mechanisms.

DOI:10.14753/SE.2021.2546

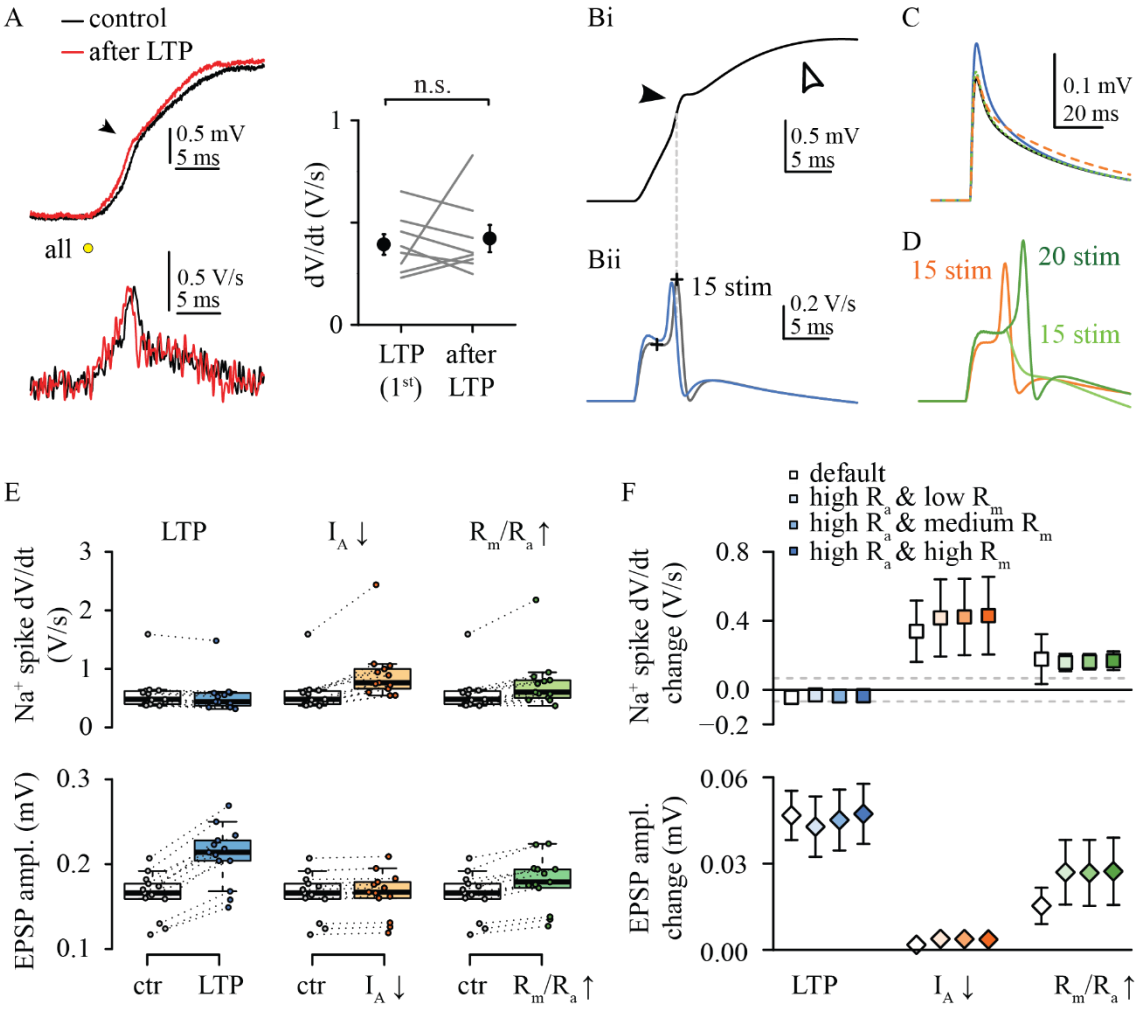

Figure 17 Changes in dendritic excitability by the LTP induction protocol cannot explain somatic increase in EPSP amplitude. *(**A**) Left, Representative voltage trace (top) and dV/dt (bottom) of the dendritic Na^+ spike evoked by the first stimulus of the LTP induction protocol (black), and >40 min after the LTP induction (red). Arrow points to fast spikelets. Right, Summary of 8 similar recordings (p=0.67, Wilcoxon test). Filled symbols and error bars represent mean±SEM. (**B-E**) Simulations in a biophysical CA1PC model. (**Bi**) Somatic membrane potential response to stimulation of 15 synapses (ISD: 1 µm, dt=0.3) on a terminal basal dendritic branch. Note the fast Na^+ (filled arrowhead) and the slower NMDA-spikes (open arrowhead). (**Bii**) dV/dt of the somatic voltage response in control condition (black) and after increasing AMPA conductance of the synapses from 0.6 to 0.84 nS (blue; NMDA conductance constant 0.8 nS). (**C**) Unitary synaptic EPSPs in control (black), after increasing the AMPA conductance (blue; LTP),*

*after decreasing K^+ channel density to 0 in the stimulated branch (dotted orange; I_A-down), or after halving R_a and quadrupling R_m in the stimulated branch (green; R_m/R_a-up). (**D**) dV/dt of the somatic voltage responses after changing local excitability through active (I_A-down, orange) or passive (R_m/R_a-up, green) mechanisms, using 15 and 20 stimuli (dark green). (**E**) Summary data from 13 stimulated basal branches. Only changing the synaptic conductance (LTP) but not changing local dendritic excitability via active (I_A-down) or passive (R_m/R_a-up) mechanisms was consistent with the experimental data (increased EPSP associated with no changes in dV/dt amplitude). Box plots represent median (line), interquartile ranges (box), and the last data point within the 1.5x interquartile range (whiskers). (**F**) Impact of LTP, I_A- down, and R_m/R_a-up conditions using different combinations of varied R_m/R_a parameters. The predicted Na^+ spike dV/dt changes by I_A-down and R_m/R_a-upconditions are above the threshold of detectability (gray dashed lines indicate SD of the measured dV/dt during the baseline). Symbols and error bars represent mean±SD. In some cases, error bars are smaller than symbols.*

Previous studies showed that LTP at a single spine can lower LTP induction threshold at nearby spines for several minutes, so that even weak stimuli can induce potentiation. Thus, we asked whether the crosstalk plasticity may be related to the weak test stimuli applied to monitor EPSPs. Since the initial selection of the four test spines involved variable numbers of pre-LTP stimuli at different spines (see Materials and Methods), we first analysed whether pre-LTP stimulation was related to the ability of spines to develop potentiation. Although we did not find a correlation between the number of pre-LTP stimuli and the magnitude of LTP by the individual spines (Spearman R=0.096, p=0.308, n=113 spines), When we separated test spines based on the number of received pre-LTP stimuli into two groups divided near the median (16 stimuli, range: 6-43; **Fig 18 A upper panel**), we found a trend for smaller EPSP amplitude change and fewer potentiated spines in the spine group receiving ≤15 pre-LTP stimuli (1.02±0.08, n=50; 22% of test spines potentiated) than in those receiving ≥16 pre-LTP stimuli (1.43±0.13, n=63; p=0.022, Mann-Whitney test, 40% of test spines potentiated, p=0.045,

χ^2 test; **Fig. 18B**). This raises the possibility that synapse activation before LTP induction by other synapses may facilitate crosstalk potentiation. Suspending test stimulation for 30 min after LTP induction (**Fig. 18A bottom panel**) did not eliminate the crosstalk (EPSP amplitude measured at 30-40 min: 1.26±0.11, n=14 experiments, 42% of test spines potentiated; **Fig. 18C**).

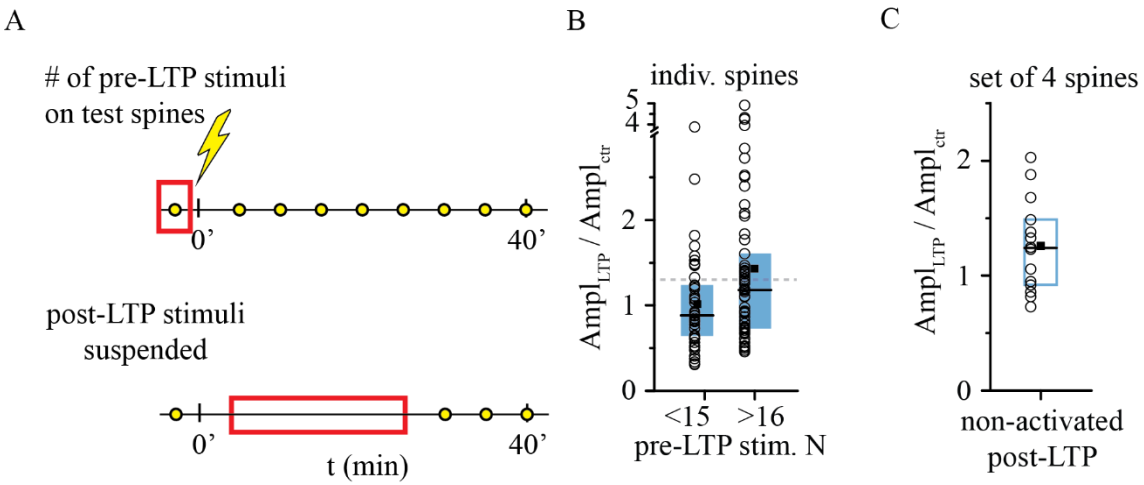

Figure 18 Effect of individual stimulations in heterosynaptic plasticity *(**A**) Schematic figure explaining the meaning of pre- and post-LTP stimulations. (**B**) Comparison of EPSP amplitude change in individual test spines that were stimulated ≤15x and ≥16x before the heterosynaptic LTP protocol. Dashed grey line indicates 30% increase. (**C**) EPSP amplitude change measured 30-40 min after the heterosynaptic LTP protocol, with postinduction test stimulation suspended for the first 30 min.*

5.8 Biophysical mechanism of crosstalk

The crosstalk mechanism was NMDAR-dependent because no potentiation developed in the presence of D-AP5 (50 μM; **Fig. 20 A-E**; EPSP amplitude: 0.90±0.07, n=10 experiments, p=0.023, significant by Holm-Bonferroni-corrected α with Mann-Whitney tests after Kruskal-Wallis test with p=0.022 for control, AP5, U0126, and VGCC blocker groups).

DOI:10.14753/SE.2021.2546

To rule out the possibility that the plasticity of the test spines was due to gradual glutamate accumulation around them during the multiple multisite stimuli of the LTP protocol at the LTP spines, in control experiments we loaded neurons with Ca^{2+} dye (OGB-1, 100 μM) and performed mock laser stimulations at a similar lateral distance from the test spine (**Fig. 19A, B**) while measuring spine Ca^{2+} signal and somatic voltage change. Neither the voltage nor the spine Ca^{2+} signals increased during the course of the mock LTP induction protocol, indicating that no gradual glutamate accumulation occurred locally in the tissue during the LTP protocol (**Fig. 19C**).

To better understand how intracellular Ca^{2+} may contribute to plasticity crosstalk, we next monitored Ca^{2+} signals in an individual test spine located ~10 μm distally from a group of eight spines on which the LTP protocol was applied (arrangement similar to that in heterosynaptic plasticity experiments) (**Fig. 19A, D-E**). We found a substantial increase of Ca^{2+} in test spines during those stimuli when d-spikes were elicited (**Fig. 19E**), most likely via the activation of VGCCs by the distally propagating spike (see also (Losonczy and Magee 2006)). Because VGCCs can play a role in some forms of LTP at CA3-CA1 synapses (Tigaret et al., 2016), we tested whether VGCCs are important for crosstalk plasticity.

DOI:10.14753/SE.2021.2546

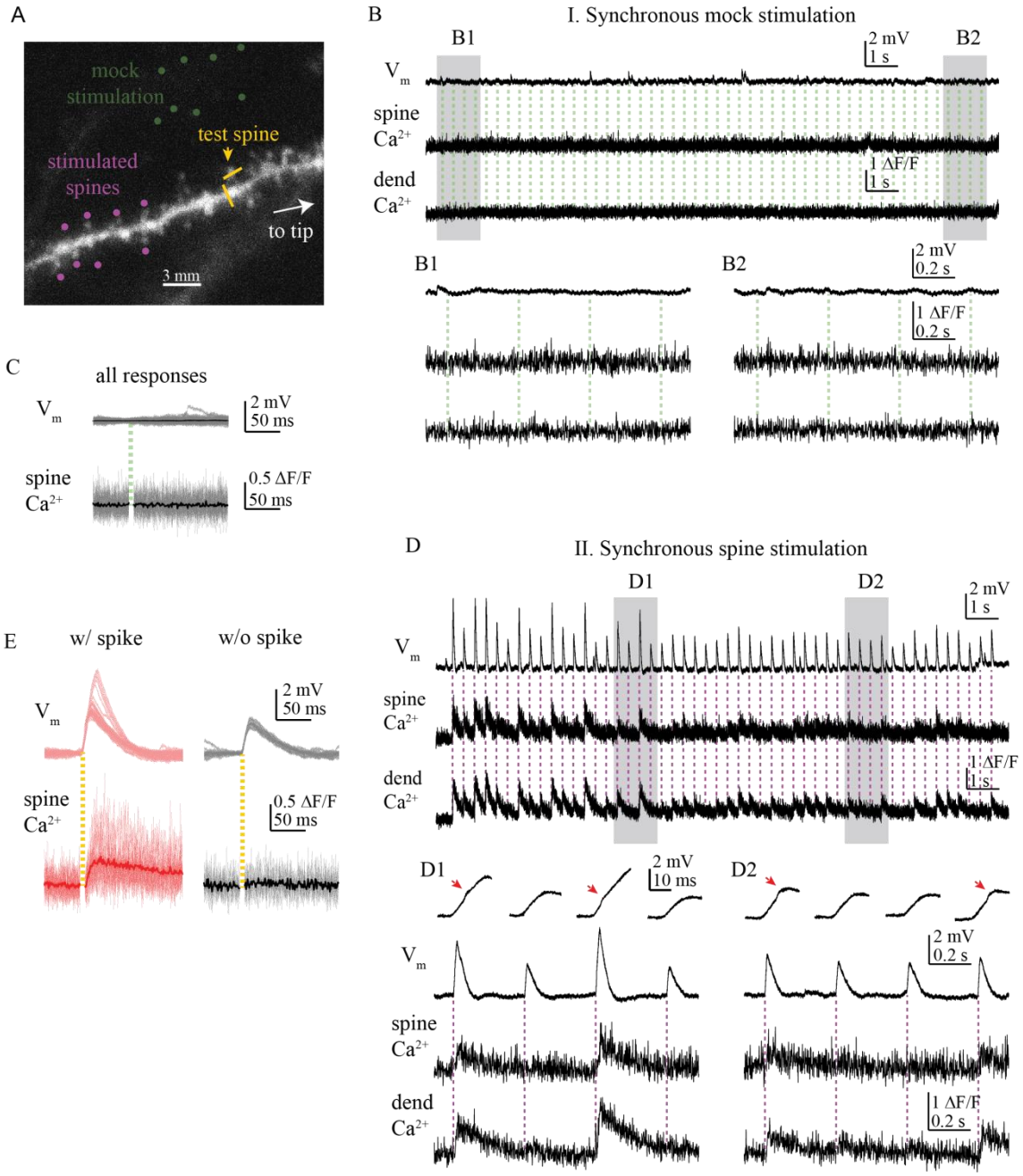

Figure 19 Ca^{2+} measurements in test spines during heterosynaptic LTP induction protocol and mock stimuli. *(A) 2P image of a dendrite loaded with OGB-1 and Alexa 594. Yellow lines indicate the position of the line scan through the head of a test spine (indicated by yellow arrowhead) and through the shaft. Magenta dots indicate uncaging sites at a group of nearby spines. Green dots indicate mock uncaging locations in the same arrangement but at a distance from the test spines. Quasi-synchronous uncaging at*

*the 9 sites was performed 50 times at 3Hz (same arrangement as used for heterosynaptic LTP induction protocol). (**B**) Somatic voltage responses and test spines head and dendrite Ca^{2+} signals during the LTP protocol with uncaging at the mock stimulation sites indicated by green dots in A. **B1** and **B2** regions show multiple stimuli enlarged. Note the lack of any voltage or spine Ca^{2+} signals evoked by the mock LTP uncaging stimuli at any time point during the protocol. (**C**) Individual stimuli from B aligned. (**D**) Representative recording showing somatic voltage responses and test spine head and dendrite Ca^{2+} signals during the LTP protocol on the spines indicated in A. **D1** and **D2** regions (lower panels) show multiple stimuli enlarged. Note the Ca^{2+} signals in the spine head during those responses that display a fast spikelet (red arrows on the enlarged initial part of the voltage traces on the top). (**E**) Stimuli in B were grouped based on the presence (left, red) or absence (right, black) of d-spike. Ca^{2+} signals in the test spine were detected only when d-spikes were evoked. Pink and grey traces are individual stimuli; red and black traces show mean ± SEM.*

In the presence of T-,R-, and L-type VGCC inhibitors (100 μM Ni^{2+} and 10 μM nimodipine), we observed an initial increase in EPSP amplitude in test spines, followed by gradual decline toward the baseline (**Fig. 20 A-C**; average EPSP amplitude at 7.5 min after LTP protocol: 1.26±0.07; at 30-40 min: 1.07±0.05, n=8, p=0.042, Wilcoxon test between time points), but the EPSP change at 30-40 min was not significantly different from that in ACSF (p=0.422, Mann-Whitney test). Thus, VGCCs are not indispensable for crosstalk but they may support stabilization of the process. Finally, inhibition of the MEK/ERK pathway by U0126, which was proposed to mediate local metaplasticity of nearby spines via small GTPases eliminated the crosstalk (test spine EPSP amplitude at 30-40 min in 20 μM U0126: 0.88±0.05, n=9, p=0.011, significant by Holm-Bonferroni-corrected α with Mann-Whitney test; **Fig. 20A-C**).

DOI:10.14753/SE.2021.2546

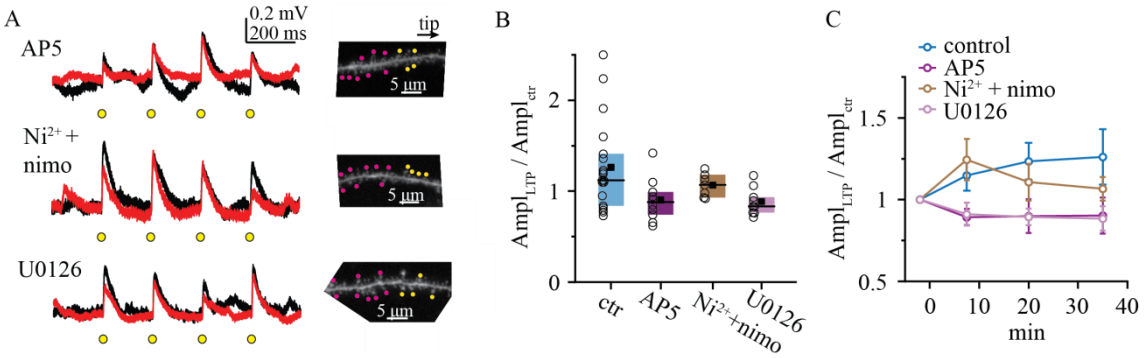

Figure 20 Mechanisms involved in heterosynaptic crosstalk *(**A**) Representative experiments (black represents baseline; red represents >30min after LTP induction) with bath application of AP5 (50 µM, top), Ni^{2+} plus nimodipine (10 and 100 µM, respectively, middle), or U0126 (20 µM, bottom). (**B**) Effect of inhibiting NMDA receptors (AP5), T-, R-, and L-type VGCCs (Ni^{2+} + nimodipine), or MEK/ERK pathway (U0126) on crosstalk plasticity. Test spines were located distally from LTP induction spines in all experiments testing different pharmacological conditions (control group includes the experiments with positive distances in Fig. 14C). (**C**) Time course of mean EPSP changes in heterosynaptic experiments under different pharmacological conditions. There is a transient increase of EPSP amplitudes in VGCC inhibitors.*

Together, the results suggest that crosstalk potentiation of synapses by nearby activity pattern evoking d-spikes may provide a less effective, but not negligible mechanism to increase synaptic strength, via signaling mediated by NMDARs and MEK/ERK activation.

DOI:10.14753/SE.2021.2546

6. DISCUSSION

While there is increasing evidence for spatiotemporally organized synaptic activity in recent studies, the interactions between individual synapses depending on the actual input pattern, have not yet been elucidated on the biophysical and molecular levels. Using combined 2PI, 2PGU, and electrophysiology, we explored how the fine-grained spatial pattern and the form of voltage integration determine synaptic cooperativity and plasticity of different excitatory synaptic input patterns along individual dendrites of CA1 pyramidal cells.

6.1 Subthreshold instantaneous interactions of spatially clustered co-active synapses

First, in order to investigate the interactions of subthreshold inputs, we examined the cooperative synaptic Ca^{2+} signaling and voltage integration by small input clusters. Our results demonstrate that NMDAR-mediated Ca^{2+} signals in individual spines are highly sensitive to the spatiotemporal activity pattern of even a few nearby synapses. However, the cooperativity was not equal along the dendritic tree, rather it showed a gradient along the dendritic branches which was consistent with the impedance profile of dendrites. In distal segments of perisomatic dendrites, surprisingly few coactive synapses (two to four) within ~10-20 μm can efficiently influence each other's function in a cooperative manner. Small clusters, consisting of just a few inputs, have been proposed to be optimal for NMDAR-rich synapses (Mel 1992). In addition, such small cluster size can be physiologically relevant according to the reports observing similar clusters of coactive synapses during spontaneous network activity. As an example, in the developing brain, neighbouring synapses on hippocampal pyramidal cell dendrites (located within 16 μm), are more likely to be coactive (Kleindienst et al., 2011). Winnubst and colleagues also demonstrated the importance of clustered synaptic coactivity in synaptic potentiation during development (Winnubst et al., 2015). Other studies, conducted in cortical pyramidal neurons, have pointed out the coordination of plasticity of neighbouring synapses upon sensory experience, which is observable in multiple cortical areas, such as in the motor cortex (Fu et al., 2012), frontal association cortex (Lai et al., 2012), and

barrel cortex (Makino and Malinow 2011). Moreover, the Dombeck lab has observed local Ca^{2+} signals independent from somatic firing in basal dendrites of CA1 pyramidal cells preceding new place field formation, consistent with local clustered input activity (Sheffield et al., 2017). Consistent with this, a recent ex vivo study showed that during sharp wave activity, clustered synapses are more likely to be active in CA1 pyramidal cells (Ishikawa and Ikegaya 2020).

The cooperative amplification of spine Ca^{2+} signals is produced by a graded NMDAR-mediated mechanism (Major et al., 2013), most likely due to effective spread of EPSPs between adjacent spines in distal compartments, alleviating the Mg^{2+} block of NMDARs and leading to supralinear Ca^{2+} influx in coactive nearby spines. Because the amplitude and kinetics of dendritic depolarization by a synapse depends on dendritic impedance, this mechanism is expected to be location dependent. Indeed, the dendritic map of synaptic Ca^{2+} cooperativity in perisomatic dendrites is consistent with the differences in local biophysical dendritic properties. In high-impedance terminal segments, small spine-to-dendrite voltage attenuation produces strong dendritic depolarization (Gulledge et al., 2012; Harnett et al., 2012; Rinzel and Rall 1974), allowing even a few closely located inputs to interact, whereas larger numbers of inputs are necessary to reach threshold for d-spikes and evoke nonlinear amplification of synaptic Ca^{2+} signals at low-impedance proximal dendritic locations. Indeed, the same mechanism affects dendritic spike properties depending on the input location and spatial pattern (Behabadi et al., 2012; Branco et al., 2010; Branco and Hausser 2011; Major et al., 2008), leading to a rich computational arsenal of the dendrite.

Here we showed the impact of dendritic location on local cooperativity of spine Ca^{2+} signals, without engaging more global, regenerative dendritic spikes. In fact, an interesting feature of the spatial gradient in the subthreshold scenario is a dissociation of nonlinearity in electrical versus Ca^{2+} signaling; while nonlinear spine Ca^{2+} signals increased in the proximodistal direction along branches, somatic EPSP integration was largely location independent. This is likely due to the different effect of depolarization on the AMPA receptor current, mainly producing EPSPs, and on NMDARs, mainly responsible for spine Ca^{2+} signals. Depolarization by an active synapse decreases

AMPAR current in neighbours through a reduction in driving force (actively counterbalanced by increased NMDAR current that leads to linearization of voltage summation), whereas the driving force for Ca^{2+} influx via the activated NMDARs is not dramatically reduced. A similar mechanism was observed in cerebellar stellate cells (Tran-Van-Minh et al., 2016). As a result of the dissociation of voltage and Ca^{2+} signaling, the uncovered local interactions in Ca^{2+} signaling among clustered synapses may remain virtually undetectable in somatic voltage recordings, as long as the compound depolarization remains subthreshold to local spikes.

Our results, including the relative location independence of mEPSP amplitude and individual spine Ca^{2+} signals as well as the increasing proximodistal gradient of spine Ca^{2+} cooperativity along thin dendrites, are consistent with relatively uniform synaptic properties in dendritic spines, and dendritic depolarization varying with location (Gulledge et al., 2012; Harnett et al., 2012). However, systematic distance-dependent differences of synaptic or voltage-dependent dendritic properties along thin branches may also influence location dependence of Ca^{2+} cooperativity. While such spatial distribution of voltage-gated channels are mostly unexplored, different gradients of synaptic density and strength along perisomatic dendrites of CA1PCs were proposed to counterbalance the inequality of synaptic strength due to impedance differences within a branch (Katz et al., 2009; Menon et al., 2013). For example of such counterbalancing differences, a proximodistal increase of AMPA receptor expression and a parallel decrease in NMDA receptors (Menon et al., 2013). Another interesting example that the NMDAR activation cause larger Ca^{2+} signals in smaller spines, which are more typical at distal dendritic locations (Walker et al., 2017). Nevertheless, unless the impact of the dendritic impedance gradient is completely neutralized, spine Ca^{2+} cooperativity is expected to increase gradually along these terminal dendrites, due to the local large depolarizations and subsequent activation of NMDA receptors.

DOI:10.14753/SE.2021.2546

6.2 Subthreshold cooperative long-term plasticity of spatially clustered synapses

The factors determining cooperativity of Ca^{2+} signaling and plasticity among synchronously active nearby synapses are incompletely understood (Carter et al., 2007; Govindarajan et al., 2011; Harnett et al., 2012; Jia et al., 2014; Winnubst et al., 2015). The rules that set the conditions to induce LTP by different dendritic distribution of synaptic input have scarcely been systematically investigated (Hardie and Spruston 2009; Letzkus et al., 2006; Sjostrom et al., 2008), and to our knowledge never at the level of individual synapses. Our finding of large Ca^{2+} signal amplification by small distal clusters may suggest that these input patterns can induce or at least contribute to specific, high Ca^{2+} dependent local molecular mechanisms. We decided to investigate whether cooperative activity of clustered synapses may allow synaptic potentiation. In order to do that, we repetitively costimulated small synapse clusters using 2P glutamate uncaging with a protocol which is similar to that used by others to evoke spike timing dependent plasticity (although with our technique, we were able to precisely control the spatiotemporal activation of a given set of synapses). We have demonstrated that subthreshold cooperative plasticity at distal segments of thin dendrites provide favourable environment for even low numbers ($\geq$3) of clustered inputs to cooperate and copotentiate; this form of interaction is efficient only in relatively distal dendritic segments, such as terminal dendrites. This finding was striking, since a recently prevailing idea has been that regenerative dendritic activity is required for clustered synaptic plasticity (Larkum and Nevian 2008) and LTP in general (Lisman and Spruston 2005). In addition, the potentiation of 3-4 synapses which was required for cooperative LTP in our experiments, is in line with the observation of Malinow and Makino in the mouse barrel cortex, where they observed similar average number of synapses per clusters that potentiated due to whisker stimulation (Makino and Malinow 2011).

Although due to the limited spatial resolution of the 2P uncaging, we cannot be sure that we always stimulated only one spine/pulse, this does not change our interpretation that subthreshold inputs can copotentiate, since their summated EPSPs never reached the threshold for dendritic spike generation. The mechanism was input specific, as EPSPs of nearby synapses that were not included in the input clusters did not

increase. Subthreshold LTP was efficient only when the coactive synapses were located within ~5-10 μm distance; it is possible that biochemical compartmentalization contributes to constraining the spatial limits for subthreshold LTP. This tight spatial requirement is stricter than what we observed at the interaction of coactive spine Ca^{2+} signals, but it is consistent with requirement of large spine Ca^{2+} signal for LTP. It is also possible, that the finite spread of LTP-related proteins and small molecules also limit the spatial extension of effective potentiation of active synapses. Again, this small coactive input number and spatial scale is remarkably consistent with that of small functional spine clusters observed in several PC types, including CA1 (Sheffield et al., 2017) and cortical PCs (Iacaruso et al., 2017; Kerlin et al., 2019; Kleindienst et al., 2011; Lee and Kirkwood 2019; Scholl et al., 2017; Takahashi et al., 2012) both *in vivo* and in *vitro*. We hypothesize that the clustered inputs at Schaffer collaterals originate from different CA3 pyramidal cells, based on the study of Druckmann and colleagues (Druckmann et al., 2014), which showed that CA3 pyramidal cells born in the same developmental time window form small clusters on dendrites of innervated CA1 pyramidal cells. In addition, a recent paper from the Spruston laboratory demonstrated that although axons arriving to CA1 pyramidal cells in lacunosum moleculare can form multiple clustered contacts on a small dendritic segment, such synaptic organization cannot be observed at Schaffer collaterals in str. radiatum, which form single contacts (Bloss et al., 2018).

Small inputs clusters are not sufficient to evoke d-spikes (Losonczy and Magee 2006), even under simulated *in vivo* conditions (Ujfalussy and Makara 2020). However, this is actually not needed for their local plasticity by the subthreshold mechanism we discovered. In fact, in the absence of substantial voltage nonlinearity in EPSP integration, activation of such small distal synapse clusters will not bias somatic output until potentiation developed, as a recently published modelling study from our lab suggests (Ujfalussy and Makara 2020); therefore, the occurrence of clustered activity might be overlooked or underestimated by somatic recording, and these small subthreshold input clusters may even have more important impact in neuronal processes than we thought before.

DOI:10.14753/SE.2021.2546

6.3 Local plasticity rules in the presence of regenerative dendritic spikes

We determined the size and spatial requirements of subthreshold input patterns for the generation of subthreshold cooperative LTP, but an also relevant question is, how the rules of plasticity are changing in the case of stronger input pattern that evoke d-spikes. In order to address this, we increased the number of costimulated inputs during the LTP protocol to reach the threshold for dendritic spike. In line with expectations, our results also support a role for local d-spikes to induce LTP, in accordance with previous work emphasizing the importance of dendritic spikes in the generation of LTP (Golding et al., 2002; Kim et al., 2015; Remy and Spruston 2007). We, however uncovered several substantial differences between subthreshold and d-spike mediated LTP induction.

In contrast to subthreshold mechanism, d-spike evoked LTP does not critically depend on the precise dendritic location, since d-spikes were able to induce LTP at both proximal and distal dendritic locations. Because the local threshold of d-spikes generation is relatively high in proximal low-impedance dendritic segments, this means that proximal synapses potentiate most likely if they are coactive with strong input patterns distributed throughout the dendrite (to elicit d-spikes) or throughout the cell (to elicit APs). At distal dendritic sites, d-spikes alleviated the strict spatial clustering requirement for LTP. Furthermore, when d-spikes were evoked, LTP could be triggered by just a few sufficiently strong activity events. LTP induced by regenerative d-spikes may thus support a rapid, effective and branch-specific (rather than tightly clustered) synaptic plasticity (Cichon and Gan 2015; Yang et al., 2014; Zhang et al., 2015) and connectivity (Druckmann et al., 2014; Lee and Kirkwood 2019). It is also likely that the propagation capacity of the d-spike (Losonczy et al., 2008), regulated by A-type K^+ currents, determine the size of the plasticity compartment. Altogether, our finding suggests that distal dendritic locations are likely to be more favourable for cooperative plasticity than proximal segments. This may also explain the observed higher density of clusters of potentiated synapses at distal compared to proximal dendritic segments evoked *in vivo* by sensory experience (Makino and Malinow 2011).

DOI:10.14753/SE.2021.2546

6.4 Heterosynaptic long term potentiation at distal dendritic locations

Since local dendritic regenerative events proved to modify the plasticity rules, we also investigated how reference spines that were not stimulated during LTP induction protocol respond to such conditions. In this case, we observed less prominent but not negligible heterosynaptic potentiation of inputs in the vicinity of synapses evoking d-spikes. While Hebbian LTP was classically postulated to be input-specific at large scale, several heterosynaptic plasticity forms have been demonstrated in dendrites on short spatial scales, usually parallel with homosynaptic LTP. The range of heterosynaptic plasticity includes not only depression and shrinkage of nearby other synapses (which is thought to be more common) (El-Boustani et al., 2018; Oh et al., 2015) but also potentiation (Govindarajan et al., 2011; Harvey and Svoboda 2007; Hedrick et al., 2016; Murakoshi et al., 2011). Specifically, LTP of some synapses may promote potentiation of other, weakly and nonsynchronously active nearby synapses via diffusion of small GTPases, on up to few tens of micrometers and minutes spatiotemporal distance (Govindarajan et al., 2011; Harvey and Svoboda 2007; Hedrick et al., 2016; Murakoshi et al., 2011), inducing the molecular mechanisms underlying heterosynaptic LTP generation. The crosstalk during metaplasticity shown by Harvey and Svoboda operated in ~10 minutes and ~10 μm, involved autocrine BDNF signaling (Harward et al., 2016). During this type of metaplasticity, Ras superfamily proteins that originate from LTP synapses can diffuse to weakly stimulated, primed spines and activate the cdc42 which can induce potentiation (Harvey and Svoboda 2007; Hedrick et al., 2016; Murakoshi et al., 2011). In addition, the Yasuda lab published a study, showing that during LTP induction in one spine, Rac1 is active for around 30 minutes, and can spread over 10 μm along the dendrite (Hedrick et al., 2016). These proteins may promote LTP either by causing direct potentiation, or by decreasing the threshold of plasticity, leading to priming the adjacent synapses for potentiation. It is tempting to speculate that the crosstalk plasticity we observed may have a similar mechanism: e.g., synaptic activation by test stimuli (in our case, ~1.5 min earlier) may prime test spines for local plasticity crosstalk from LTP-induction spines, mediated via the MEK/ERK pathway, which is known to be an important pathway in plasticity mechanisms. Unfortunately, measuring plasticity of

unstimulated synapses is not feasible with our experimental method, as the only readout of plasticity is the change of evoked EPSPs, and our technique is not optimal to examine structural plasticity. Thus, it is difficult to determine to what extent our heterosynaptic crosstalk plasticity depends on activity; although our analysis suggests a relationship, further experiments with alternative techniques will be needed to address this question more extensively.

Moreover, using Ca^{2+} imaging in unstimulated spines during LTP induction protocol, we observed a significant increase in the Ca^{2+} signal in the presence of dendritic spikes; this increased level may also promote the potentiation, possibly through the activation of LTP related slower molecular mechanisms.

6.5 Implications

The above results highlight fundamental location-dependent differences in synaptic learning rules, even in a single dendritic branch. For LTP at proximal dendritic segments, regenerative dendritic events seem essential. LTP does not only affect pre-existing synapses, but also take part in the long-term stabilization of nascent dendritic spines (Hill and Zito 2013), thus location-dependent plasticity rules may affect synaptic connectivity (Bono et al., 2017). Spatially heterogeneous plasticity rules may also result in distance-dependent bias in synaptic tuning properties (Iacaruso et al., 2017; Scholl et al., 2017) even in adult brain. For example, proximal inputs may be more likely to be cotuned with the soma, while distal inputs more likely cotuned with their neighbours (Iacaruso et al., 2017; Scholl et al., 2017). These results may indicate that different forms of information can be stored via different plasticity rules along a single dendritic branch, depending on the location of the input pattern representing the information. Subthreshold and suprathreshold LTP may also be hierarchically organized so that initial gradual potentiation of repeatedly activated small distal input clusters would help to reach d-spike threshold, recruiting a second, spatially less constrained and faster mechanism that may eventually also evoke somatic AP firing activating global Hebbian synaptic plasticity. In

addition, models suggest that information stored by synaptic clusters is more stable and long-lasting than that stored by unclustered synapses (Bono et al., 2017).

What can be the role of plasticity crosstalk in information coding? Modification of synapse strength by activity of other inputs may seem unfavorable at first sight due to degradation of input specificity, which theoretically can lead to an over-excitable network state. However, integrated storage of synaptic information representing events that occur within a time window of minutes may be behaviourally relevant, as it could bind temporally separate yet associated components (including less salient ones) of a complex experience onto a dendritic segment (Govindarajan et al., 2006; Kastellakis et al., 2016; Wiegert and Oertner 2015), allowing subsequent simultaneous recurrence of the components to be retrieved more efficiently through dendritic amplification. In addition, since plasticity crosstalk is local, it would only affect segments receiving robust local input (although a possible compensatory effect by homeostatic plasticity also needs to be considered). It is also important to highlight, that heterosynaptic plasticity was much less reliable compared to homosynaptic LTP; less spines were potentiated, whereas some of them showed a mild decrease in their EPSP amplitude, potentially suggesting a parallel compensation mechanism. Supporting the relevance of mechanisms promoting copotentiation of temporally separated inputs, another unorthodox form of LTP has been recently described in CA1PCs that is induced by long dendritic plateau potentials and strengthens inputs that were active a short interval (few seconds) earlier or later, leading to place field generation (Bittner et al., 2017).

In conclusion, our results reveal a large room for cooperative synaptic plasticity to occur locally in dendrites without somatic output, allowing even silent neurons to store information, and increasing the computational capacity of individual cells. The fine-scale distribution of active synapses and the local electrical properties of the dendrites, together with other conventional plasticity rules (Clopath and Gerstner 2010; Feldman 2012), can determine the capacity of input patterns to evoke long-term plasticity. The preferential strengthening (and possibly persistence) of specific arrangements of synaptic connections may contribute to experience-related emergence and refinement of neuronal tuning (Sheffield et al., 2017), and ultimately to the creation of highly specific synaptic engrams

DOI:10.14753/SE.2021.2546

of memory traces (Govindarajan et al., 2006). Deciphering the local biophysical processes of synaptic plasticity is not only necessary to understand the computational principles underlying the development of behaviourally relevant and flexible representations by cortical circuits, but may also help to achieve more powerful artificial learning algorithms paralleling the performance of the living brain.

DOI:10.14753/SE.2021.2546

7. CONCLUSIONS

Using a combination of various technical approaches such as *in vitro* 2P imaging, 2P glutamate uncaging combined with whole cell current-clamp recordings, as well as modelling, we elucidated the local interactions of spatially colocalized coactive synaptic inputs along the dendritic branches of CA1 pyramidal cells in acute adult rat hippocampal slices.

We first showed that subthreshold activation of small input clusters can lead to cooperative NMDAR dependent supralinear Ca^{2+} signal amplification in the co-active synapses in a location-dependent manner, observed at distal but not at proximal dendritic locations. At distal locations, interactions of coactive inputs can be detected even when the interspine distance (ISD) of two co-active synapses is around 20 µm, albeit the size of Ca^{2+} signal amplification decreases with the distance between cooperating synapses.

Based on the local large spine Ca^{2+} signal produced by cooperativity at distal synapses we investigate synaptic plasticity of small clusters of coactive inputs can be induced. Repetitive subthreshold co-stimulation (50x at 3 Hz) of 3-4 synapses by 2-photon glutamate uncaging evoked input specific cooperative LTP. Similar to the Ca^{2+} amplification of clustered co-active synapses, the efficacy of subthreshold LTP also matched the passive impedance profile of dendritic branches, although on a finer scale the required interspine distance was stricter (≤~5 µm), suggesting that, large local intracellular Ca^{2+} concentration are needed to induce LTP.

Evoking dendritic spikes using stronger input patterns during LTP stimulation changed the local plasticity rules in several aspects. We have shown that regenerative voltage signals were crucial for inducing LTP at proximal dendritic locations.

At distal locations, the magnitude of LTP was not affected by d-spikes, but d-spikes alleviated the tight spatial requirement of input distribution, transforming the potentiation from local restricted plasticity to a more extended, perhaps branch specific form. In addition, substantially smaller number of synchronous stimulation was sufficient for potentiation in the presence of d-spikes (5x @ 3Hz).

DOI:10.14753/SE.2021.2546

In addition to homosynaptic plasticity of the coactive synapses, d-spikes led to local heterosynaptic crosstalk, resulting in potentiation of nearby non-synchronous synapses. This potentiation was less efficient compared to homosynaptic LTP, but was above chance level. Heterosynaptic LTP was mediated by NMDARs and the MEK/ERK pathway, and our data suggest that VGCCs may have a stabilizing role. In addition, using in silico modelling we reinforced our findings as the long term increase of EPSPs during heterosynaptic LTP could not be explained by changes in dendritic excitability.

DOI:10.14753/SE.2021.2546

8. ÖSSZEFOGLALÁS

Doktori képzésem során kollégáimmal *in vitro* módszerekkel vizsgáltuk a CA1-es piramissejtek dendritjeire beérkező serkentő bemenetek kölcsönhatásait 2P-glutamát felszabadítás segítségével, és az ennek következményeképp kialakuló lokális plaszticitási folyamatokat felnőtt, hím Wistar patkányokban.

Mivel a dendritikus integrációban a beérkező serkentő bemenetek mintázata is meghatározó, ezért fontos kérdés, hogy a funkcionálisan hasonló bemenetek vajon véletlenszerűen helyezkednek-e el a dendritágakon, vagy strukturáltan, térben közel egymáshoz. Utóbbira egyre több bizonyíték van a szakirodalomban, viszont keveset tudunk arról, hogy az egymással szomszédos, szinkron aktív bemenetek között milyen kölcsönhatások zajlanak le, ha a szinaptikusan kiváltott depolarizáció nem vált ki regeneratív feszültségválaszt. Az eredményeink azt mutatták, hogy a szinkron aktív bemenetek hatására az aktív dendrittüske fejekben NMDA receptor függő nemlineáris Ca^{2+} jelerősödés figyelhető meg, ami korrelál a piramissejtek dendritfájának impedancia profiljával.

Ez a Ca^{2+} jel amplifikáció vezetett a feltételezéshez, hogy a szinkron klaszter aktivitás során megnövekedett intracelluláris Ca^{2+} elősegítheti a szinapszisok hosszútávú plaszticitását. 2P glutamát felszabadítás segítségével egy speciális LTP protokollal sikerült igazolnunk a távoli dendritszakaszokon ismételten együtt aktivált kis bemenet klaszterek (3-4 szinapszis) homoszinaptikus potencírozódását, melyhez nem volt szükség regeneratív feszültségválaszhoz, viszont a bemeneteknek viszonylag szoros közelségben kellett elhelyezkednie. Azt is megvizsgáltuk, hogy mennyiben különböznek ezek a plaszticitási szabályok, ha erősebb bemenet mintázattal stimulálunk, amely regeneratív dendritikus feszültségválaszt generál. Ilyen körülmények között képesek voltunk közeli dendritszakaszon is kiváltani LTP-t, míg a távoli szakaszokon nem növekedett a potencírozódás mértéke, ugyanakkor kevesebb stimulus alkalmazásával, egymástól távolabb elhelyezkedő szinapszisok is potencírozódtak. Regenerativ dendritikus tüske kiváltása esetén megfigyeltünk továbbá NMDAR-függő heteroszinaptikus plaszticitást is, melynek kialakulása a MEK/ERK jelátviteli útvonalhoz köthető.

DOI:10.14753/SE.2021.2546

9. SUMMARY

We investigated the interactions of spatially clustered excitatory inputs and the local rules of synaptic cooperativity in long-term potentiation in dendrites of hippocampal CA1 pyramidal neurons *in vitro*.

Accumulating evidence indicates that functionally related inputs may be spatially colocalized along dendrites, however, the subthreshold interactions of such input clusters and their local plasticity rules are not well elucidated. My PhD work was based on findings of our lab, revealing that co-activation of spatially clustered synapses leads to NMDAR dependent nonlinear Ca^{2+} signal amplification in the activated spine heads even during linear voltage summation. The magnitude of the observed spine Ca^{2+} amplification correlated with the increasing dendritic impedance profile along individual dendrites.

As large postsynaptic Ca^{2+} signals are essential for long-term synaptic potentiation, we hypothesized that repeated coactivation of small input clusters can induce their plasticity, depending on dendritic location. Indeed, repetitive subthreshold co-activation of 3-4 tightly clustered synapses at distal dendritic locations led to NMDAR dependent, input specific homosynaptic potentiation even in the absence of regenerative voltage events. We also examined local plasticity rules when stronger input patterns reached the threshold for dendritic spike generation. We found that at proximal dendritic locations, d-spikes (or bAPs) are required for LTP generation. At distal locations, the magnitude of LTP was not increased further by activation of d-spikes, however, the tight spatial requirement for potentiation was alleviated, and fewer co-stimulation trials were sufficient to evoke plasticity. We have also shown an NMDAR dependent heterosynaptic plasticity in nonsynchronously active neighbouring synapses, a phenomenon that was less reliable than homosynaptic LTP and depended on the MEK/ERK signalization pathway. In summary, our results uncover the diversity of synaptic plasticity rules based on the fine-scale distribution of active synapses and local electrical properties of the dendrites.

10. BIBLIOGRAPHY

Abbott LF, Nelson SB. (2000) Synaptic plasticity: taming the beast. Nat Neurosci, 3 Suppl: 1178-1183.

Abraham WC, Bear MF. (1996) Metaplasticity: the plasticity of synaptic plasticity. Trends Neurosci, 19: 126-130.

Abrahamsson T, Cathala L, Matsui K, Shigemoto R, Digregorio DA. (2012) Thin dendrites of cerebellar interneurons confer sublinear synaptic integration and a gradient of short-term plasticity. Neuron, 73: 1159-1172.

Ainge JA, van der Meer MA, Langston RF, Wood ER. (2007) Exploring the role of context-dependent hippocampal activity in spatial alternation behavior. Hippocampus, 17: 988-1002.

Amaral DG, Ishizuka N, Claiborne B. (1990) Neurons, numbers and the hippocampal network. Prog Brain Res, 83: 1-11.

Amaral DG, Witter MP. (1989) The three-dimensional organization of the hippocampal formation: a review of anatomical data. Neuroscience, 31: 571-591.

Andersen, P. (2007). The hippocampus book. Oxford University Press, Oxford; New York, 2007:51-52.

Andersen, P. (2007). The hippocampus book. Oxford University Press, Oxford; New York, 2007:71-72.

Andersen, P. (2007). The hippocampus book. Oxford University Press, Oxford; New York, 2007:67-68.

Andersen, P. (2007). The hippocampus book. Oxford University Press, Oxford; New York, 2007:305-306.

Andersen P, Bliss TVP, Skrede KK. (1971) Unit analysis of hippocampal population spikes. Exp Brain Res, 13: 208-221.

Bannister NJ, Larkman AU. (1995) Dendritic morphology of CA1 pyramidal neurones from the rat hippocampus: I. Branching patterns. J Comp Neurol, 360: 150-160.

Baudry M, Zhu G, Liu Y, Wang Y, Briz V, Bi X. (2015) Multiple cellular cascades participate in long-term potentiation and in hippocampus-dependent learning. Brain Res, 1621: 73-81.

Behabadi BF, Polsky A, Jadi M, Schiller J, Mel BW. (2012) Location-dependent excitatory synaptic interactions in pyramidal neuron dendrites. PLoS Comput Biol, 8: e1002599.

Benarroch EE. (2013) HCN channels: function and clinical implications. Neurology, 80: 304-310.

Bienkowski MS, Bowman I, Song MY, Gou L, Ard T, Cotter K, Zhu M, Benavidez NL, Yamashita S, Abu-Jaber J, Azam S, Lo D, Foster NN, Hintiryan H, Dong HW. (2018) Integration of gene expression and brain-wide connectivity reveals the multiscale organization of mouse hippocampal networks. Nat Neurosci, 21: 1628-1643.

Bischofberger J, Engel D, Li L, Geiger JR, Jonas P. (2006) Patch-clamp recording from mossy fiber terminals in hippocampal slices. Nat Protoc, 1: 2075-2081.

Bittner KC, Andrasfalvy BK, Magee JC. (2012) Ion channel gradients in the apical tuft region of CA1 pyramidal neurons. PLoS One, 7: e46652.

Bittner KC, Milstein AD, Grienberger C, Romani S, Magee JC. (2017) Behavioral time scale synaptic plasticity underlies CA1 place fields. Science, 357: 1033-1036.

Bliss TV, Collingridge GL. (1993) A synaptic model of memory: long-term potentiation in the hippocampus. Nature, 361: 31-39.

Bliss TV, Lomo T. (1973) Long-lasting potentiation of synaptic transmission in the dentate area of the anaesthetized rabbit following stimulation of the perforant path. J Physiol, 232: 331-356.

Bloodgood BL, Sabatini BL. (2007a) Ca(2+) signaling in dendritic spines. Curr Opin Neurobiol, 17: 345-351.

Bloodgood BL, Sabatini BL. (2007b) Nonlinear regulation of unitary synaptic signals by CaV(2.3) voltage-sensitive calcium channels located in dendritic spines. Neuron, 53: 249-260.

Bloss EB, Cembrowski MS, Karsh B, Colonell J, Fetter RD, Spruston N. (2018) Single excitatory axons form clustered synapses onto CA1 pyramidal cell dendrites. Nat Neurosci, 21: 353-363.

Bono J, Wilmes KA, Clopath C. (2017) Modelling plasticity in dendrites: from single cells to networks. Curr Opin Neurobiol, 46: 136-141.

Bosch M, Castro J, Saneyoshi T, Matsuno H, Sur M, Hayashi Y. (2014) Structural and molecular remodeling of dendritic spine substructures during long-term potentiation. Neuron, 82: 444-459.

Bozon B, Kelly A, Josselyn SA, Silva AJ, Davis S, Laroche S. (2003) MAPK, CREB and zif268 are all required for the consolidation of recognition memory. Philos Trans R Soc Lond B Biol Sci, 358: 805-814.

Branco T, Clark BA, Hausser M. (2010) Dendritic discrimination of temporal input sequences in cortical neurons. Science, 329: 1671-1675.

Branco T, Hausser M. (2011) Synaptic integration gradients in single cortical pyramidal cell dendrites. Neuron, 69: 885-892.

Brandon MP, Bogaard AR, Libby CP, Connerney MA, Gupta K, Hasselmo ME. (2011) Reduction of theta rhythm dissociates grid cell spatial periodicity from directional tuning. Science, 332: 595-599.

Briz V, Hsu YT, Li Y, Lee E, Bi X, Baudry M. (2013) Calpain-2-mediated PTEN degradation contributes to BDNF-induced stimulation of dendritic protein synthesis. J Neurosci, 33: 4317-4328.

Buzsaki G. (2002) Theta oscillations in the hippocampus. Neuron, 33: 325-340.

Buzsaki G. (2015) Hippocampal sharp wave-ripple: A cognitive biomarker for episodic memory and planning. Hippocampus, 25: 1073-1188.

Carter AG, Soler-Llavina GJ, Sabatini BL. (2007) Timing and location of synaptic inputs determine modes of subthreshold integration in striatal medium spiny neurons. J Neurosci, 27: 8967-8977.

Cash S, Yuste R. (1998) Input summation by cultured pyramidal neurons is linear and position-independent. J Neurosci, 18: 10-15.

Cash S, Yuste R. (1999) Linear summation of excitatory inputs by CA1 pyramidal neurons. Neuron, 22: 383-394.

Celikel T, Szostak VA, Feldman DE. (2004) Modulation of spike timing by sensory deprivation during induction of cortical map plasticity. Nat Neurosci, 7: 534-541.

Cenquizca LA, Swanson LW. (2007) Spatial organization of direct hippocampal field CA1 axonal projections to the rest of the cerebral cortex. Brain Res Rev, 56: 1-26.

Chistiakova M, Bannon NM, Bazhenov M, Volgushev M. (2014) Heterosynaptic plasticity: multiple mechanisms and multiple roles. Neuroscientist, 20: 483-498.

Cichon J, Gan WB. (2015) Branch-specific dendritic Ca(2+) spikes cause persistent synaptic plasticity. Nature, 520: 180-185.

Citri A, Malenka RC. (2008) Synaptic plasticity: multiple forms, functions, and mechanisms. Neuropsychopharmacology, 33: 18-41.

Clopath C, Gerstner W. (2010) Voltage and Spike Timing Interact in STDP - A Unified Model. Front Synaptic Neurosci, 2: 25.

Colgin LL. (2013) Mechanisms and functions of theta rhythms. Annu Rev Neurosci, 36: 295-312.

Collingridge GL. (1992) The Sharpey-Schafer Prize Lecture. The mechanism of induction of NMDA receptor-dependent long-term potentiation in the hippocampus. Exp Physiol, 77: 771-797.

Corkin S. Lasting consequences of bilateral medial temporal lobectomy: Clinical course and experimental findings in HM. In: Seminars in neurology Vol. 4, 1984: 249-259.

Crunelli V, Mayer ML. (1984) Mg2+ dependence of membrane resistance increases evoked by NMDA in hippocampal neurones. Brain Res, 311: 392-396.

Dam AM. (1980) Epilepsy and neuron loss in the hippocampus. Epilepsia, 21: 617-629.

Danielson NB, Zaremba JD, Kaifosh P, Bowler J, Ladow M, Losonczy A. (2016) Sublayer-Specific Coding Dynamics during Spatial Navigation and Learning in Hippocampal Area CA1. Neuron, 91: 652-665.

Day M, Carr DB, Ulrich S, Ilijic E, Tkatch T, Surmeier DJ. (2005) Dendritic excitability of mouse frontal cortex pyramidal neurons is shaped by the interaction among HCN, Kir2, and Kleak channels. J Neurosci, 25: 8776-8787.

Deguchi Y, Donato F, Galimberti I, Cabuy E, Caroni P. (2011) Temporally matched subpopulations of selectively interconnected principal neurons in the hippocampus. Nat Neurosci, 14: 495-504.

Derkach V, Barria A, Soderling TR. (1999) Ca2+/calmodulin-kinase II enhances channel conductance of alpha-amino-3-hydroxy-5-methyl-4-isoxazolepropionate type glutamate receptors. Proc Natl Acad Sci U S A, 96: 3269-3274.

Deshmukh SS, Knierim JJ. (2013) Influence of local objects on hippocampal representations: Landmark vectors and memory. Hippocampus, 23: 253-267.

Desjardins AE, Li YX, Reinker S, Miura RM, Neuman RS. (2003) The influences of Ih on temporal summation in hippocampal CA1 pyramidal neurons: a modeling study. J Comput Neurosci, 15: 131-142.

Dougherty KA, Islam T, Johnston D. (2012) Intrinsic excitability of CA1 pyramidal neurones from the rat dorsal and ventral hippocampus. J Physiol, 590: 5707-5722.

Druckmann S, Feng L, Lee B, Yook C, Zhao T, Magee JC, Kim J. (2014) Structured synaptic connectivity between hippocampal regions. Neuron, 81: 629-640.

Dudai Y, Morris RG. (2013) Memorable trends. Neuron, 80: 742-750.

Eichenbaum H. (2013) What H.M. taught us. J Cogn Neurosci, 25: 14-21.

Eichenbaum H. (2017) The role of the hippocampus in navigation is memory. J Neurophysiol, 117: 1785-1796.

El-Boustani S, Ip JPK, Breton-Provencher V, Knott GW, Okuno H, Bito H, Sur M. (2018) Locally coordinated synaptic plasticity of visual cortex neurons in vivo. Science, 360: 1349-1354.

English JD, Sweatt JD. (1997) A requirement for the mitogen-activated protein kinase cascade in hippocampal long term potentiation. J Biol Chem, 272: 19103-19106.

Feldman DE. (2012) The spike-timing dependence of plasticity. Neuron, 75: 556-571.

Frank AC, Huang S, Zhou M, Gdalyahu A, Kastellakis G, Silva TK, Lu E, Wen X, Poirazi P, Trachtenberg JT, Silva AJ. (2018) Hotspots of dendritic spine turnover facilitate clustered spine addition and learning and memory. Nat Commun, 9: 422.

Freund TF, Buzsaki G. (1996) Interneurons of the hippocampus. Hippocampus, 6: 347-470.

Frey U, Morris RG. (1997) Synaptic tagging and long-term potentiation. Nature, 385: 533-536.

Frick A, Magee J, Koester HJ, Migliore M, Johnston D. (2003) Normalization of Ca2+ signals by small oblique dendrites of CA1 pyramidal neurons. J Neurosci, 23: 3243-3250.

Froemke RC, Letzkus JJ, Kampa BM, Hang GB, Stuart GJ. (2010) Dendritic synapse location and neocortical spike-timing-dependent plasticity. Front Synaptic Neurosci, 2: 29.

Fu M, Yu X, Lu J, Zuo Y. (2012) Repetitive motor learning induces coordinated formation of clustered dendritic spines in vivo. Nature, 483: 92-95.

Galloni AR, Laffere A, Rancz E. (2020) Apical length governs computational diversity of layer 5 pyramidal neurons. Elife, 9.

Gambino F, Pages S, Kehayas V, Baptista D, Tatti R, Carleton A, Holtmaat A. (2014) Sensory-evoked LTP driven by dendritic plateau potentials in vivo. Nature, 515: 116-119.

Gentet LJ, Stuart GJ, Clements JD. (2000) Direct measurement of specific membrane capacitance in neurons. Biophys J, 79: 314-320.

Giannakopoulos P, Hof PR, Michel JP, Guimon J, Bouras C. (1997) Cerebral cortex pathology in aging and Alzheimer's disease: a quantitative survey of large hospital-based geriatric and psychiatric cohorts. Brain Res Brain Res Rev, 25: 217-245.

Golding NL, Spruston N. (1998) Dendritic sodium spikes are variable triggers of axonal action potentials in hippocampal CA1 pyramidal neurons. Neuron, 21: 1189-1200.

Golding NL, Staff NP, Spruston N. (2002) Dendritic spikes as a mechanism for cooperative long-term potentiation. Nature, 418: 326-331.

Goldstein SS, Rall W. (1974) Changes of action potential shape and velocity for changing core conductor geometry. Biophys J, 14: 731-757.

Gordon U, Polsky A, Schiller J. (2006) Plasticity compartments in basal dendrites of neocortical pyramidal neurons. J Neurosci, 26: 12717-12726.

Govindarajan A, Israely I, Huang SY, Tonegawa S. (2011) The dendritic branch is the preferred integrative unit for protein synthesis-dependent LTP. Neuron, 69: 132-146.

Govindarajan A, Kelleher RJ, Tonegawa S. (2006) A clustered plasticity model of long-term memory engrams. Nat Rev Neurosci, 7: 575-583.

Gulledge AT, Carnevale NT, Stuart GJ. (2012) Electrical advantages of dendritic spines. PLoS One, 7: e36007.

Hardie J, Spruston N. (2009) Synaptic Depolarization Is More Effective than Back-Propagating Action Potentials during Induction of Associative Long-Term Potentiation in Hippocampal Pyramidal Neurons. Journal of Neuroscience, 29: 3233-3241.

Harnett MT, Makara JK, Spruston N, Kath WL, Magee JC. (2012) Synaptic amplification by dendritic spines enhances input cooperativity. Nature, 491: 599-602.

Harvey CD, Svoboda K. (2007) Locally dynamic synaptic learning rules in pyramidal neuron dendrites. Nature, 450: 1195-1200.

Harvey CD, Yasuda R, Zhong H, Svoboda K. (2008) The spread of Ras activity triggered by activation of a single dendritic spine. Science, 321: 136-140.

Harward SC, Hedrick NG, Hall CE, Parra-Bueno P, Milner TA, Pan E, Laviv T, Hempstead BL, Yasuda R, McNamara JO. (2016) Autocrine BDNF-TrkB signalling within a single dendritic spine. Nature, 538: 99-103.

Hayashi Y, Shi SH, Esteban JA, Piccini A, Poncer JC, Malinow R. (2000) Driving AMPA receptors into synapses by LTP and CaMKII: requirement for GluR1 and PDZ domain interaction. Science, 287: 2262-2267.

Hebb DO. The organization of behavior; a neuropsychological theory. Wiley, Oxford, England, 1949.

Hedrick NG, Harward SC, Hall CE, Murakoshi H, McNamara JO, Yasuda R. (2016) Rho GTPase complementation underlies BDNF-dependent homo- and heterosynaptic plasticity. Nature, 538: 104-108.

Hill TC, Zito K. (2013) LTP-induced long-term stabilization of individual nascent dendritic spines. J Neurosci, 33: 678-686.

Hitti FL, Siegelbaum SA. (2014) The hippocampal CA2 region is essential for social memory. Nature, 508: 88-92.

Hoffman DA, Magee JC, Colbert CM, Johnston D. (1997) K+ channel regulation of signal propagation in dendrites of hippocampal pyramidal neurons. Nature, 387: 869-875.

Holthoff K, Kovalchuk Y, Konnerth A. (2006) Dendritic spikes and activity-dependent synaptic plasticity. Cell Tissue Res, 326: 369-377.

Holtmaat A, Caroni P. (2016) Functional and structural underpinnings of neuronal assembly formation in learning. Nat Neurosci, 19: 1553-1562.

Iacaruso MF, Gasler IT, Hofer SB. (2017) Synaptic organization of visual space in primary visual cortex. Nature, 547: 449-452.

Ishikawa T, Ikegaya Y. (2020) Locally sequential synaptic reactivation during hippocampal ripples. Sci Adv, 6: eaay1492.

Jarsky T, Roxin A, Kath WL, Spruston N. (2005) Conditional dendritic spike propagation following distal synaptic activation of hippocampal CA1 pyramidal neurons. Nat Neurosci, 8: 1667-1676.

Jia H, Varga Z, Sakmann B, Konnerth A. (2014) Linear integration of spine Ca2+ signals in layer 4 cortical neurons in vivo. Proc Natl Acad Sci U S A, 111: 9277-9282.

Johnston D, Brown TH. (1983) Interpretation of voltage-clamp measurements in hippocampal neurons. J Neurophysiol, 50: 464-486.

Johnston D, Christie BR, Frick A, Gray R, Hoffman DA, Schexnayder LK, Watanabe S, Yuan LL. (2003) Active dendrites, potassium channels and synaptic plasticity. Philos Trans R Soc Lond B Biol Sci, 358: 667-674.

Johnston D, Hoffman DA, Colbert CM, Magee JC. (1999) Regulation of back-propagating action potentials in hippocampal neurons. Curr Opin Neurobiol, 9: 288-292.

Johnston D, Hoffman DA, Magee JC, Poolos NP, Watanabe S, Colbert CM, Migliore M. (2000) Dendritic potassium channels in hippocampal pyramidal neurons. J Physiol, 525 Pt 1: 75-81.

Jones MW, McHugh TJ. (2011) Updating hippocampal representations: CA2 joins the circuit. Trends Neurosci, 34: 526-535.

Kampa BM, Clements J, Jonas P, Stuart GJ. (2004) Kinetics of Mg2+ unblock of NMDA receptors: implications for spike-timing dependent synaptic plasticity. J Physiol, 556: 337-345.

Kandel ER. (2001) The molecular biology of memory storage: a dialogue between genes and synapses. Science, 294: 1030-1038.

Kandel ER, Dudai Y, Mayford MR. (2014) The molecular and systems biology of memory. Cell, 157: 163-186.

Kastellakis G, Silva AJ, Poirazi P. (2016) Linking Memories across Time via Neuronal and Dendritic Overlaps in Model Neurons with Active Dendrites. Cell Rep, 17: 1491-1504.

Katz Y, Menon V, Nicholson DA, Geinisman Y, Kath WL, Spruston N. (2009) Synapse distribution suggests a two-stage model of dendritic integration in CA1 pyramidal neurons. Neuron, 63: 171-177.

Kerchner GA, Nicoll RA. (2008) Silent synapses and the emergence of a postsynaptic mechanism for LTP. Nat Rev Neurosci, 9: 813-825.

Kerlin A, Mohar B, Flickinger D, MacLennan BJ, Dean MB, Davis C, Spruston N, Svoboda K. (2019) Functional clustering of dendritic activity during decision-making. Elife, 8.

Kessels HW, Malinow R. (2009) Synaptic AMPA receptor plasticity and behavior. Neuron, 61: 340-350.

Kim Y, Hsu CL, Cembrowski MS, Mensh BD, Spruston N. (2015) Dendritic sodium spikes are required for long-term potentiation at distal synapses on hippocampal pyramidal neurons. Elife, 4.

Klausberger T. (2009) GABAergic interneurons targeting dendrites of pyramidal cells in the CA1 area of the hippocampus. Eur J Neurosci, 30: 947-957.

Kleindienst T, Winnubst J, Roth-Alpermann C, Bonhoeffer T, Lohmann C. (2011) Activity-dependent clustering of functional synaptic inputs on developing hippocampal dendrites. Neuron, 72: 1012-1024.

Knierim JJ, Neunuebel JP, Deshmukh SS. (2014) Functional correlates of the lateral and medial entorhinal cortex: objects, path integration and local-global reference frames. Philos Trans R Soc Lond B Biol Sci, 369: 20130369.

Kogan JH, Frankland PW, Silva AJ. (2000) Long-term memory underlying hippocampus-dependent social recognition in mice. Hippocampus, 10: 47-56.

Lai CS, Franke TF, Gan WB. (2012) Opposite effects of fear conditioning and extinction on dendritic spine remodelling. Nature, 483: 87-91.

Larkum ME, Kaiser KM, Sakmann B. (1999a) Calcium electrogenesis in distal apical dendrites of layer 5 pyramidal cells at a critical frequency of back-propagating action potentials. Proc Natl Acad Sci U S A, 96: 14600-14604.

Larkum ME, Nevian T. (2008) Synaptic clustering by dendritic signalling mechanisms. Curr Opin Neurobiol, 18: 321-331.

Larkum ME, Nevian T, Sandler M, Polsky A, Schiller J. (2009) Synaptic integration in tuft dendrites of layer 5 pyramidal neurons: a new unifying principle. Science, 325: 756-760.

Larkum ME, Zhu JJ. (2002) Signaling of layer 1 and whisker-evoked Ca2+ and Na+ action potentials in distal and terminal dendrites of rat neocortical pyramidal neurons in vitro and in vivo. J Neurosci, 22: 6991-7005.

Larkum ME, Zhu JJ, Sakmann B. (1999b) A new cellular mechanism for coupling inputs arriving at different cortical layers. Nature, 398: 338-341.

Laviv T, Scholl B, Parra-Bueno P, Foote B, Zhang C, Yan L, Hayano Y, Chu J, Yasuda R. (2020) In Vivo Imaging of the Coupling between Neuronal and CREB Activity in the Mouse Brain. Neuron, 105: 799-812 e795.

Lee CM, Stoelzel C, Chistiakova M, Volgushev M. (2012) Heterosynaptic plasticity induced by intracellular tetanization in layer 2/3 pyramidal neurons in rat auditory cortex. J Physiol, 590: 2253-2271.

Lee HK, Barbarosie M, Kameyama K, Bear MF, Huganir RL. (2000) Regulation of distinct AMPA receptor phosphorylation sites during bidirectional synaptic plasticity. Nature, 405: 955-959.

Lee HK, Kirkwood A. (2019) Mechanisms of Homeostatic Synaptic Plasticity in vivo. Front Cell Neurosci, 13: 520.

Lee SJ, Escobedo-Lozoya Y, Szatmari EM, Yasuda R. (2009) Activation of CaMKII in single dendritic spines during long-term potentiation. Nature, 458: 299-304.

Letzkus JJ, Kampa BM, Stuart GJ. (2006) Learning rules for spike timing-dependent plasticity depend on dendritic synapse location. J Neurosci, 26: 10420-10429.

Lisman J, Spruston N. (2005) Postsynaptic depolarization requirements for LTP and LTD: a critique of spike timing-dependent plasticity. Nat Neurosci, 8: 839-841.

Lorente de Nó R. Studies on the structure of the cerebral cortex. II, II. Johann Ambrosius Barth, Leipzig, 1934.

Losonczy A, Magee JC. (2006) Integrative properties of radial oblique dendrites in hippocampal CA1 pyramidal neurons. Neuron, 50: 291-307.

Losonczy A, Makara JK, Magee JC. (2008) Compartmentalized dendritic plasticity and input feature storage in neurons. Nature, 452: 436-441.

Lu H, Park H, Poo MM. (2014) Spike-timing-dependent BDNF secretion and synaptic plasticity. Philos Trans R Soc Lond B Biol Sci, 369: 20130132.

Lynch GS, Dunwiddie T, Gribkoff V. (1977) Heterosynaptic depression: a postsynaptic correlate of long-term potentiation. Nature, 266: 737-739.

Magee J, Hoffman D, Colbert C, Johnston D. (1998) Electrical and calcium signaling in dendrites of hippocampal pyramidal neurons. Annu Rev Physiol, 60: 327-346.

Magee JC. (1999) Dendritic Ih normalizes temporal summation in hippocampal CA1 neurons. Nat Neurosci, 2: 848.

Magee JC, Cook EP. (2000) Somatic EPSP amplitude is independent of synapse location in hippocampal pyramidal neurons. Nat Neurosci, 3: 895-903.

Magee JC, Johnston D. (1997) A synaptically controlled, associative signal for Hebbian plasticity in hippocampal neurons. Science, 275: 209-213.

Major G, Larkum ME, Schiller J. (2013) Active properties of neocortical pyramidal neuron dendrites. Annu Rev Neurosci, 36: 1-24.

Major G, Polsky A, Denk W, Schiller J, Tank DW. (2008) Spatiotemporally graded NMDA spike/plateau potentials in basal dendrites of neocortical pyramidal neurons. J Neurophysiol, 99: 2584-2601.

Makara JK, Losonczy A, Wen Q, Magee JC. (2009) Experience-dependent compartmentalized dendritic plasticity in rat hippocampal CA1 pyramidal neurons. Nat Neurosci, 12: 1485-1487.

Makara JK, Magee JC. (2013) Variable dendritic integration in hippocampal CA3 pyramidal neurons. Neuron, 80: 1438-1450.

Makino H, Malinow R. (2009) AMPA receptor incorporation into synapses during LTP: the role of lateral movement and exocytosis. Neuron, 64: 381-390.

Makino H, Malinow R. (2011) Compartmentalized versus global synaptic plasticity on dendrites controlled by experience. Neuron, 72: 1001-1011.

Malik R, Dougherty KA, Parikh K, Byrne C, Johnston D. (2016) Mapping the electrophysiological and morphological properties of CA1 pyramidal neurons along the longitudinal hippocampal axis. Hippocampus, 26: 341-361.

Markram H, Lubke J, Frotscher M, Sakmann B. (1997) Regulation of synaptic efficacy by coincidence of postsynaptic APs and EPSPs. Science, 275: 213-215.

Masurkar AV, Srinivas KV, Brann DH, Warren R, Lowes DC, Siegelbaum SA. (2017) Medial and Lateral Entorhinal Cortex Differentially Excite Deep versus Superficial CA1 Pyramidal Neurons. Cell Rep, 18: 148-160.

Matsuzaki M, Ellis-Davies GC, Nemoto T, Miyashita Y, Iino M, Kasai H. (2001) Dendritic spine geometry is critical for AMPA receptor expression in hippocampal CA1 pyramidal neurons. Nat Neurosci, 4: 1086-1092.

Matsuzaki M, Honkura N, Ellis-Davies GC, Kasai H. (2004) Structural basis of long-term potentiation in single dendritic spines. Nature, 429: 761-766.

Mayer ML, Westbrook GL, Guthrie PB. (1984) Voltage-dependent block by Mg2+ of NMDA responses in spinal cord neurones. Nature, 309: 261-263.

Mel BW. (1992) NMDA-based pattern discrimination in a modeled cortical neuron. Neural Comput, 4: 502-517.

Menon V, Musial TF, Liu A, Katz Y, Kath WL, Spruston N, Nicholson DA. (2013) Balanced synaptic impact via distance-dependent synapse distribution and complementary expression of AMPARs and NMDARs in hippocampal dendrites. Neuron, 80: 1451-1463.

Milojkovic BA, Zhou WL, Antic SD. (2007) Voltage and calcium transients in basal dendrites of the rat prefrontal cortex. J Physiol, 585: 447-468.

Mower AF, Kwok S, Yu H, Majewska AK, Okamoto K, Hayashi Y, Sur M. (2011) Experience-dependent regulation of CaMKII activity within single visual cortex synapses in vivo. Proc Natl Acad Sci U S A, 108: 21241-21246.

Muller D, Hefft S, Figurov A. (1995) Heterosynaptic interactions between LTP and LTD in CA1 hippocampal slices. Neuron, 14: 599-605.

Murakoshi H, Wang H, Yasuda R. (2011) Local, persistent activation of Rho GTPases during plasticity of single dendritic spines. Nature, 472: 100-104.

Nevian T, Larkum ME, Polsky A, Schiller J. (2007) Properties of basal dendrites of layer 5 pyramidal neurons: a direct patch-clamp recording study. Nat Neurosci, 10: 206-214.

Nguyen PV, Woo NH. (2003) Regulation of hippocampal synaptic plasticity by cyclic AMP-dependent protein kinases. Prog Neurobiol, 71: 401-437.

Nicoll RA. (1988) The coupling of neurotransmitter receptors to ion channels in the brain. Science, 241: 545-551.

Nicoll RA, Kauer JA, Malenka RC. (1988) The current excitement in long-term potentiation. Neuron, 1: 97-103.

Nimchinsky EA, Sabatini BL, Svoboda K. (2002) Structure and function of dendritic spines. Annu Rev Physiol, 64: 313-353.

Norenberg A, Hu H, Vida I, Bartos M, Jonas P. (2010) Distinct nonuniform cable properties optimize rapid and efficient activation of fast-spiking GABAergic interneurons. Proc Natl Acad Sci U S A, 107: 894-899.

Nowak L, Bregestovski P, Ascher P, Herbet A, Prochiantz A. (1984) Magnesium gates glutamate-activated channels in mouse central neurones. Nature, 307: 462-465.

O'Keefe J, Conway DH. (1978) Hippocampal place units in the freely moving rat: why they fire where they fire. Exp Brain Res, 31: 573-590.

O'Keefe J, Dostrovsky J. (1971) The hippocampus as a spatial map. Preliminary evidence from unit activity in the freely-moving rat. Brain Res, 34: 171-175.

O'keefe J, Nadel L. The hippocampus as a cognitive map. Oxford: Clarendon Press1978.

Oh WC, Parajuli LK, Zito K. (2015) Heterosynaptic structural plasticity on local dendritic segments of hippocampal CA1 neurons. Cell Rep, 10: 162-169.

Okuyama T, Kitamura T, Roy DS, Itohara S, Tonegawa S. (2016) Ventral CA1 neurons store social memory. Science, 353: 1536-1541.

Oliva A, Fernandez-Ruiz A, Buzsaki G, Berenyi A. (2016) Spatial coding and physiological properties of hippocampal neurons in the Cornu Ammonis subregions. Hippocampus, 26: 1593-1607.

Packard MG, McGaugh JL. (1996) Inactivation of hippocampus or caudate nucleus with lidocaine differentially affects expression of place and response learning. Neurobiol Learn Mem, 65: 65-72.

Pelkey KA, Chittajallu R, Craig MT, Tricoire L, Wester JC, McBain CJ. (2017) Hippocampal GABAergic Inhibitory Interneurons. Physiol Rev, 97: 1619-1747.

Penzes P, Cahill ME, Jones KA, Srivastava DP. (2008) Convergent CaMK and RacGEF signals control dendritic structure and function. Trends Cell Biol, 18: 405-413.

Pittenger C, Kandel ER. (2003) In search of general mechanisms for long-lasting plasticity: Aplysia and the hippocampus. Philos Trans R Soc Lond B Biol Sci, 358: 757-763.

Polsky A, Mel BW, Schiller J. (2004) Computational subunits in thin dendrites of pyramidal cells. Nat Neurosci, 7: 621-627.

Poucet B, Save E, Lenck-Santini PP. (2000) Sensory and memory properties of hippocampal place cells. Rev Neurosci, 11: 95-111.

Rall W. (1960) Membrane potential transients and membrane time constant of motoneurons. Exp Neurol, 2: 503-532.

Remy S, Beck H, Yaari Y. (2010) Plasticity of voltage-gated ion channels in pyramidal cell dendrites. Curr Opin Neurobiol, 20: 503-509.

Remy S, Spruston N. (2007) Dendritic spikes induce single-burst long-term potentiation. Proc Natl Acad Sci U S A, 104: 17192-17197.

Rhodes P. (2006) The properties and implications of NMDA spikes in neocortical pyramidal cells. J Neurosci, 26: 6704-6715.

Rinzel J, Rall W. (1974) Transient response in a dendritic neuron model for current injected at one branch. Biophys J, 14: 759-790.

Robinson NTM, Descamps LAL, Russell LE, Buchholz MO, Bicknell BA, Antonov GK, Lau JYN, Nutbrown R, Schmidt-Hieber C, Hausser M. (2020) Targeted Activation of Hippocampal Place Cells Drives Memory-Guided Spatial Behavior. Cell, 183: 1586-1599 e1510.

Rogerson T, Cai DJ, Frank A, Sano Y, Shobe J, Lopez-Aranda MF, Silva AJ. (2014) Synaptic tagging during memory allocation. Nat Rev Neurosci, 15: 157-169.

Rolls ET. (2018) The storage and recall of memories in the hippocampo-cortical system. Cell Tissue Res, 373: 577-604.

Rondi-Reig L, Petit GH, Tobin C, Tonegawa S, Mariani J, Berthoz A. (2006) Impaired sequential egocentric and allocentric memories in forebrain-specific-NMDA receptor knock-out mice during a new task dissociating strategies of navigation. J Neurosci, 26: 4071-4081.

Roth A, Hausser M. (2001) Compartmental models of rat cerebellar Purkinje cells based on simultaneous somatic and dendritic patch-clamp recordings. J Physiol, 535: 445-472.

Schiller J, Major G, Koester HJ, Schiller Y. (2000) NMDA spikes in basal dendrites of cortical pyramidal neurons. Nature, 404: 285-289.

Scholl B, Wilson DE, Fitzpatrick D. (2017) Local Order within Global Disorder: Synaptic Architecture of Visual Space. Neuron, 96: 1127-1138 e1124.

Shah MM, Hammond RS, Hoffman DA. (2010) Dendritic ion channel trafficking and plasticity. Trends Neurosci, 33: 307-316.

Sheffield ME, Dombeck DA. (2015) Calcium transient prevalence across the dendritic arbour predicts place field properties. Nature, 517: 200-204.

Sheffield MEJ, Adoff MD, Dombeck DA. (2017) Increased Prevalence of Calcium Transients across the Dendritic Arbor during Place Field Formation. Neuron, 96: 490-504 e495.

Shen K, Meyer T. (1999) Dynamic control of CaMKII translocation and localization in hippocampal neurons by NMDA receptor stimulation. Science, 284: 162-166.

Simms BA, Zamponi GW. (2014) Neuronal voltage-gated calcium channels: structure, function, and dysfunction. Neuron, 82: 24-45.

Sjostrom PJ, Hausser M. (2006) A cooperative switch determines the sign of synaptic plasticity in distal dendrites of neocortical pyramidal neurons. Neuron, 51: 227-238.

Sjostrom PJ, Rancz EA, Roth A, Hausser M. (2008) Dendritic excitability and synaptic plasticity. Physiol Rev, 88: 769-840.

Sliwa J, Plante A, Duhamel JR, Wirth S. (2016) Independent Neuronal Representation of Facial and Vocal Identity in the Monkey Hippocampus and Inferotemporal Cortex. Cereb Cortex, 26: 950-966.

Soderling TR, Derkach VA. (2000) Postsynaptic protein phosphorylation and LTP. Trends Neurosci, 23: 75-80.

Song S, Miller KD, Abbott LF. (2000) Competitive Hebbian learning through spike-timing-dependent synaptic plasticity. Nat Neurosci, 3: 919-926.

Spruston N, Jaffe DB, Johnston D. (1994) Dendritic attenuation of synaptic potentials and currents: the role of passive membrane properties. Trends Neurosci, 17: 161-166.

Spruston N, Jaffe DB, Williams SH, Johnston D. (1993) Voltage- and space-clamp errors associated with the measurement of electrotonically remote synaptic events. J Neurophysiol, 70: 781-802.

Stuart GJ, Spruston N. (2015) Dendritic integration: 60 years of progress. Nat Neurosci, 18: 1713-1721.

Szoboszlay M, Lorincz A, Lanore F, Vervaeke K, Silver RA, Nusser Z. (2016) Functional Properties of Dendritic Gap Junctions in Cerebellar Golgi Cells. Neuron, 90: 1043-1056.

Takahashi H, Magee JC. (2009) Pathway interactions and synaptic plasticity in the dendritic tuft regions of CA1 pyramidal neurons. Neuron, 62: 102-111.

Takahashi N, Kitamura K, Matsuo N, Mayford M, Kano M, Matsuki N, Ikegaya Y. (2012) Locally synchronized synaptic inputs. Science, 335: 353-356.

Takao K, Okamoto K, Nakagawa T, Neve RL, Nagai T, Miyawaki A, Hashikawa T, Kobayashi S, Hayashi Y. (2005) Visualization of synaptic Ca2+ /calmodulin-dependent protein kinase II activity in living neurons. J Neurosci, 25: 3107-3112.

Tigaret CM, Olivo V, Sadowski J, Ashby MC, Mellor JR. (2016) Coordinated activation of distinct Ca(2+) sources and metabotropic glutamate receptors encodes Hebbian synaptic plasticity. Nat Commun, 7: 10289.

Tonnesen J, Katona G, Rozsa B, Nagerl UV. (2014) Spine neck plasticity regulates compartmentalization of synapses. Nat Neurosci, 17: 678-685.

Tran-Van-Minh A, Abrahamsson T, Cathala L, DiGregorio DA. (2016) Differential Dendritic Integration of Synaptic Potentials and Calcium in Cerebellar Interneurons. Neuron, 91: 837-850.

Tran-Van-Minh A, Caze RD, Abrahamsson T, Cathala L, Gutkin BS, DiGregorio DA. (2015) Contribution of sublinear and supralinear dendritic integration to neuronal computations. Front Cell Neurosci, 9: 67.

Ujfalussy BB, Makara JK. (2020) Impact of functional synapse clusters on neuronal response selectivity. Nat Commun, 11: 1413.

Vervaeke K, Lorincz A, Nusser Z, Silver RA. (2012) Gap junctions compensate for sublinear dendritic integration in an inhibitory network. Science, 335: 1624-1628.

Vetter P, Roth A, Hausser M. (2001) Propagation of action potentials in dendrites depends on dendritic morphology. J Neurophysiol, 85: 926-937.

Victor M, Agamanolis D. (1990) Amnesia due to Lesions Confined to the Hippocampus: A Clinical-Pathologic Study. J Cogn Neurosci, 2: 246-257.

Volianskis A, France G, Jensen MS, Bortolotto ZA, Jane DE, Collingridge GL. (2015) Long-term potentiation and the role of N-methyl-D-aspartate receptors. Brain Res, 1621: 5-16.

Vossler MR, Yao H, York RD, Pan MG, Rim CS, Stork PJ. (1997) cAMP activates MAP kinase and Elk-1 through a B-Raf- and Rap1-dependent pathway. Cell, 89: 73-82.

Walker AS, Neves G, Grillo F, Jackson RE, Rigby M, O'Donnell C, Lowe AS, Vizcay-Barrena G, Fleck RA, Burrone J. (2017) Distance-dependent gradient in NMDAR-driven spine calcium signals along tapering dendrites. Proc Natl Acad Sci U S A, 114: E1986-E1995.

Weber JP, Andrasfalvy BK, Polito M, Mago A, Ujfalussy BB, Makara JK. (2016) Location-dependent synaptic plasticity rules by dendritic spine cooperativity. Nat Commun, 7: 11380.

Wiegert JS, Oertner TG. (2015) Neighborly synapses help each other out. Nat Neurosci, 18: 326-327.

Williams SR, Stuart GJ. (2002) Dependence of EPSP efficacy on synapse location in neocortical pyramidal neurons. Science, 295: 1907-1910.

Williams SR, Stuart GJ. (2003) Role of dendritic synapse location in the control of action potential output. Trends Neurosci, 26: 147-154.

Winnubst J, Cheyne JE, Niculescu D, Lohmann C. (2015) Spontaneous Activity Drives Local Synaptic Plasticity In Vivo. Neuron, 87: 399-410.

Wood ER, Dudchenko PA, Robitsek RJ, Eichenbaum H. (2000) Hippocampal neurons encode information about different types of memory episodes occurring in the same location. Neuron, 27: 623-633.

Xu C, Krabbe S, Grundemann J, Botta P, Fadok JP, Osakada F, Saur D, Grewe BF, Schnitzer MJ, Callaway EM, Luthi A. (2016) Distinct Hippocampal Pathways Mediate Dissociable Roles of Context in Memory Retrieval. Cell, 167: 961-972 e916.

Yang G, Lai CS, Cichon J, Ma L, Li W, Gan WB. (2014) Sleep promotes branch-specific formation of dendritic spines after learning. Science, 344: 1173-1178.

Zhang Y, Cudmore RH, Lin DT, Linden DJ, Huganir RL. (2015) Visualization of NMDA receptor-dependent AMPA receptor synaptic plasticity in vivo. Nat Neurosci, 18: 402-407.

Zhu JJ, Qin Y, Zhao M, Van Aelst L, Malinow R. (2002) Ras and Rap control AMPA receptor trafficking during synaptic plasticity. Cell, 110: 443-455.

DOI:10.14753/SE.2021.2546

11. BIBLIOGRAPHY OF CANDIDATE'S PUBLICATION

Publications related to the Ph.D. dissertation

- Weber, J. P., Andrásfalvy, B. K., Polito, M., Magó, Á., Ujfalussy, B. B., Makara, J.K. (2016). Location-dependent synaptic plasticity rules by dendritic spine cooperativity. Nat Commun. 7:11380

- Magó Á., Weber, J. P., Ujfalussy B. B., Makara, J. K. (2020). Synaptic Plasticity Depends on the Fine-Scale Input Pattern in Thin Dendrites of CA1 Pyramidal Neurons. J Neurosci. 40, 2593-2605.

Other publications

- Raus Balind, S., Magó, Á., Ahmadi, M., Kis, N., Varga-Németh, Z., Lőrincz, A., Makara, J. K. (2019). Diverse synaptic and dendritic mechanisms of complex spike burst generation in hippocampal CA3 pyramidal cells. Nat Commun. 10, 1859

DOI:10.14753/SE.2021.2546

12. ACKNOWLEDGEMENTS

First of all, I would like to thank to Judit Makara for the opportunity to work in her lab, her friendly but critical support and guidance to learn the techniques, her patience and to get to know the beauty of the world of dendrites. I am also grateful for her help to improve my presentation qualities and she was always open-minded for my ideas. I would also like to thank to Jens Peter Weber, who helped me a lot during the cooperativity project, and provided me practical technical advices. The help of Bertalan Andrásfalvy, who always helped me when there were any serious problems with the patch-clamp setup, and he always had some cheerful comment even during the most desperate times. I would like to thank to Balázs Benedek Ujfalussy, who provided a valuable model in my project and he always had useful critical comments, which increased the quality of my work. I am also grateful to Zsófia Varga-Németh, for her friendship and that she always ensured to have enough solutions, and cut the best brain slices, providing the perfect conditions for great experiments. I would also like to thank to Snezana Raus Balind, who is also a great friend and a good colleague. I would like to thank to the rest of the Makara lab for the good atmosphere, and for the Nusser and Szabadics lab for the great and exciting discussions during journal clubs.

I would like to thank to Brunner János who was my internal reviewer, who gave useful comments, suggestions and asked very good questions about my thesis.

I would like to thank to József Bóna, my highschool biology teacher, who introduced me the beauty of science and he saw potential in me even when my marks did not give any reasons.

I am grateful to my friends, who were always there when I needed them and helped to relax, and Kata Kenesei, who pushed me to write and finish my thesis and my PhD.

Finally, I would like to thank to my family, especially to my mother, father and my brother for the support, help and patience during my whole life.